UNIVERSITY OF UDINE

PhD research in Agro-Environmental Science
Cycle XXVIII
Coordinator: prof.ssa Maria De Nobili

DISSERTATION

Relationship Between Nanoparticles and Higher Plants

DOCTOR OF PHILOSOPHY
Alessandro Mattiello

SUPERVISOR
Prof. Luca Marchiol

ACADEMIC YEAR 2015/2016

Contents

1 General Introduction

1.1 Nanoparticles and Nanomaterials Definition

1.1.1 First Mentioning of Nanoparticles

The introduction of the concept of nanotechnologies could be assigned to the Nobel prize in physics Richard Feynman, who described in a lecture entitled "There's plenty of room at the bottom" dated December 1959 the problems of manipulating the matter at very small scale level but also the enormous possibilities offered by this technological improvement, in particular he thought what would happen if we could arrange the atoms one by one the way we want them.

He also anticipated the idea of how difficult the manipulation and the control of things at this small scale are because atoms at this scale behave like nothing on a large scale, for they satisfy the law of quantum mechanics. "We are working with different laws and we expect different things. At the atomic level, we have new kinds of forces and new kind of possibilities, new kind of effects" (Feynman, 1959).

1.1.2 Definition of Nanoparticles

The term nano is adapted from the Greek word meaning "dwarf." When used as a prefix, it implies 10^{-9}. A nanometer (nm) is one billionth of a meter, or roughly the length of three atoms side by side (Figure 1). A NP is defined as a microscopic particle with at least one dimension less than 100 nm (Kaushik et al., 2010).

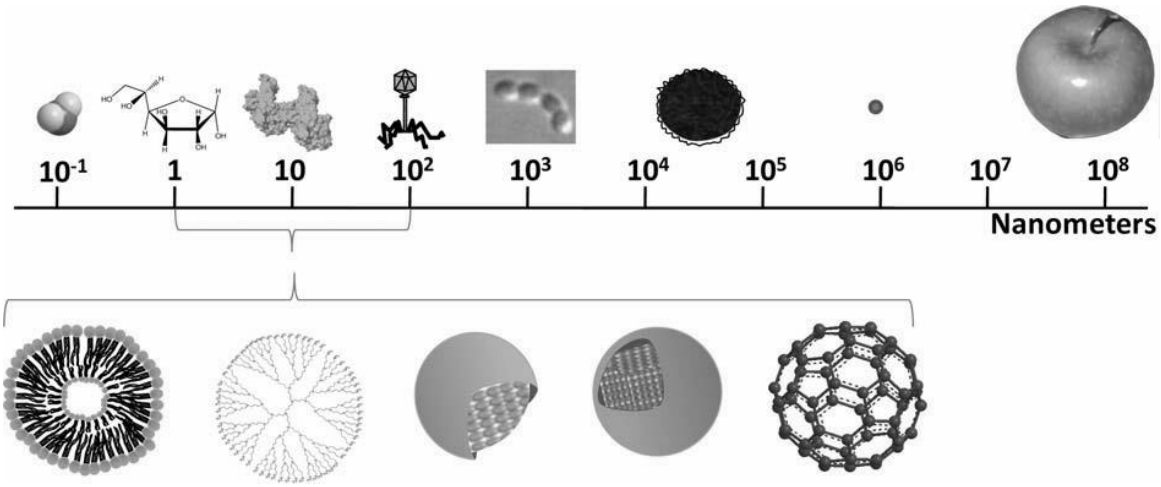

Figure 1: Logarithmical length scale showing size of nanomaterials compared to biological component and definition of 'nano' and 'micro' sizes (USEPA, 2005).

1.1.3 Definition of Nanomaterials

When two or more NPs are stick together, they are defined nanomaterial (NM). The European Commission has recently (2011) adopted a recommendation on the definition of NM. According to which 'nanomaterial' means a natural, incidental or manufactured material containing particles, in an unbound state or as an aggregate or as an agglomerate and where, for 50 % or more of the particles in the number size distribution, one or more external dimensions is in the size range 1-100 nm. In specific cases and where warranted by concerns for the environment, health, safety or competitiveness the number size distribution threshold of 50 % may be replaced by a threshold between 1 and 50 % (Savolainen et al., 2013). NPs in the dry state can be in two forms: agglomerated (held by weaker van der Waals forces) and aggregated (hard bonds between primary particles due to sintering) (Figure 2) (Jiang et al., 2009).

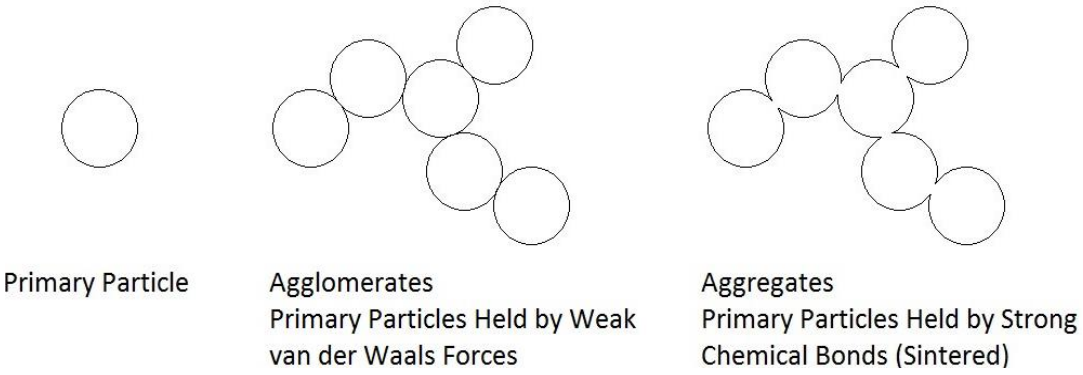

Figure 2: Various states and configurations of particles in dry state.

1.2 Nanoparticles Characteristics

The small scale of the nanoparticles gives to them their prominent physical characteristic; the increase in their surface-to-volume ratio with the decrease in size (Maskos and Stauber, 2011) (Figure 3).

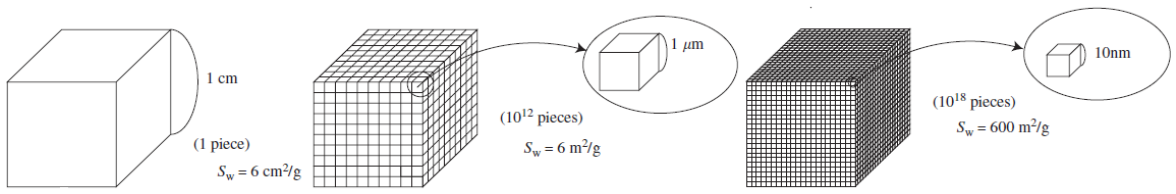

Figure 3: Change of the surface area by miniaturization of a solid cube assuming the solid density of 1 g/cm^3 (Yokoyama et al., 2012).

This feature gives to the NPs and their corresponding NMs characteristics such as physical, chemical, electronic, electrical, mechanical, magnetic, thermal, dielectric, optical and biological properties opposed to bulk materials (Schmid, 1992; Daniel and Astruc, 2004).

1.2.1 Morphological Properties

The biological properties are related to the morphological ones, the NPs result to be absorbed more easily through the biological membrane. This characteristic is reflected on the Enhanced Permeation and Retention (EPR) effect, which is the property of the NPs to accumulate in tumoral tissues much more than they do in normal tissues because the affected cells have enlarged cell gap of this part.

Other NPs properties related to their morphological characteristic, in particular with their large specific surface area, are the increase of their reactivity, solubility and sintering performances related with the mass, heat transfer between the particles and their surroundings from the morphological viewpoint apart from the control of the surface and inner structures of the nanoparticles. Furthermore, the crystal structure of the particles may change with the particle size in the nanosized range in some cases.

1.2.2 Thermal Properties

Another intrinsic characteristic of the elements, which changes at the nano size level, is the melting point. This is due as the atoms and molecules that are located at the particle surface become influential in the nanometer order. The melting point of the material decreases from that of the bulk material because atoms tend to be able to move easier at the lower temperature.

1.2.3 Electromagnetic Properties

The NPs differ from the bulk materials also for the electromagnetic properties: the dielectric constant, defined as the capacity of an element to screen the electrostatic interaction, tends to increase considerably as the particles become smaller than about 20 nm.

Another intrinsic elemental electromagnetic property, which changes, is the Curie point, defined as the point changing from the ferroelectric material to the paraelectric phase, and which reduces drastically with the decreasing particle size below 20–30 nm.

As a result of such change in the electromagnetic properties of nanoparticles, a stable element like gold as a bulk shows unique catalytic characteristics as nanomaterials (Verma et al., 2002).

1.2.4 Optical Properties

As the size of particles becomes in the several nanometers range, they absorb the light with a specific wavelength as the plasmon absorption (Handy et al., 2008) caused by the plasma oscillation of the electrons and the transmitted light with different color depending upon the kind of metal and particle size is obtained (Pacheco-Blandino, 2012).

Thanks to this physical property, the NPs show the color phenomena with splendid tinting strength, color saturation and transparency compared with the conventional pigments for the paint in the submicron size and the tinting strength per unit volume higher than that of organic pigments. Furthermore, since the nanoparticles are smaller than the wavelength of visible light and the light scattering by the particles becomes negligible, higher transparency can be obtained with the nanoparticles than the conventional pigment.

Concerning the light emitting performance, the indirect transition type substances like silicon and germanium, which do not emit the light as bulk material, give high light emitting efficiency as the direct transition type substances as a result of quantum effect, when the particle size is reduced down to several nanometers.

1.2.5 Mechanical Properties

The hardness of the crystalline materials generally increases with the decreasing crystalline size, and the mechanical strength of the materials considerably increases by micronizing the structure of the metal and ceramic material or composing them in the nano range (Roger et al., 2005; Seames et al., 2002).

Furthermore, with the ceramic material having crystalline size less than several hundred nanometers, the unique super-plastic phenomenon is seen extended several to several thousand times from the original size at the elevated temperature over 50 % of the melting point (Linak et al., 2000), which may provide the possibility of forming and processing of ceramics like metallic materials.

1.3 NPs Tipologies

Particles in the nano-sized range have been present on earth for millions of years and they were used by mankind for thousands of years (Nowack and Bucheli, 2007) (Figure 4).

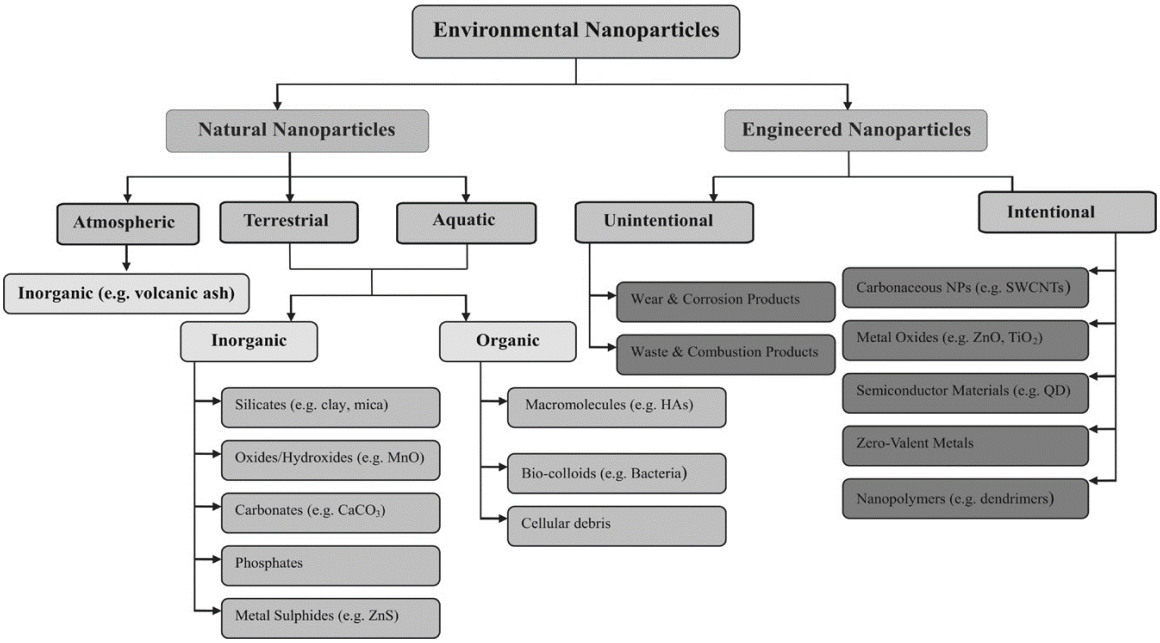

Figure 4: Categories of nanoparticles present in the environment (Bhatt and Tripathi, 2011).

1.3.1 Natural Nanoparticles

The existence of naturally occurring NPs in water, air and soil is known from the beginning of earth's history as they have been recorded from 10,000 years old glacial ice cores (Murr et al., 2004) and there is evidence of natural NP formation in sediments at the Cretaceous-Tertiary (K-T) boundary (Elsila et al., 2005).

Several mechanisms create NPs in the environment and these can be either geological or biological.

Geological mechanisms include physicochemical weathering, authigenesis/neoformation (e.g., in soils) and volcanic activity (Handy et al., 2008). These geological processes typically produce inorganic NPs.

Weathering is the result of physical (abrasion) or chemical (dissolution) decomposition of rock material, to produce a powder. Part of this powder will naturally exist as NP, either as a primary effect of the decomposition, or through further physical/chemical weathering.

Authigenesis/neoformation is the reverse of the previous process. It takes place when chemical degradation eventually results in high enough concentrations of certain dissolved species to exceed the saturation in solution of a phase, leading to its nucleation and growth. The early forming nuclei of authigenic or neoformed phases are sub-nanometric in size and may either re-dissolve, grow to form larger particles, or remain nanosized.

Volcanic eruptions, including also geysers and other geothermal/hydrothermal activities produce a variety of particle sizes, which include NPs. Meteorite impacts may also result in NPs formation (Handy et al., 2008).

Another big source of natural inorganic NPs is sea salt aerosols emitted from seas and oceans around the world. These aerosols are formed by water evaporation and when wave-produced water drops are ejected into the atmosphere. Their size ranges from 100 nm to several microns.

Nanoparticles can also form in bodies of water through precipitation, as a result of temperature changes and evaporation (Buzea et al., 2007).

Another natural NPs source is represented by biological mechanisms that typically produce organic nanomolecules, although some organisms can produce mineral granules in cells.

Many biological processes typically operate at the nanoscale and many biological entities, from proteins/peptides, DNA/RNA, ATP, to viruses are nanosized. Some of these are clearly released into the environment directly from the organism (e.g., mucoprotein exudates from algae and animals, dispersion of virus particles), and in addition may also be released during the degradation of biological matter in the environment (Handy et al., 2008).

1.3.2 Anthropic Nanoparticles

Humans have created NMs for millennia, as NPs are byproducts of simple combustion (with sizes down to several nm) and food cooking (Buzea et al., 2007). More recently, the principal sources of anthropic NPs are represented by chemical manufacturing, welding, ore refining and smelting, combustion in vehicle and airplane engines (Rogers et al., 2005), combustion of treated pulverized sewage sludge (Seames et al., 2002), and combustion of coal and fuel oil for power generation (Linak et al., 2000).

1.3.2.1 Byproduct NMs

One of the principal NMs byproduct is the soot for instance that is a product of the incomplete combustion of vegetation and coal and it has a particle size in the nanometer-micrometer range and therefore falls partially within the ‘‘nanoparticle’’ domain (Nowack and Bucheli, 2007).

Nowadays the principal source of byproduct NPs is represented by diesel and automobile exhaust; they are the primary source of atmospheric nano- and microparticles in urban areas (USEPA, 2002). Most particles from vehicle exhaust are in the size range of 20-130 nm for diesel engines and 20-60 nm for gasoline engines and are typically approximately spherical

in shape. Carbon nanotubes and fibers, already a focus of ongoing toxicological studies, were recently found to be present in engine exhaust as a byproduct of diesel combustion (Evelyn et al., 2002) and also in the environment near gas-combustion sources (Soto et al., 2005). Nanoparticles constitute 20% of the particles mass but more than 90% of the number of diesel generated particles (Kittelson, 2001).

Another chronical source of NPs is represented by indoor activities, which generate considerable amounts of particulate matter. NPs are generated through common indoor activities, such as: cooking, smoking, cleaning, and combustion (e.g. candles, fireplaces). Examples of indoor nanoparticles are: textile fibers, skin particles, spores, dust mites droppings, chemicals, smoke from candles, cooking, and cigarettes (Buzea et al., 2007).

Occupational activities, such as welding, mining, or building demolition (Buzea et al., 2007; Rosati et al., 2005) are also an important source of nanoparticle (Pacheco-Blandino et al., 2012). Particulate matter concentrations can rise to very high levels when large buildings are demolished, especially the respirable ones with diameter smaller than 10 microns and the dust cloud can travel tens of kilometers and affect the neighboring regions of the collapsed building site (Bhatt and Tripathi, 2011).

1.3.2.2 Engineered NMs

While byproducts NMs are created by human activity from millennia, the engineered nanoparticles (ENPs) have been on the market for some time and are commonly used in cosmetics, sporting goods, tires, stain-resistant clothing, sunscreens, toothpaste, food additives, etc. These NMs constitute a small minority of environmental NMs (Buzea et al., 2007).

Nowadays the ENPs can be divided into several classes, such as, carbonaceous NMs, metal oxides, semi-conductor materials, zero-valent metals and nanopolymers (Bhatt and Tripathi, 2011).

1.3.2.2.1 Carbonaceus NMs

The carbonaceous NMs include fullerene compounds, nanotubes and nanowires.

The discovery of first fullerene in 1985 marked the origin of this class. Fullerenes possess a regular truncated icosahedron, the vertices of which bear the carbon atoms (Kroto et al., 1985) (Figure 5).

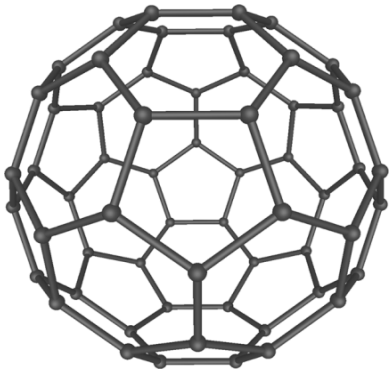

Figure 5: Fullerene (C-60).

Carbonaceus NMs are naturally non-ionogenic, but acquire charge under selective conditions. They have a negative zeta potential (Brant et al., 2005) and exhibit unique optical, mechanical, elastic and thermal properties (Kroto et al., 1985).

In 1991, the carbon nanotube (CNT) was synthesized (Klaine et al., 2008). It is a cylindrical fullerene derivative, which is formed by sheets of carbon atoms covalently bonded to form one-dimensional hollow cylindrical shape (Smart et al., 2005). There are two classes of CNTs: single-walled (SWCNTs) and multi-walled (MWCNTs) carbon nanotubes (Figure 6).

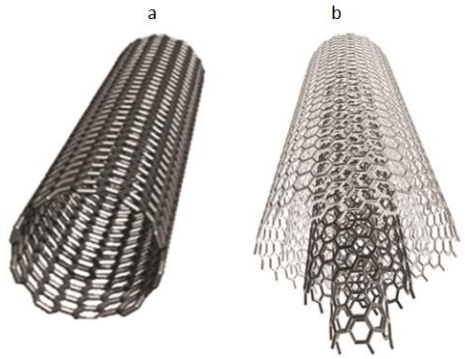

Figure 6: Schematic diagram of single-walled carbon nanotube (SWCNT) (a) and multi-walled carbon nanotube (MWCNT) (b) (Choudhary and Gupta, 2011).

SWCNTs are structurally single-layered graphene sheets rolled up in cylindrical shapes of approximately 1 nm diameter and several micrometers of length, whereas MWCNTs possess two or more concentric layers with varying length and diameters.

Carbon nanotubes possess mechanical, thermal, photochemical and electrical properties (Arepalli et al., 2001). Together with fullerenes they offer a wide application in human health area, plastics, catalysts, battery and fuel electrodes, super capacitors, water purification system, orthopedic implants, conductive coating, adhesives and composites,

sensors, and components in the electronics, aircrafts, aerospace and automotive industries (Klaine et al., 2008).

1.3.2.2.2 Metal Oxide NMs

Metal oxides belong to the second class of ENPs and they include both individual ones (such as Zinc oxide [ZnO], Titanium dioxide [TiO_2], Cerium dioxide [CeO_2], Chromium dioxide [CrO_2], Molybdenum trioxide [MoO_3], Bismuth trioxide [Bi_2O_3]) and binary oxides (such as, Lithium Cobalt dioxide [$LiCoO_2$], Indium Tin oxide [$In_xSn_yO_z$]). Metal oxides have specific catalytic, optical and physical properties.

The ZnO NP has emerged as one of the most promising oxide materials because of its numerous industrial applications in the fields of medicine, pigments, catalysts, ceramics, and rubber additives (Wang et al., 2010; Kumar and Khare, 2008). ZnO nanostructures have also potential applications in solar cells, electrodes, sensors, transparent UV protection films, UV light emission, surface acoustic waves, and magneto-optical devices (Wang et al., 2010; Kumar and Khare, 2008; Kumar et al., 2009; Zhuge et al., 2010). These wide range of applications are due to their electrical, optical, and magnetic properties (Al-Salman and Abdullah, 2013).

The TiO_2 NPs have been applied in photocatalytic water splitting (Fujishima and Honda, 1972; Ni et al., 2011), purification of pollutants (Hashimoto et al., 2005; Wold, 1993; Pozzo et al., 1997; Carp et al., 2004; Fujishima et al., 2008), photocatalytic self-cleaning, photocatalytic antibacterial (Hashimoto et al., 2005; Fujishima et al., 2008; Blake et al., 1999; Fujishima et al., 2000), photo-induced super hydrophilicity material (Hashimoto et al., 2005; Carp et al., 2004; Fujishima et al., 2000). The TiO_2 NPs is used also in photovoltaics (Carp et al., 2004; Grätzel, 1999; Grätzel, 2001; Grätzel, 2005) and photosynthesis applications (Carp et al., 2004).

The TiO_2 NPs have been used in a lot of applications because provide increased surface area at which photo-induced reactions may occur, enhancing light absorption rate, increasing surface photoinduced carrier density, enhancing photo-reduction rate, and resulting in higher surface photoactivity. At the same time, the high surface-volume ratio of the NPs enhances the surface absorption of OH^- and H_2O, increasing the photocatalytic reaction rate (Lan et al., 2013).

The CeO_2 has long been employed as a bound catalyst in catalytic converters for diesel engines and it is now finding application as a NP additive to diesel fuels. Its usage as a fuel additive has been associated with reduced fuel consumption and reduced emissions of combustion derived NPs and unburned hydrocarbons (O'Brien and Cummins, 2011). CeO_2

NPs has recently gained also a wide range of applications that includes coatings, electronics, biomedical and energy (Cassee et al., 2011). In particular, like glass polishing material (Bekyarova et al., 1998) in the abrasive process of the Chemo-Mechanical Polishing (CMP) (Jiang et al., 1998). As a coating for corrosion protection for metals and alloys (Hamdy, 2006; Zhong et al., 2008), UV-blockers and filters (Tsunekawa et al., 2000; Morimoto et al., 1999; Tsunekawa et al., 2000a Yamashita et al., 2002) high temperature oxidation resistant coating (Patil et al., 2002), sunscreens (Masut et al., 2000).

As an additive to glass to protect light-sensitive material (Lin et al., 1994) or in ceramics (Bhaduri et al., 1988; Messing et al., 1993), as an oxidation catalyst (Yakimova et al., 2009) or selective hydrogenation catalysis of unsaturated compounds (Fierro et al., 1987; Sim et al., 1991).

In the energy industry like: an oxygen ion conductor in solid oxide full cells (Yahiro et al., 1988), electrolyzers (Marina and Pederson, 2008; Inaba and Tagawa, 1996), oxygen pumps, amperometric monitors (Hirano et al., 1996), solar cells (Corma et al., 2004), photocatalytic oxidation of water for the generation of hydrogen gas (Bamwenda and Arakawa, 2000; Chung and Park, 1996) and like an anode material for lithium ion battery system (Zhou et al., 2007a).

The CeO_2 NPs can be used in biomedical field like protection of primary cells from the detrimental effects of radiation therapy (Tarnuzzer et al., 2005), neuroprotection to spinal cord neurons, prevention of retinal degeneration induced by intercellular peroxide (Das et al., 2007), potent antioxidant in cell culture model (Patil et al., 2007) thanks to free-radical scavenger (Babu et al., 2007).

The CeO_2 NPs can be used like slurry in semiconductor fabrication (Jiang et al., 1998), like buffer layers with silicon wafer (Tashiro et al., 2002) or gates for metal-oxide semiconductor device (Galata et al., 2007).

Other utilizations of CeO_2 NPs are: high temperature oxidation safe guards (Zhou et al., 2007), and gas sensor (Stefanik and Tuller, 2001), low-temperature water gas shift catalyst (Hilaire et al., 2001), removal organics from wastewater (Matatov-Meytal and Sheintuch, 1998), photodegradation of toluene in the gas phase (Hernández-Alonso et al., 2004), photocatalytic behavior under sunlight irradiation to degrade dyes (Zhai et al., 2007; Borker and Salker, 2007).

The CeO_2 NPs have been used in these wide range of applications because it shows absorption properties in the UV, low photocatalytic, antioxidants properties (Truffault et al., 2013), high thermal stability (Trovarelli et al., 1999), facile electrical conductivity and

diffusivity (Zhou et al., 2007b), high hardness, specific chemical reactivity (Chen and Chang, 2005), ability to store and transport oxygen as large oxygen storage capacity (Shahin et al., 2005) and high refractive index (Goharshadi et al., 2011).

The last two metal oxide NPs represent the most produced ones (Table 1).

Table 1: Safety of Manufactured Nanomaterials: About, UOECD Environment Directorate, OECD.org, 18 July 2007. Small Sizes that Matter: Opportunities and Risks of Nanotechnologies, Joint report of the Allianz Center for Technology and the OECD International Futures Programme, ed. Dr. Christoph Lauterwasser, OECD.org 18 July 2007 (modified from Brar et al., 2010).

Source	Type of nanoparticle	Quantity tons	Application
Metals and alkaline earth metals	Ag/Fe/Pt groups metals	High	Antimicrobials, paints, coatings, medical use, food packaging/Water treatment/Catalysts
	Sn/Cu	Unknown	Paints/microelectronics
	Al	High	Metallic coating/plating
	Zr	High	
	Se/Ca/Mg	Low	Nutraceuticals, health supplements
Metal oxides	$TiO_2/CeO_2/SiO_2$	High	Cosmetics, paints, coatings/Fuel catalyst/Paints, coatings
	ZnO/Al_2O_3	Low	Cosmetics, paints, coatings/Usually substrate bound, paintings
Carbon materials	Carbon black	High	Substrate bound, but released with tyre wear
	Carbon nanotubes/Fullerenes (C60-C80)	Medium–High	Used in a variety of composite materials/Medical and cosmetics use
Miscellaneous	Nanoclay/Ceramic	High	Plastic packaging Nanoclay High Plastic packaging/Coatings
	Quantum dots/Organic nanoparticles	Low	Different compositions/Vitamins, medicines, carriers for medicines and cosmetics, food

1.3.2.2.3 Semi-conductor Materials

The third class of ENPs constitutes nanometer sized semi-conductor nanocrystals, known as quantum dots (QDs) with their size ranges between 2 and 10 nm (Schmid, 2004).

Quantum dots refer to the quantum confinement of electrons and whole carriers at dimensions smaller than the Bohr radius. They possess a reactive core consisting of metal, like iron (Fe) or semi-conductor from groups II and IV, like Cadmium selenide (CdSe) and Zinc selenide (ZnSe), or III and V, like Indium phosphide (InP). The core is protect by a shell, made up of a Silica or ZnS monolayer that protects the core from oxidation and enhances the photoluminescence yield (Klaine et al., 2008) (Figure 7).

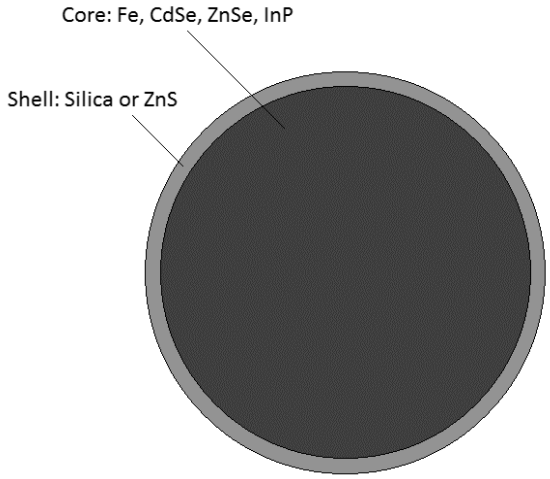

Figure 7: Quantum dots.

Although to QDs have been largely used in medical applications such as medical imaging and targeted therapeutics, they are now being extended to include solar cells and photovoltaics, security inks, photonics and telecommunications (Alivisatos et al., 2005).

Quantum dots possess unique optical, in particular high luminescence and stability against photobleaching, electrical (Logothetidis, 2006; Hoshino et al., 2004), magnetic and catalytic properties (Murray et al., 2001).

1.3.2.2.4 Zero-valent Metals

The fourth class of ENPs includes zero-valent metals that are usually prepared by reduction of metal salts to the zero valency state (Bhatt and Tripathi, 2011).

Zero-valent metals, have found usage in nitrate removal from water, soil and sediments and also for detoxification of organochlorine pesticides and polychlorinated biphenyls (Zhang, 2003), textile products, baby-products, vacuum cleaners, washing machines, toothpastes, as vector in tumor therapy, in electronics and catalyst (Klaine et al., 2008).

Zero-valent metal nanoparticles exhibit an important phenomenon called as Surface Plasmon Resonance (SPR), which is caused the interaction of incident light and free electrons in the materials (Noguez, 2007) and this imparts to metal ENPs unique optical properties (Bhatt and Tripathi, 2011). These particles are also characterized by high surface area to volume ratio, high level of stepped surface and high surface energy (Zhang et al., 1998).

1.3.2.2.5 Nanopolymers

The fifth class of ENPs is represented by dendrimers. Dendrimers are globular, nano-sized (1–100 nm) macromolecules with a particular architecture constituted of three distinct domains. (i) a core at the center of dendrimer consisting of an atom or a molecule having at least two identical chemical functions; (ii) several branches, emanating from the core, constituted of repeat units having at least one branch junction, whose repetition is organized in a geometrical progression that results in a series of radially concentric layers called "generations"; and (iii) many terminal functional groups, generally located at the surface of dendritic architecture. These surface groups are vital in determining the properties of dendritic macromolecules (Kesharwani et al., 2014) (Figure 8).

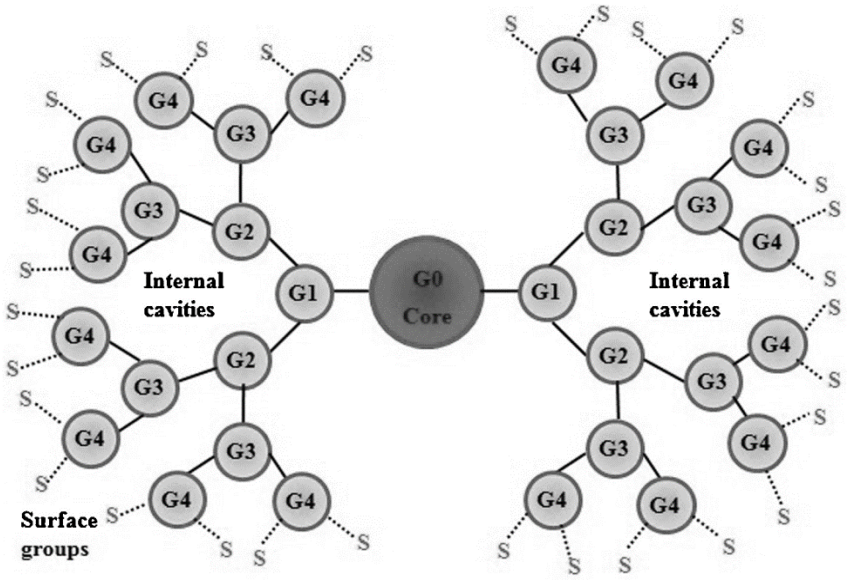

Figure 8: Schematic representation of general structure of dendrimer (Kesharwani et al., 2014).

Dendrimers are three-dimensional (3D), hyperbranched, nanoscale polymeric architectures (Hasanzadeh et al., 2014). Since they assume highly asymmetric shapes and with increase in branching they adopt a globular structure (Watkins et al., 1997).

Dendrimers can be used for many applications in different fields ranging from biology, material sciences, and surface modification to enantioselective catalysis. These include

macrocapsules, nanolatex, colored glasses, chemical sensors, modified electrodes, DNA transfecting agents, therapeutic agents for prion diseases, hydrogels, drug delivery, and DNA chips (Klaine et al., 2008).

The principal characteristic of dendrimers is their monodispersity hence the capacity to construct them with a well-defined molecular structure unlike linear polymers. Monodispersity offers researchers the possibility to work with a tool useful for well-defined and reproducible scalable size (Kesharwani et al., 2014).

Dendrimers have also improved physical, chemical, and biological properties compared to traditional polymers (Logothetidis, 2006), like high surface functionality, hydrophilicity and high mechanical and chemical stability (Hasanzadeh et al., 2014) and some unique properties related to their globular shape and the presence of internal cavities offering the possibility as medical nanovehicles (Logothetidis, 2006).

1.4 NPs Production

In general, there are two ways for the production of NPs: top-down or bottom-up methodology.

– Top-down approaches are defined as those by which NPs or well-organised assemblies are directly generated from bulk materials via the generation of isolated atoms by using various distribution techniques.

– Bottom-up strategies involve molecular components as starting materials linked with chemical reactions, nucleation and growth process to promote the formation of more complex clusters.

The majority of the top-down strategies involve physical methods while the bottom-up involve chemical and organic methods (Ju-Nam and Lead, 2008) (Figure 9).

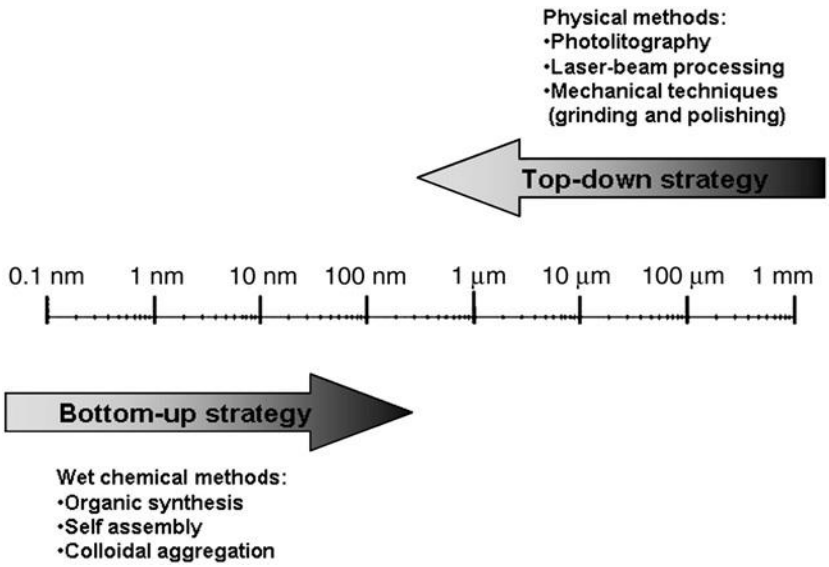

Figure 9: Top-down and bottom-up strategies (Ju-Nam and Lead, 2008).

1.4.1 Physical Methods

In the physical methods, which do not change the initial chemical composition, the bulk materials are transformed into the nano scale via their interaction with photons, heat or ions or even by mechanical milling (Wendera et al., 2013). In the case of photons, it is possible to highlight the laser-based techniques, such as laser ablation, Pulsed Laser Deposition (PLD) and laser-induced particle fragmentation (Gelesky et al., 2005). Laser ablation (Mafuné et al., 2001) enables to obtain colloidal NPs solutions in a variety of solvents. Nanoparticles are formed during the condensation of a plasma plume produced by the laser ablation of a bulk metal plate dipped in a liquid solution. This technique is considered as a 'green technique' alternative to the chemical reduction method for obtaining noble metal nanoparticles (MNPs). However, the main drawback of this methodology is the high energy required per unit of MNPs produced and the little control over the growth rate of the MNPs (Nath and Banerjee, 2013).

When matter is transformed by heat, the bulk material is evaporated and recrystallized on the nano scale (Dai et al., 2003). On the other hand, as it is implicit in its name, mechanical milling is based on milling the bulk particulate starting material until it is finely divided into nanometric particles. The transformation of matter via interaction with ions is based on the moment transfer between ions that collide on the surface of bulk materials, pulling out atoms or small clusters of the target material that are then directed to a substrate, where they begin to nucleate and grow (Wendera et al., 2013). These techniques allow a

preparation of highly ordered NPs with a narrow shape and size distribution on substrates (Aeschlimann et al., 2009; Lamprecht et al., 1999; Berndt et al., 2009).

1.4.2 Chemical Methods

In the chemical methods, which change the initial chemical composition, the molecular species are transformed into NPs. The chemical methods can be divided into two major techniques: Chemical Vapor Deposition (CVD) with liquid phase synthesis and colloidal synthesis (CS).

In the CVD process, the vaporized precursor compounds react in the gas phase, usually at high temperatures, and the nanostructures are obtained as powders or as films over substrates (Hao et al., 2005; Okumura et al., 1998; Reina et al., 2009; Sivula et al., 2009). The control of the size of the materials in the CVD process is achieved by tuning the reaction parameters, such as temperature, flow rate and relative precursor quantities (Wendera et al., 2013). An example of CVD process is the technique Inert Gas Condensation (IGC) which is the most widely used method for MNPs synthesis at laboratory-scale. In IGC, metals are evaporated in ultrahigh vacuum chamber filled with helium or argon gas at typical pressure of few hundreds Pascal. The evaporated metal atoms lose their kinetic energy by collisions with the gas, and condense into small particles. These particles then grow by Brownian coagulation and coalescence and finally form nano-crystals (Nath and Banerjee, 2013).

The CS method is based on reactions between reactants in solution (Burda et al., 2005). In this case, the size and shape of NPs are controlled via reaction conditions and stabilizing agents (Wendera et al., 2013). The crystallographic control over the nucleation and growth of noble MNPs has most widely been achieved using colloidal methods (Tao et al., 2008; Turkevich et al., 1951; Frens, 1972; Brust and Kiely, 2002). In general, MNPs are synthesized by reducing metal salt with chemical reducing agents like borohydride, hydrazine, citrate, etc., followed by surface modification with suitable capping ligands to prevent aggregation and to confer additional surface properties. Occasional use of organic solvents in this synthetic process often raises environmental questions. At the same time, these approaches produce multi-shaped NPs that require purification by differential centrifugation and consequently have low yield. Thus, the development of reliable experimental protocols for the synthesis of NMs over arrange of chemical compositions, sizes, and high monodispersity is one of the challenging issues in current nanotechnology. In this context, current efforts are focused on the development of green and biosynthetic

technologies for production of nanocrystals with desired size and shape (Nath and Banerjee, 2013). These techniques yield a mass production of small NPs (Ju-Nam and Lead, 2008). Both chemical and physical methods have their advantages and can be complementary but each methodology has got some disadvantages (Wendera et al., 2013). The NPs ensembles obtained with the chemical techniques have a broad size and shape distribution (Ouacha et al., 2005; Hubenthal, 2009; Stietz, 2001; Binns, 2001) and harmful byproducts are released. On the other hand, the NPs ensembles with the physical techniques are extremely time-consuming and expensive (Wendera et al., 2013). For these reasons there is a significant interest in the development of environmentally friendly and sustainable methods (Narayanan and Sakthivel, 2011).

1.4.3 Green Chemistry

Recently, biosynthesis of NPs, especially MNPs, with the aid of novel, non-toxic, eco-friendly, and convenient biological materials namely bacteria (Shivaji et al., 2011), yeast (Questera et al., 2013), fungi (Rajakumar et al., 2012), biomolecules (Venkatpurwar et al., 2011), and plant extracts (Kaviya et al., 2011) are under much investigation (Mortiz and Geszke-Mortiz, 2013).

1.4.3.1 Bacteria

Bacteria are the most abundant microorganisms on Earth; they are prokaryotic cells greatly diversified in size, shape, and means of gaining energy and live in all kinds of habitats, including extreme environments that exhibit, for example, extremely high or low temperatures, acidity, alkalinity, and salt or sulfur concentrations. The organisms that inhabit these extreme habitats, referred to as extremophiles, are so well adapted that they readily grow and multiply.

Some species of bacteria have developed the ability to resort to specific defense mechanisms to quell stresses like toxicity of foreign metal ions or metals; even at high metal ion concentrations some of these organisms can survive and grow. (Questera et al., 2013). For this characteristic and their relative ease of manipulation the bacteria have been most extensively researched for synthesis of metallic NPs (Thakkar et al., 2010).

Studies have shown some bacteria are able to reduce metal ions and deposit them as NPs inside the cell, others can synthesize them both intra- and extracellularly.

The extracellular synthesis of metal NPs, in particular silver, by reduction of silver ions to nanometer range involves NADH- dependent reductase enzyme. The reductase enzyme

gets its electrons from NADH, which is then oxidized to NAD^+. The enzyme too gets oxidized at the same time by the reduction of silver ions to nanosilver.

The intracellular method involves a special ion transportation in the microbial cell. The cell wall of the micro-organisms plays an important role. The mechanism involves electrostatic interaction of the positive charge of the metal ions with negative charge of the cell wall. The enzymes which are present within the cell wall reduce the ions to nanoparticles and these nanoparticles get diffused off through the cell wall (Hulkoti and Taranath, 2014).

Independently of the bacterial species used as a reducing agent, the majority of the resulting synthesized NPs present polydispersity. Nevertheless, some studies report promising results with narrower particle size ranges. Attempting to optimize or control size and shape of synthesized NPs, studies have reported incubation assays using different ambient conditions varying temperature and pH, changing incubation time, and/or metal precursor concentration (Questera et al., 2013).

1.4.3.2 Yeast

All yeast genera can accumulate different heavy metals. They have the ability to accumulate significant amounts of highly toxic metals. Enzymatic oxidation or reduction, absorption at the cell wall and in some cases consequent chelating with extracellular peptides or polysaccharides, controlled cell membrane transport of heavy metals towards or their active efflux from the cell are the different mechanisms developed by these species overcoming the toxic effects of heavy metals (Breierová et al., 2002).

Detoxification mechanisms in yeast cells is brought about by glutathione (GSH) and two groups of metal-binding ligands-metallothioneins and phytochelatins (PC).

The yeasts can also synthetize MNPs at the extracellular level with the involvement of carboxyl, hydroxyl, and amide groups on the cell surfaces (Questera et al., 2013).

In most of the yeast species studied, these molecules determine the mechanism for the formation of nanoparticles and stabilize the complexes. Yeasts are mainly known for their ability to synthesize semiconductor nanoparticles, particularly cadmium sulfide (CdS). Recent studies have shown the ability of yeasts to form other nanoparticle as well (Hulkoti and Taranath, 2014).

The advantages of using yeast is that the obtained NPs are dense aggregate of nearly monodisperse, spherical, homogenous particles (Questera et al., 2013). Moreover the peptides produced by yeasts form a coating which avoids the particles to clump together and also do not cause Ostwald ripening, resulting in a higher stability than the chemically

synthesized nanoparticles. Finally the presence of peptide-coating provides the nanoparticles with a hydrophilic surface without additional preparation steps.

The problem of NPs production with yeasts is due to the stringent control of intracellular metal ions required by them to avoid negative or lethal effects (Hulkoti and Taranath, 2014).

1.4.3.3 Fungi

Fungi as well as eukaryotic organisms that live in a wide variety of natural habitats (Questera et al., 2013).

Thanks to their tolerance and metal bioaccumulation ability, fungi are taking the center stage of studies on biological generation of MNPs (Sastry et al., 2003) and semiconductor NPs (Hulkoti and Taranath, 2014).

Fungi like bacteria and yeasts can synthesize metal NPs both extracellularly and intracellularly.

A lot of cases were reported in which different genera of fungi can synthesize semiconductor NPs extracellularly by the release of reductase enzymes into the solution (Hulkoti and Taranath, 2014) or metal NPs by using both NADH-dependent reductases and a shuttle quinone extracellular process (Questera et al., 2013). Moreover fungi are able to exudate a wide range of proteins, polysaccharides and organic acids which have the ability to differentiate the different crystal shapes and were also able to direct their growth into spherical crystals and the coating of proteins moiety brought about a stabilization of the NPs (Hulkoti and Taranath, 2014).

The fungi can also synthesize metal NPs intracellularly, the process start with the electrostatic interaction between the metal ions and the positively charged groups such as lysine residues in enzymes (Mukherjee et al., 2001) or negatively charged carboxylate groups mediated by enzymes present in the cell wall of the mycelia. After the metal ion is bioreducted to produce metal NPs followed by stabilization and/or encapsulation of the same by a suitable capping agent (Thakkar et al., 2010).

The bioreduction is made by the enzymes present in the cell wall which reduce the metal ions and resulting in the formation of metal nuclei, that grows by further reduction of metal ions and accumulation on these nuclei.

Then after the incapsulation process, the metal nuclei diffuse through the cell wall (Nath and Banerjee, 2013; Hulkoti and Taranath, 2014).

A distinct advantage of using fungi in nanoparticle synthesis is the ease in their scale-up. Further advantages of using a fungal-mediated green approach for synthesis of metal NPs

include economic viability and easiness in handling biomass (Kaushik et al., 2010). In addition, using fungi it is possible to obtain monodisperse NPs with well-defined dimensions.

Compared to bacteria, fungi could be used as a source for the production of large amount of NPs. This is due to the fact that fungi secrete more amounts of proteins which directly translate to higher productivity of NPs formation (Mohanpuria et al., 2008).

A significant drawback of using these bio-entities in nanoparticles synthesis is that the genetic manipulation of eukaryotic organisms as a means of overexpressing specific enzymes is relatively much more difficult than that in prokaryotes.

Another disadvantage is that the majority of the filamentous fungi (eg, Aspergillus fumigatus) that have reportedly been used for the purpose of extracellular biomass free synthesis of metal NPs are pathogenic to plants and/or humans. This makes handling and disposal of the biomass a major inconvenience toward commercialization of the process (Kaushik et al., 2010).

Microorganisms can be utilized to produce NPs but the rate of synthesis is slow and only limited number of sizes and shapes are amenable (Kharissova et al., 2013).

1.4.3.4 Plants

Among the organisms mentioned above, plant based materials seem to be the best candidates, mostly because they are suitable for large-scale 'biosynthesis' of NPs (Iravani, 2011) and in contrast with microbial cultures and downstream processing plants do not need expensive methodologies for maintaining their productivity (Narayanan and Sakthivel, 2011). Finally, comparing to fungi and bacteria they do not require a long incubation time for the reduction of metal ions. Therefore, compared to bacteria and fungi, plants are better candidates for the synthesis of NPs (Nath and Banerjee, 2013). The production of NPs with plants can be done with two different approaches. The first approach uses the whole plant and the second uses the plant extracts.

1.4.3.4.1 In-planta

The idea to utilize plant on purpose to NPs production became from the knowledge of plant scientist who have known for a long time that certain metals are essential for normal biological function. More recently it has been determined that some plants are able to hyperaccumulate metals, up to concentrations several hundreds of times more of those found in non hyperaccumulating plants (Brooks et al., 1998; McGrath and Zhao, 2003). It is thought that this provides a measure of protection for the plant from insects and others herbivores. This observation is the basis for the technology known as phytoextraction, i.e.

the process of using plants to beneficially absorb mineral species from groundwater, soil and sediments. There are four broad applications of phytoextraction: (i) phytomining, where valuable naturally occurring elements are harvested (Brooks et al., 1998; Anderson et al., 1999), (ii) phytoremediation, where non-naturally occurring contaminants are stabilized or recovered for secure disposal or reuse (McGrath and Zhao, 2003; Salt et al., 1998), (iii) functional foods, where essential minerals are added to a crop whilst it is growing (Guerinot and Salt, 2001), and (iv) phytosynthesis, where plants are used as biological factories for synthesis of MNPs (Gardea-Torresdey et al., 2002; Gardea-Torresdey et al., 2003). The capacity of plants to uptake even very low levels of metals ions from large volume of soil and bioconcentrate them into their biomass and accumulate in tissues (Narayanan and Sakthivel, 2011) have attracted the curiosity of scientists. Recent experiments have demonstrated that in some cases live plants show the ability to absorb metals from the outside and accumulate them in their tissues in the form of nanostructures (Gardea-Torresdey et al., 2002; Gardea-Torresdey et al., 2003; Armendariz et al., 2004; Harris and Bali, 2008). The reduction process was presumed to be mediated by the presence of secondary metabolites present in the cells (Narayanan and Sakthivel, 2011).

1.4.3.4.2 Ex-planta

The plant extract is the most commonly used agent to produce MNPs (Questera et al., 2013) because it is readily scalable and may be less expensive (Iravani, 2011) compared with the utilization of whole plants (Armendariz et al., 2004; Beattiew and Haverkamp, 2011; Kumar and Yadav, 2009; Marshall et al., 2007). Plant extracts may act both as reducing and stabilizing agents in the synthesis of NPs. The source of the plant extract is known to influence the characteristics of the NPs (Kumar and Yadav, 2009). This is because different extracts contain different concentrations and combinations of organic reducing agents (Mukunthan and Balaji, 2012). Typically, a plant extract-mediated bioreduction involves mixing the aqueous extract with an aqueous solution of the relevant metal salt. The reaction occurs at room temperature and is generally complete within a few minutes. Regarding the number of different chemicals involved, the bioreduction process is relatively complex (Mittal et al., 2013).

The plant initially tested and most widely used is alfalfa (*Medicago sativa*). By using alfalfa extract, distinctive metallic nanostructures were synthesized under diverse environmental conditions. For instance, using the same protocol for synthesis but under varying pH, differences in NP shapes and sizes are achieved (Ascencio et al., 2003; Herrera-Becerra et

al., 2007). Besides alfalfa, a number of other plants were successfully employed for the production of metallic NPs.

Silver and gold are the two most extensively applied metals in NP production, and the use of plant extracts of discrete species resulted in a wide variety of shapes and sizes. The incubation of metal ions with plant extracts under changing environmental conditions or in altered ratios led to some interesting results as well. While some authors found that the size and shape of NPs are not significantly influenced by incubation time, temperature, or extract concentration (Cruz et al., 2010), others found that varying the amount of extract resulted in differences in nanoparticle size and shape (Shankar et al., 2005; Kasthuri et al., 2009). Distinctive concentrations of ionic solution led to the formation of different sized particles as well, and additionally, variation in temperature influenced the shape and size of resulting NPs (Jia et al., 2009; Song et al., 2009). Changing the pH value affects the absorption rate and results as well in varying nanoparticle size and shape (Philip, 2010). Thus, the size and shape of NPs synthesized by using plant extracts depends on several factors such as plant species, ratio of metal salt to extract in the reaction medium, pH, temperature, and/or reaction time. Moreover, plant waste material like banana (Bankar et al., 2010), *Citrus sinensis* (Kaviya et al., 2011), pomegranate (Ahmad et al., 2012), and *Annona squamosal* (Kumar et al., 2012) peel were used to prepare extracts and successfully produced MNPs (Questera et al., 2013).

Recently much work has been done with regard to plant assisted reduction of MNPs and the respective role of phytochemicals. The main responsible phytochemicals have been identified as terpenoids, flavones, ketones, aldehydes, amides and carboxylic acids. The main water soluble phytochemicals are flavones, organic acids and quinones which are responsible for immediate reduction.

The phytochemicals present in *Bryophyllum* sp. (Xerophytes), *Cyprus* sp. (Mesophytes) and *Hydrilla* sp. (Hydrophytes) were studied for their role in the synthesis of silver NPs. The Xerophytes were found to contain emodin, an anthraquinone which could undergo redial tautomerization leading to the formation of silver NPs. The Mesophytes contain three types of benzoquinones, namely, cyperoquinone, dietchequinone and remirin. It was suggested that gentle warming followed by subsequent incubation resulted in the activation of quinones leading to particle size reduction. Catechol and protocatechaldehyde were reported in the Hydrophytes studied along with other phytochemicals. It was reported that catechol under alkaline conditions gets transformed into protocatechaldehyde and finally

into protocatecheuic acid. Both these processes liberated hydrogen and it was suggested that it played a role in the synthesis of the NPs (Jha et al., 2009).

1.5 Nanotoxicology

Nanotechnology is one of the fastest growing and most promising technologies in our society (Simon et al., 2011). Possible fields for the use of ENM include advanced materials, display technologies, electronics, nutrition, cosmetics, medical drug designing, and numerous other applications.

On the other hand, this exciting technological progress may also be associated with risks (Piccinno et al., 2012).

ENM may undergo a wide range of weathering or "aging" processes that will alter their surface chemistry and, therefore, transport and potential exposure routes. These transformations occur through processes such as redox reactions, interactions with organic macromolecules such as Natural Organic Matter (NOM) or cellular material, dissolution, or adsorption of known pollutants (e.g., As, Hg, Polychlorinated Biphenyls (PCBs), Polycyclic Aromatic Hydrocarbons (PAHs)). In air, manufactured and incidental NPs might be expected to condense low volatility compounds (organics and sulfate) (Robinson et al., 2007).

Photocatalytic NPs (e.g., TiO_2) might in turn photooxidize the condensed material. Interactions between NPs and organic macromolecules (Saleh et al., 2005; Hardman, 2006) such as NOM, proteins, surfactants, and polyelectrolytes modify aggregation and deposition kinetics and therefore transport and potential exposure routes.

Environmental and physiological conditions also modify reactivity of NMs as evidenced by changes in the toxicity of manufactured, natural, and incidental NPs (Maynard and Kuemple. 2005; Oberdörster et al., 2005), the generation of Reactive Oxygen Species (ROS) (Wiesner et al., 2009; Lee et al., 2007), and reduced redox activity (Phenrat et al., 2008; Phenrat et al., 2009). Additionally, other chemical species that interact NMs with may themselves be altered in the process. For example, NPs may alter the conformation of proteins (Chen and Mikecz, 2005; Linse S at al., 2007) interfering with cell signaling and possibly gene transcription. Likewise as NPs may impact organisms, organisms may impact NPs. The accessibility of adsorbed or chemically bound macromolecules that stabilize NPs against aggregation may also prevent biological attack and increase NPs persistence. Alternatively, bacteria may enhance the solubility of iron oxide NPs (Ha et al., 2006) or

enhance the bioavailability of adsorbed heavy metals such as mercury (Hg) (Jew et al., 2006). Photolysis, oxidation, and subsequent dissolution (in the case of inorganic NPs) can release toxic metals into the environment, alter NP morphology and other properties (Derfus et al., 2004; Jin et al., 2001; Zhang et al., 2007), and ultimately provide removal mechanisms for NPs in the environment.

Predicting the ecosystem impacts of NMs requires significant empirical progress in understanding (i) abiotic interactions between NMs and natural substrates and solutions, (ii) interactions between NMs and an ecosystem's primary uptake compartments (plants, fungi, and bacteria) and the longevity and reversibility of ecological sources and sinks and (iii) the resulting consequences of NMs exposure for productivity, organic matter decomposition, and trophic transfer. NMs may also have indirectly detrimental effects on ecosystems through their interactions with existing environmental contaminants (Wiesner et al., 2009). In particular the uptake, translocation and toxicity of NPs to humans, animals and, in a few cases, to plants have been studied in diverse experimental setups. The accumulation, persistence and impact of NPs on plant metabolism and development depend on the size, concentration and chemistry of NPs, as well as the chemical milieu of the subcellular sites to which the NPs are deposited. NPs can be toxic to plant tissues, owing to chemical or physical effects. Thus, NPs act as catalysts and interactors or, upon dissolution, as soluble metal ions. Physical toxicity is linked to association with cell structures or mechanical clogging.

NPs interact with biological systems by five main modes: (i) chemical effects as metal ions in solution upon dissolution; (ii) mechanical effects owing to hard spheres and defined interfaces; (iii) catalytic effects on surfaces; (iv) surface effects owing to binding of proteins to the surface, either by non-covalent or covalent mechanisms or oxidative effects; and (v) changes in the chemical environment (pH) (Dietz and Herth, 2011).

1.5.1 Chemical Effects

Toxic metals interference with cellular processes often causes redox imbalances and oxidative stress in metal-exposed plants. Some metals, such as Cu and Fe, transfer electrons to O_2 as acceptors to form O_2- or to H_2O_2 to form the extremely reactive ·OH radical. These Reactive Oxygen Species (ROS) may lead to unspecific oxidation of proteins and membrane lipids or may cause DNA injury (Schnützendübel and Polle, 2002; Sharma and Dietz, 2008). These reactions enhance oxidative stress in the affected cells (Dietz and Herth, 2011).

1.5.2 Mechanical Effects

Mechanical effects depend on particle size and not on particle chemistry. They include the filling of pores, which are then unavailable for other transport processes. An example is the inhibition of water transport in the presence of high NP concentrations in the soil. The reduced water availability caused by external nanoparticles appeared to involve a rapid physical inhibition of apoplastic flow through nanosized root cell wall pores and consequently inhibited leaf growth and transpiration (Asli and Neumann, 2009).

1.5.3 Catalytic Effects

Many metals, including Ag, Pt, Pd, Au, Fe and Co, catalyze chemical reactions, such as reduction–oxidation reactions (Dietz and Herth, 2011). Metal ions at cell-compatible low concentrations are usually bound to constitutive or inducible chelators, including phytochelatins, organic acids, metallothionein and ferritin (Hall, 2002) or they are compartmentalized by transport processes (Hall and Williams, 2003). The toxicity symptoms seen in the presence of excessive amounts of heavy metals may be due to a range of interactions at the cellular/molecular level. Toxicity may be result from the binding of metal to sulphydryl groups in proteins, leading to an inhibition of activity or disruption of structure, or from the displacing of an essential element resulting in deficiency effects (van Assche and Clijster, 1990).

1.5.4 Surface Effects

Particles with an oxidic surface often form a layer of ·OH groups at the surface, which are negatively charged and thereby attract positively charged side groups of proteins (Larsen et al., 2005). Once the proteins are bound to the particles, they are either no longer available for their function or function with lower efficiency. A more extreme effect occurs if side groups of proteins bind covalently to the particles, such as cysteines to Au surfaces, because this type of binding is permanent.

Most published studies on NP toxicity in plants have addressed easily scored parameters, such as germination rate and growth-related features with positive, negative or no effects (Ma et al., 2010).

1.6 Plants and Nanoparticles Relashionship

Plants have evolved in the presence of natural nanomaterials (NMs). However, the probability of plant exposure to NMs has increased to a greater extent with the ongoing

increasing production and use of engineered nanomaterials (ENMs) in a variety of instruments and goods (Pan and Xing, 2010), via the addition of biosolids to agricultural fields (Suppan, 2013; Tourinho et al., 2012; Hong J et al., 2013; Colman et al., 2013) or through the application of nanoenabled agricultural (Suppan et al., 2013: Gogos et al., 2012; Mura et al., 2013) and soil remediation (Pan and Xing, 2010; Liu and Lal, 2012) technologies for crop production is not far from reality. This practice repeated overtime could result in soil accumulation of ENMs, which opens an important route of ENMs entry into the food chain (Gardea-Torresdey et al., 2014). ENMs can also reach the plants through, accidental release, contaminated soil/sediments, or atmospheric fallouts. Little is known about the impact of ENMs on food crops, and their possible effects in the food chain are unknown (Darlington et al., 2009; Pidgeon et al., 2009).

The NMs go thorugh a wide range of biotransformation in soil and plant tissues and the knowledge of this aspect is critical to understanding the physiological, biochemical, molecular and genetic modifications in the exposed plants (Dimpka et al., 2012). The biotransformation potential of ENMs in crops varies greatly, dependent on both nanoparticle type and plant species, as well as potentially other unknown factors. However, it is clear that accumulation and translocation within crop species occurs and therefore may represent an important route for transfer of ENMs into the food chain, presenting an unknown exposure and risk to humans and other species. The accumulation of component metals (e.g., Ti uptake from *n*TiO_2 treatment) in plant edible tissues or in seeds for the next generation is an important aspect of nanomaterial fate and effects assessment and may have implications for human health and agricultural productivity (Gardea-Torresdey et al., 2014).

This brought anoter concern about the potential trophic transfer of ENMs within terrestrial food webs which is probably the most poorly understood phenomena when assessing ENM fate, disposition and effects. Several studies have demonstrated potential trophic transfer of ENMs among microscopic organisms or invertebrates in aquatic systems (Ferry et al., 2009; Zhu et al., 2010; Holbrook et al., 2008; Werlin et al., 2011;. Kulacki et al., 2012).

Recently some work have started to investigate the terrestrial trophic transfer and biomagnification of ENMs. The results certainly demonstrate the potential and perhaps probable trophic transfer and accumulation/biomagnification of ENMs in terrestrial systems and raise the likelihood of human exposure through dietary uptake as an issue in need of rapid and intense investigation (Gardea-Torresdey et al., 2014).

The ENMs when take contact with plants could also alter their agronomic traits (e.g., growth, biomass production, number of leaves, and chlorophyll content), which can directly influence the resulting yield parameters (number of fruit per plant, fruit weight, diameter, length) when grown to full maturity (Gardea-Torresdey et al., 2014).

Recently it has been also demonstrated the ENMs could affect the crop nutritional content directly consumed by humans but this aspect has not been fully investigated yet (Gardea-Torresdey et al., 2014).

Food crops resulted to be susceptible to ENMs contamination through material accumulation in soil from continuous biosolid amendment in agricultural fields, and possibly through the application of nanotechnology in agriculture and soil remediation efforts. However, there is very limited understanding on the extent of ENMs entry into the food supply and the resulting implications on environmental and human health (Gardea-Torresdey et al., 2014).

Important questions that need to be resolved by further study.

First, predictive quantitative modeling ENMs fate and disposition within agricultural soils that accommodates both repeated applications of effluent and biosolids from wastewater treatment plants, as well as the use of nanoenabled agricultural products and/or soil remediation techniques, is needed.

Second, nanophytotoxicity assessment of ENMs in forms that are being developed for agricultural and remediation techniques should be undertaken.

Third, studies exploring ENMs impacts on plants during different modes of application preferably at long-term exposure, should be performed. Longterm studies provide a more realistic and holistic approach for determining the implications of ENMs on soil health and microbial functions, as well as on the physiological and yield responses of plants. While short-term studies give a unique opportunity for understanding the mechanism of ENMs impacts in plants, full life cycle studies are critical to understanding plant response to chronic and perhaps low dose exposure (Gardea-Torresdey et al., 2014).

2 Aims

The aims of my PhD research are the evaluation of:

- The plants capacity to synthesize NPs from the ionic form of the element added to the growth media and investigate which are the principal metabolites involved in the process.
- The possible toxic effects caused by the interaction between NPs and plants in the early plant development stages and also along their entire life cycle. These toxic effects will be evaluated at different levels (morphologic, metabolic, genetic and phenologic).
- The plant capacity to uptake the NPs and translocate them through the plant tissues.
- The possible nutritional modification in the seeds obtained from plants cultivated in the presence of NPs.

Marchiol *et al. Nanoscale Research Letters* 2014, **9**:101
http://www.nanoscalereslett.com/content/9/1/101

Nanoscale Research Letters
a SpringerOpen Journal

NANO EXPRESS Open Access

In vivo synthesis of nanomaterials in plants: location of silver nanoparticles and plant metabolism

Luca Marchiol[1*], Alessandro Mattiello[1], Filip Pošćić[1], Cristiana Giordano[2] and Rita Musetti[1]

Abstract

Metallic nanoparticles (MeNPs) can be formed in living plants by reduction of the metal ions absorbed as soluble salts. It is very likely that plant metabolism has an important role in MeNP biosynthesis. The *in vivo* formation of silver nanoparticles (AgNPs) was observed in *Brassica juncea*, *Festuca rubra* and *Medicago sativa*. Plants were grown in Hoagland's solution for 30 days and then exposed for 24 h to a solution of 1,000 ppm $AgNO_3$. In the leaf extracts of control plants, the concentrations of glucose, fructose, ascorbic acid, citric acid and total polyphenols were determined. Total Ag content in plant fractions was determined by inductively coupled plasma atomic emission spectroscopy. Despite the short exposure time, the Ag uptake and translocation to plant leaves was very high, reaching 6,156 and 2,459 mg kg^{-1} in *B. juncea* and *F. rubra*, respectively. Ultrastructural analysis was performed by transmission electron microscopy (TEM), and AgNPs were detected by TEM X-ray microanalysis. TEM images of plant fractions showed the *in vivo* formation of AgNPs in the roots, stems and leaves of the plants. In the roots, AgNPs were present in the cortical parenchymal cells, on the cell wall of the xylem vessels and in regions corresponding to the pits. In leaf tissues, AgNPs of different sizes and shapes were located close to the cell wall, as well as in the cytoplasm and within chloroplasts. AgNPs were not observed in the phloem of the three plant species. This is the first report of AgNP synthesis in living plants of *F. rubra*. The contents of reducing sugars and antioxidant compounds, proposed as being involved in the biosynthesis of AgNPs, were quite different between the species, thus suggesting that it is unlikely that a single substance is responsible for this process.

Keywords: *Festuca rubra*; *Medicago sativa*; *Brassica juncea*; Silver; Nanoparticles; Biosynthesis; Plant metabolites

MSC 2010: 92 Biology and other natural sciences; 92Cxx Physiological, cellular and medical topics; 92C80 Plant biology

3.1 Background

In recent years, remarkable progress has been made in developing nanotechnology. This has led to the fast growth of commercial applications that involve the use of a great variety of manufactured nanomaterials (Klaine et al., 2008). One trillion dollars' worth of nanotechnology-based products is expected on the market by the year 2015 (Hernandez-Viezcas et al., 2013). Metallic nanoparticles (MeNPs), one of the building blocks of nanotechnology, have a variety of applications due to their unique properties.

Synthesis of MeNPs can be carried out by using traditional technologies that use chemical and physical methods with a 'top-down' approach (Kawazoe and Meech, 2005). However, such methods are expensive and have a low production rate; moreover, they are harmful as the chemicals used are often poisonous and not easily disposable due to environmental issues (Kowshik et al., 2003).

A relatively new and largely still poorly explored area of research is the biosynthesis of nanomaterials following a 'bottom-up' approach (Mohanpuria et al., 2008). Several biological systems (fungi, yeasts, bacteria and algae) are able to produce MeNPs at ambient temperature and pressure without requiring hazardous agents and generating poisonous by-products (Iravani, 2011; Kharissova et al., 2012).

Although a large number of papers have been published on the biosynthesis of MeNPs using phytochemicals contained in the extracts of a number of plant species (Haverkamp, 2011), so far little has been understood about this process when it occurs in living plants.

The plant-mediated MeNP synthesis that is promoted via plant extracts occurs in three different steps (Lukman et al., 2011; Rodríguez-León et al., 2013).

The first step (induction phase) is a rapid ion reduction and nucleation of metallic seeds. Such small, reactive and unstable crystals spontaneously aggregate and transform into large aggregates (growth phase). When the sizes and shapes of the aggregates become energetically favourable, some biomolecules act as capping agents stabilizing the nanoparticles (termination phase). Eventhough this appears conceptually to be similar to biomineralization (Skinner, 2003), this process in live plants is still poorly known. In particular, the role of plant metabolism is not yet understood in any depth.

The first experimental evidence of the synthesis of MeNPs in living vascular plants was reported by Gardea-Torresdey et al. (2002) who observed the formation of Au nanoparticles of different sizes and structures in plants of *Medicago sativa* (alfalfa) grown on agar medium enriched with $AuCl_4$. *Brassica juncea* (Indian mustard) was the second species in

which the synthesis of MeNPs was studied (Haverkamp et al., 2007; Marshall et al., 2007). Besides alfalfa and Indian mustard, some other plant species have been tested for the capacity to synthesize MeNPs (Iravani, 2011; Quester et al., 2013).

One of the key questions regarding this process is whether MeNP synthesis occurs outside the plant tissues with MeNPs transported through the root membrane into the plant or whether MeNPs are formed within plants by the reduction of the metal, previously taken up in ionic form by the roots. At present, the second hypothesis is the most accepted one. Plant-mediated MeNP formation was demonstrated by Sharma et al., using XANES and EXAFS, which provided evidence of Au reduction and the formation of AuNPs within the tissues of *Sesbania drummondii*.

Interspecific differences (*M. sativa* vs. *B. juncea*) in the synthesis of MeNPs in response to experimental parameters such as Ag exposure time and concentration have been highlighted by Harris and Bali (2008). Finally, Starnes et al. (2010) studied the effects of managing some environmental parameters (e.g. temperature and photosynthetically active radiation regime) on the nucleation and growth of AuNPs in some plant species, demonstrating empirical evidence on the feasibility of in planta NP engineering in order to produce nanomaterials of a wide variety of sizes and shape, which therefore have different physical and chemical properties.

The aims of our work were (i) to confirm the in vivo formation of silver nanoparticles (AgNPs) in *B. juncea*, *M. sativa* and *F. rubra* and (ii) to observe the location of AgNPs in plant tissues and cells in order (iii) to evaluate the possible relationship with plant metabolites.

3.2 Methods

3.2.1 Seed Germination and Plant Growth

Seeds of Indian mustard (*B. juncea* cv. Vittasso), red fescue (*F. rubra*) and alfalfa (*M. sativa* cv. Robot), previously washed with 1% H_2O_2 for 15 min and subsequently rinsed with deionized water, were placed in the dark in Petri dishes containing germinating paper and distilled water.

Fifteen days after germination, the seedlings were transferred to a hydroponic system (1^{-l} pots) containing a half-strength modified aerated Hoagland's solution. The nutrient solution was replaced every 7 days. The plants were grown for a cycle of 30 days on a laboratory bench lit by fluorescence lamps providing an average photosynthetically active radiation

(PAR) at the top of the plants of 500 μmol m^{-2} s^{-1} with a 16:8-h (light/dark) photoperiod. Ambient temperature was maintained at 22°C ± 2°C.

At the end of the growth cycle, the nutrient solution was removed and the root mass of the plant material was washed three times with deionized water. After washing, the growth solution was replaced with 1,000 ppm $AgNO_3$ (99.9999% salt; Sigma-Aldrich, St. Louis, MO, USA) solution and with deionized water (control). After 24 h, both treated and control plants (n = 6) were harvested.

3.2.2 Plant Tissue Collection

Ultrastructural analyses were performed by transmission electron microscopy. Fresh samples of plant tissues were collected after 24 h from the roots, along the stems and from fully expanded leaves near the primary veins. A subset of plants (three replicates per species) were used for inductively coupled plasma optical emission spectroscopy (ICP-OES) analysis.

3.2.3 TEM Analysis

Samples of plant tissues, as reported above, were excised, cut into small portions (2 × 3 mm) and fixed for 2 h at 4°C in 0.1% (wt/vol) buffered sodium phosphate and 3% (wt/vol) glutaraldehyde at pH 7.2. They were then postfixed with 1% osmium tetroxide (wt/vol) in the same buffer for 2 h, dehydrated in an ethanol series and embedded in Epon/Araldite epoxy resin (Electron Microscopy Sciences, Fort Washington, PA, USA). Serial ultrathin sections from each of the species were cut with a diamond knife, mounted on Cu grids, stained in uranyl acetate and lead citrate, and then observed under a Philips CM 10 (FEI, Eindhoven, The Netherlands) transmission electron microscope (TEM) operating at 80 kV.

3.2.4 TEM X-ray Microanalysis

The nature of precipitates observed in plant tissues was determined by TEM (PHILIPS CM 12, FEI, Eindhoven, The Netherlands) equipped with an EDS-X-ray microanalysis system (EDAX, software EDAX Genesis, AMETEK, Mahwah, NJ, USA). The images were recorded by a Megaview G2 CCD camera (software iTEM FEI, AnalySIS Image Processing, Olympus, Shinjuku-ku, Japan).

3.2.5 ICP-OES Analysis

Plant fractions were carefully washed with deionized water. Roots were additionally washed in slightly acidic (4% HCl) milliQ water for 10 min and then rinsed three times in

milliQ water. The material was then ovendried at 105°C for 24 h and nitric acid-digested in a microwave oven (MARS Xpress, CEM, Matthews, NC, USA) according to the USEPA 3052 method (USEPA 1995). After mineralization, the plant extracts were filtered (0.45-µm PTFE), diluted (1:20) and analyzed.

Total content of Ag was determined by an ICP-OES (Vista MPX, Varian Inc., Palo Alto, CA, USA). The accuracy of the analytical procedure adopted for ICP-OES analysis was checked by running standard solutions every 20 samples. Yttrium was used as the internal standard. A reagent blank and certified reference material (NIST SRM® 1573) were included for quality control of analysis.

3.2.6 Plant Metabolism Parameters

In control plants, leaf samples were collected (n = 3), immediately frozen in liquid nitrogen and stored at −80°C with the aim of determining the following parameters from leaf extracts: (i) glucose (GLC) and (ii) fructose (FRU) contents, (iii) ascorbic acid (AA) and (iv) citric acid (CA) contents, and (v) total polyphenol (PP) content.

The content of GLC and FRU in leaves was evaluated by measuring the NADPH absorption after successive additions of the coupling enzymes glucose-6-P-dehydrogenase, hexokinase, phosphoglucose-isomerase and invertase (Bergmeyer et al., 1974) using a UV/visible spectrophotometer (Tecan GENios Microplate Reader, Männedorf, Switzerland) at 340 nm.

AA was estimated by a colorimetric 2.6-dichlorophenol-indophenol (DIP) method (Keller and Schwager, 1977). The AA content was estimated using a UV/visible spectrophotometer (Novaspec II, Pharmacia Biotech AB, Uppsala, Sweden) at 520 nm.

CA content was determined by measuring the NADH oxidation after addition of L-malate dehydrogenase, L-lactate dehydrogenase, oxaloacetate and pyruvate (Dagley, 1974) using a UV/visible spectrophotometer (Novaspec II, Pharmacia Biotech AB, Uppsala, Sweden) at 340 nm.

Finally, according to Marinova et al. (2005), PP leaf content was determined following a modified Folin-Ciocalteu method (Singleton and Rossi, 1965). After incubation, the absorbance of the leaf extracts was determined using a UV/visible spectrophotometer (Novaspec II, Pharmacia Biotech AB, Uppsala, Sweden) at 750 nm.

The enzymatic test kit was purchased from R-Biopharm AG (Darmstadt, Germany).

3.2.7 Data Analysis

Plants were arranged in a randomized design (nine plants per species per treatment, one plant per pot). One-way analysis of variance (ANOVA) was carried out to test the differences in the plants' behaviour. The statistical significance of differences between mean values was determined using Bonferroni's test ($p < 0.05$). Different letters in Tables 1 and 2 are used to indicate means that were statistically different at $p < 0.05$. Statistical analysis was performed using the SPSS program (ver. 17, SPSS Inc., Chicago, IL, USA).

3.3 Results

3.3.1 Silver Concentration in Plant Tissues

We observed a quick Ag root sorption that resulted in a rapid and progressive darkening of root tissues and subsequently of the other plant fractions. Preliminary observation demonstrated that after 48 h of exposure to a solution of $AgNO_3$ at 1,000 ppm, the cell structures in leaf tissues were seriously injured. Since one of the aims of our experiment was to observe the distribution of AgNPs within the cell structures of different species, we decided to shorten the Ag exposure to 24 h; however, despite the shorter exposure, the Ag uptake was very high and these plants also appeared stressed.

The concentrations of Ag in the plant fractions were determined by ICP analysis. Data for roots, stems and leaves are reported in Table 1.

Table 1: Concentration of Ag in the roots, stems and leaves of the plants and Ag TF

Species	Ag roots (mg kg $^{-1}$ DW)	Ag stem (mg kg $^{-1}$ DW)	Ag leaves (mg kg $^{-1}$ DW)	TF (mg kg $^{-1}$ DW)
B. juncea	82.292 a	57.729 a	6.156 a	7.48 a
	(5.394)	(598)	(516)	(0.92)
F. rubra	62.365 b	2.777 c	2.495 b	3.94 b
	(1.990)	(2.738)	(258)	(0.36)
M. sativa	19.715 c	25.241 b	4.31 c	0.022 c
	(2.369)	(5.004)	(0.84)	(0.003)

The means (n = 3) with the same letter were not significantly different (Bonferroni's test; $p < 0.05$). The mean standard error (n = 3) is in brackets. TF, translocation factor; DW, dry weight.

Comparing the behavior of the three species, some statistically significant differences can be evidenced. In the roots of *B. juncea*, the Ag concentration reached its highest value compared to the other species ($F2,6 = 79.3$, $p<0.001$). However, even the lowest value (19,715 mg kg^{-1} in *M. sativa*) was almost twice the concentration of Ag in the solution provided to the plants. With regard to the shoots ($F2,6 = 74.7$, $p < 0.001$), the highest Ag level was observed again in *B. juncea* while the lowest was observed in *F. rubra* (Table 1). As for the Ag accumulation in leaves, ANOVA also showed significant differences among the species ($F2,6 = 86.3$, $p < 0.001$).

Analyzing the magnitude of Ag accumulation in the fractions from the different species, we can observe three different strategies. In *B. juncea*, the Ag concentration decreased progressively from roots to leaves (Table 1). In the case of *F. rubra*, about 95% of the Ag concentration was held in the roots. In *M. sativa*, a root-to-shoot Ag translocation was allowed while in the leaves the Ag concentration is very low (Table 1). The different strategies are briefly summarized by the translocation factor ($TF = [Ag]_{leaves} / [Ag]_{roots}$); the statistical significance of TF values ($F2,6 = 43.7$, $p < 0.001$) confirms such different behaviour of the species.

3.3.2 Plant Metabolism Compounds

In Table 2, the concentrations of the primary sugars GLC and FRU and the antioxidants AA, CA and PP recorded in the studied species are shown. As expected, because the species belong to different botanical families, the concentrations of the metabolites were quite different.

Table 2: Content of GLC, FRU, AA, CA and PP in the leaves of the plants

Species	GLC (mmol kg $^{-1}$ FW)	FRU (mmol kg $^{-1}$ FW)	AA (mg kg $^{-1}$ DW)	CA (mg kg $^{-1}$ DW)	PP (mg kg $^{-1}$ DW)
B. juncea	1.61 b	2.17 b	3.878 a	10.2 a	711 a
	(0.64)	(1.07)	(548)	(0.48)	(48.6)
F. rubra	70.4 a	57.8 a	119 c	11.2 a	580 b
	(12.9)	(14.7)	(92.4)	(2.59)	(37)
M. sativa	8.17 b	7.37 b	1459 b	5.12 a	528 b
	(0.58)	(0.57)	(359)	(1.68)	(18.9)

The means (n = 3) with the same letter were not significantly different (Bonferroni's test; $p < 0.05$). The mean standard error (n = 3) is in brackets. GLC, glucose; FRU, fructose; AA, amino acid; CA, citric acid; PP, polyphenols; FW, fresh weight.

With regard to the primary sugars, ANOVA indicated that the grass, *F. rubra*, had a significantly higher concentration of GLC (70.4 mg kg^{-1}, $F_{2,6} = 25.6$, $p < 0.01$) and FRU (57.8 mg kg−1, $F_{2,6} = 13.04$, $p < 0.01$) compared to other species, while in *B. juncea* and *M. sativa*, considerably lower values of both the sugars were found (Table 2).

Regarding the content of AA, there were statistically significant differences among the species ($F_{2,6} = 24.8$, $p < 0.01$). The AA concentration varied from 3,878 and 119 mg kg^{-1} measured for *B. juncea* and *F. rubra*, respectively (Table 2).

The ANOVA also showed significant differences among the species for the content of PP ($F_{2,6} = 6.56$, $p < 0.05$). The highest amount of PP was found again in *B. juncea*, while *F. rubra* and *M. sativa* had similar low PP contents.

Finally, no significant differences among the species were recorded for the concentration of CA ($F_{2,6} = 3.29$, $p = 0.108$) (Table 2).

3.3.3 Ag-like Particle Distribution in Plants and Ultrastructural Modifications Induced by Treatment

The subcellular localization of Ag-like particles was assessed in the different organs (roots, stems and leaves) of *B. juncea*, *F. rubra* and *M. sativa* up to 24 h of metal exposure. Nanoparticles were visible in the tissues of the treated plants as dark, electron-dense roundish aggregates (Figures 1, 2, 3). After 24 h of treatment, TEM observations showed a similar distribution of the particles in the three plant species.

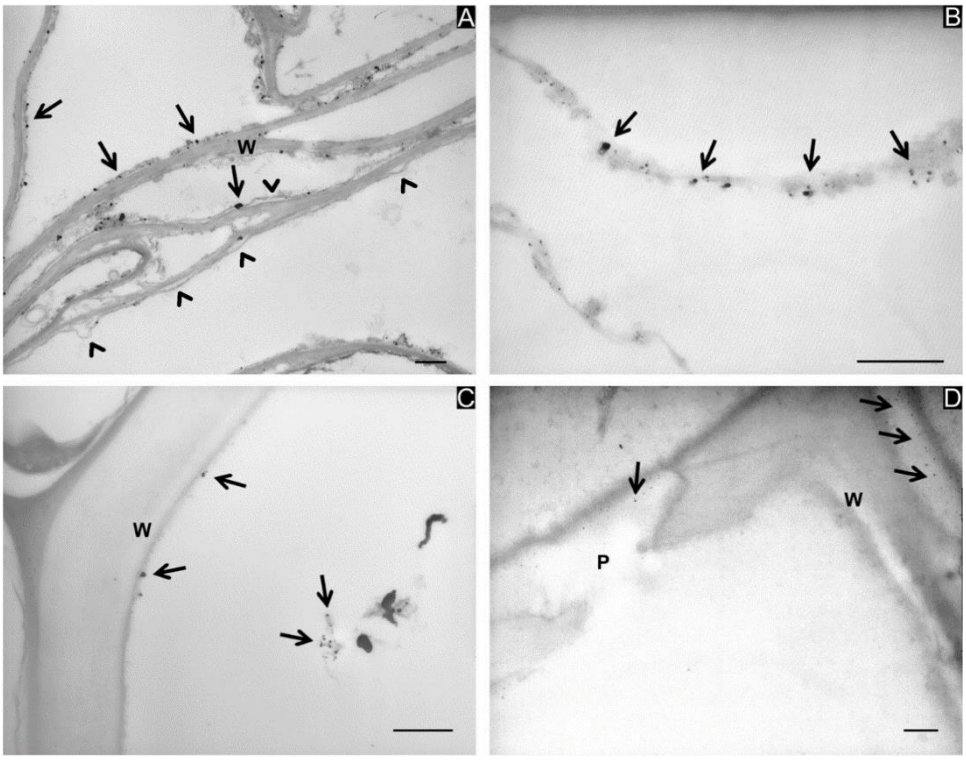

Figure 1: Localization of Ag particles in the roots of *Festuca rubra* (A) and *Medicago sativa* (B, C, D). Electron-dense Ag spots are visible on the plasmalemma of the cortical parenchymal cells (A and B, arrows). In (A), arrowheads indicate the detachment of the plasmalemma from the cell wall. In (C), small particles are visible on the cell wall (W) and in the lumen of a xylem vessel (arrows). In (D), a detail of a xylem vessel showing the beginning of deposition of electron-dense Ag particles at the vessel pit (P) is visible (arrows). Bars correspond to 500 nm.

In the roots, electron-dense Ag spots were present in the cortical parenchymal cells. The spots were localized mainly on the plasmalemma (Figure 1A,B, arrows). Small Ag particles were also found on the cell wall of the xylem vessels, in the cell lumen (Figure 1C, arrows) and in areas corresponding to the pits (P in Figure 1D, arrows). The ultrastructure of root tissues appeared significantly modified by Ag treatment even though the different cell compartments were still recognizable. The main changes concerned the cortical parenchymal cells where the plasmalemma was often detached from the cell wall (Figure 1A, arrowheads).

Unlike the roots, numerous electron-dense Ag particles of different sizes, often forming consistent aggregates, appeared in the shoots in association with different cell compartments (Figure 2) such as cell walls (Figure 2A,B, arrows), chloroplasts (Chl in Figure 2B, arrows), plasmalemma and cytoplasm (Cyt in Figure 2C,D, arrows).

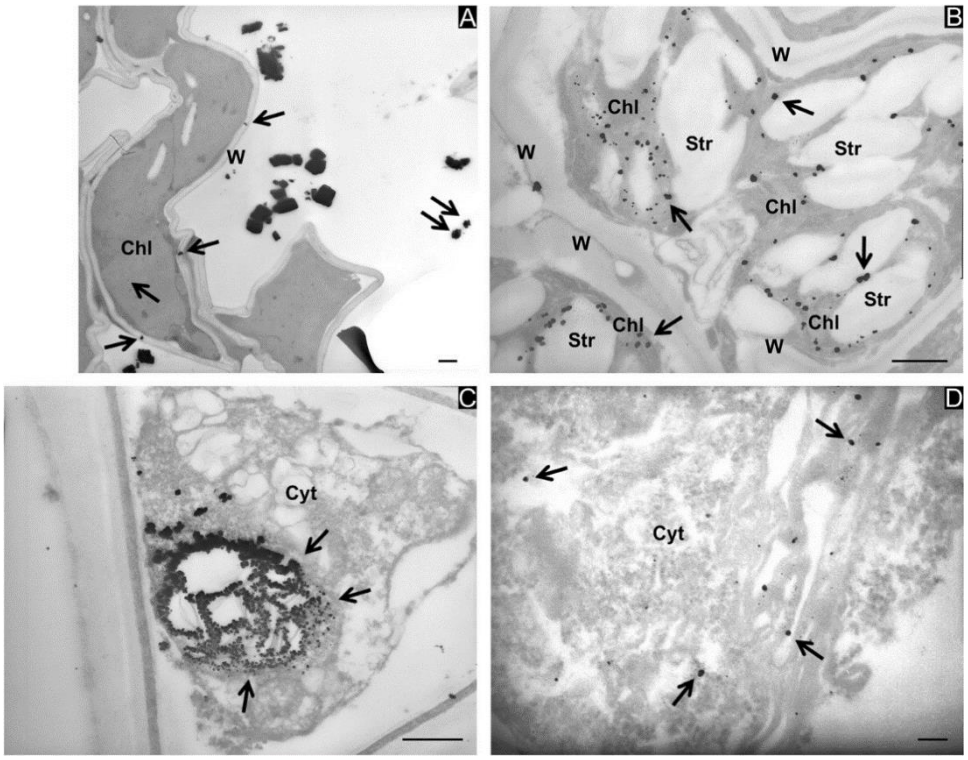

Figure 2: Ag particles in shoots of *Brassica juncea* (A, C), *Festuca rubra* (B) and *Medicago sativa* (D). Electron-dense Ag precipitates are found in association with different cell compartments. In (A), Ag precipitates appear as big electron-dense accumulations in the extracellular spaces among cortical parenchymal cells and as small spots on the cell walls (W) and on chloroplasts (Chl, arrows). In the parenchymal cells of vascular tissues, precipitates are found in the chloroplast stroma (B, Chl, arrows) and in the cytoplasm (Cyt), which often appears condensed (C and D, arrows). Organelles such as mitochondria, endoplasmic reticulum and vacuoles are not distinguishable. Note the big starch accumulations into the chloroplasts (B, Str). Bars correspond to 500 nm in (A, B, C) and 100 nm in (D).

In the xylem, Ag precipitates were distributed along the cell wall and, to a lesser extent, in the cell lumen (not shown). Ag treatment led to severe consequences in the stem tissues of the three plant species. In fact, the parenchymal cells of the stem showed anomalous shapes (Figure 2A). Cells had the appearance of being plasmolyzed, and the consequent condensation of the cytoplasm (Cyt in Figure 2C,D) made recognition of the organelles difficult. The chloroplasts were altered by disorganization of the lamellae (Chl in Figure 2B) and by anomalous formation of starch granules (Str in Figure 2B).

In leaf tissues, Ag-like precipitates with different shapes and sizes (Figure 3A, arrows) were observed in association with the cell wall (W in Figure 3A) as well as the cytoplasm (Cyt in Figure 3B, arrows) and chloroplasts (Chl in Figure 3C, arrows).

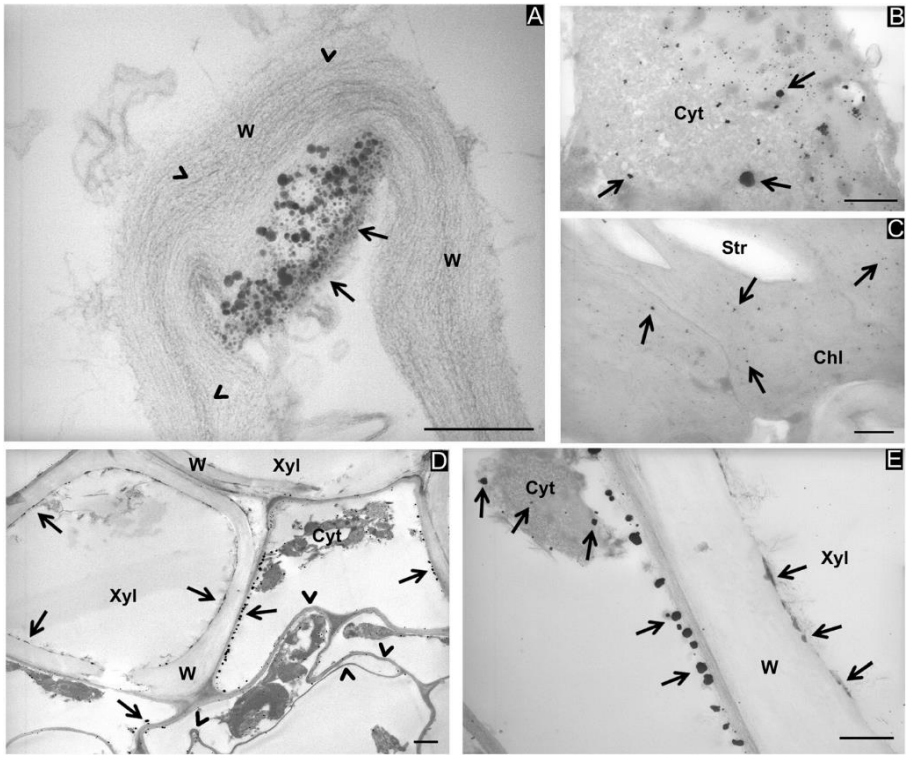

Figure 3: Ag particles in the leaves of *Brassica juncea*. Precipitates of different sizes are visible in the parenchymal cells (A, B, C). They are localized in the inner side of cell walls (A, W, arrows), in the condensed cytoplasm (B, Cyt, arrows) and in the chloroplasts (C, Chl, arrows). The wall architecture was modified, showing not compacted microfibrils (A, arrowheads). In (D), a xylem vessel (Xyl) contains numerous precipitates along the cell wall (W, arrows). In (E), the surrounding cells show also numerous precipitates, along the plasmalemma (arrows) and in the condensed cytoplasm (Cyt, arrows). Bars correspond to 250 nm in (A, B, C), 1,000 nm in (D) and 500 nm in (E).

Electron-dense particles had also accumulated along the plasmalemma (Figure 3D,E, arrows). Similar to the observations in stems, precipitates were also present in the cell walls of the xylem elements (Xyl in Figure 3D,E, arrows). Precipitates were never observed in the phloem of the three plant species.

As observed in the stems, Ag treatment also caused severe modifications to the cell structures in the leaf tissues. Parenchymal cells also seemed to have been plasmolyzed with an associated cytoplasmic condensation (Cyt in Figure 3B,E), chloroplasts contained large starch granules (Str in Figure 3C), and the walls were distorted (Figure 3D, arrowheads).

3.3.4 X-ray Microanalyses and Ag-like Particle Identification

X-ray microanalysis was performed on the electrondense Ag-like particles observed in the different tissues of the three plant species. Some representative images of electron-dense precipitates recovered from the roots of *F. rubra* are shown in Figure 4 and those from the leaves of *M. sativa* and *B. juncea* in Figures 5 and 6, respectively. The presence of C, Os, U and Pb was due to sample preparation, and Cu was due to the grids used as section support.

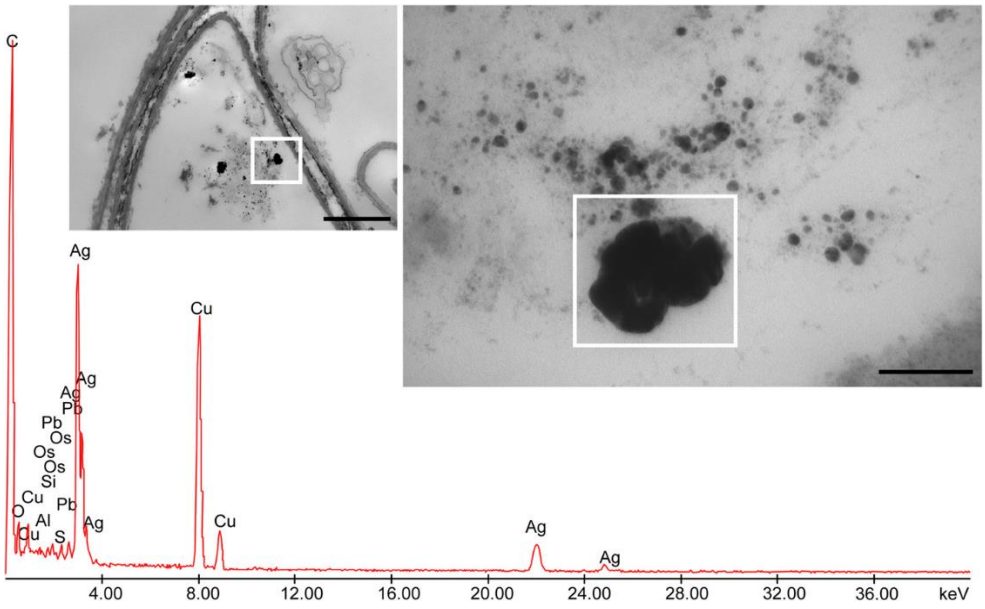

Figure 4: Electron-dense precipitates recovered from root cortical parenchymal cell of *Festuca rubra* and X-ray spectra of elements. Bar corresponds to 1,000 nm. Insets represent enlarged region where X-ray microanalyses have been performed. Bar corresponds to 200 nm. Ag peaks, at 23 keV, were well visible.

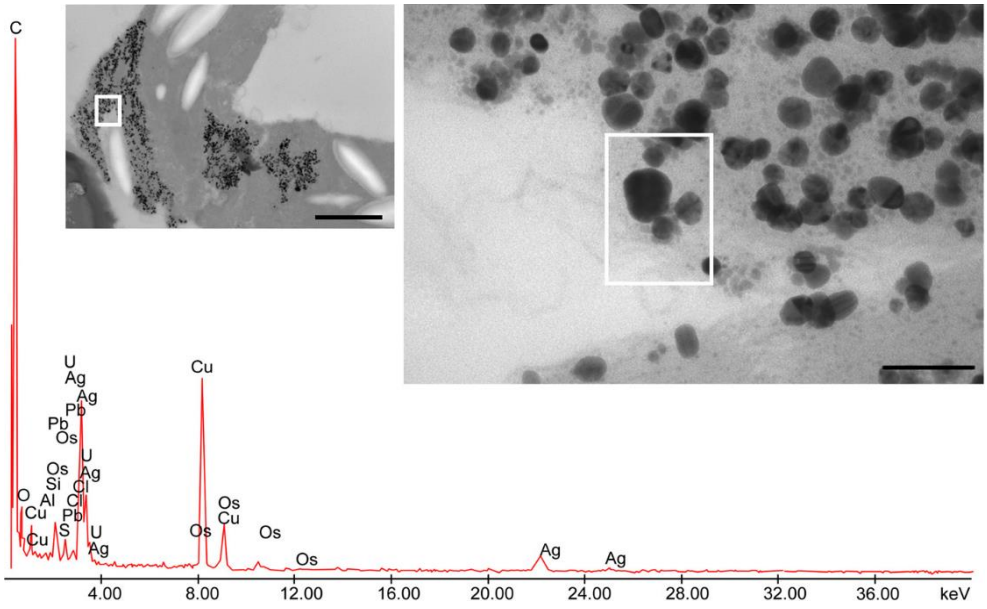

Figure 5: Electron-dense precipitates recovered from leaf parenchymal cell of *Medicago sativa* and X-ray spectra of elements. Bar corresponds to 1,000 nm. Insets represent enlarged region where X-ray microanalyses have been performed. Bar corresponds to 100 nm. Ag peaks, at 23 keV, were well visible. The presence of C, Os, U and Pb was due to sample preparation, and Cu was due to the grids used as section support.

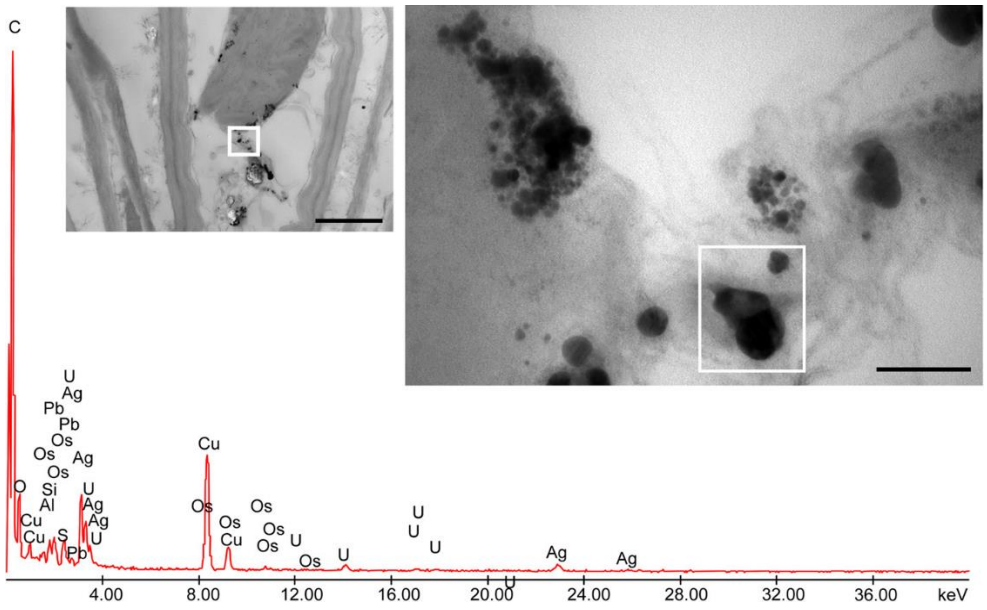

Figure 6: Electron-dense precipitates recovered from leaf parenchymal cell of *Brassica juncea* and X-ray spectra of elements.Bar corresponds to 1,000 nm. Insets represent enlarged region where X-ray microanalyses have been performed. Bar corresponds to 100 nm. Ag at 23 keV, were well visible. The presence of C, Os, U and Pb was due to sample preparation, and Cu was due to the grids used as section support.

3.4 Discussion

Plants are able to take up silver, although this element has no biological functions (Adriano, 2001). The typical level of Ag in plant tissue is <1 ppm (Smith and Carson, 1977). When the ionic form of Ag occurs in low concentrations in the soil, it accumulates evenly throughout the whole plant. At much higher concentrations, Ag accumulation increases in the plant roots, but it is poorly translocated to the shoots (Klein et al., 1975).

This also occurs when plants are grown in hydroponics. Our data confirms the major Ag accumulation in plant roots. Also, we demonstrated how different the root-to-leaf Ag mobilization can be among different species. According to Harris and Bali (2008), *B. juncea* and *F. rubra* are much more efficient than *M. sativa* in Ag uptake and translocation. TEM analyses confirmed the presence of AgNPs through all the plant tissues of the three species, in the form of single particles and/or intracellular clusters of different sizes and shapes. This fact suggests that after entering through the root apparatus, AgNPs are able to move to remote positions and to form aggregates throughout the plants. The movement probably occurs through the vascular system, but it is unclear whether particles were transported as nanosized individuals or as aggregates. Twenty-four hours after treatment, roots showed aggregates that appeared to be blocked to further movement at the plasmalemma of the cortical tissues, while isolated nanoparticles have been mainly found close to the root vascular core, in the xylem pits and in the vessel lumen. This could indicate that a small proportion of AgNPs aggregate at the root level and the others move from parenchymal cells to the xylem mainly as nanosized individuals, to be subsequently transported to the other plant organs where they form clusters. The fact that particles can move through the xylem is in agreement with the report of Corredor et al. (2009), who suggested that iron-carbon nanoparticles, after injection into *Cucurbita pepo* tissues, were able to spread through the xylem away from the application point.

AgNP localization inside the cells is widely addressed in the literature. It has been reported that Ag is able to displace other cations from electropositive sites located on the cell walls, membranes and DNA molecules, thanks to its strong electronegative potential. A long time before the current investigations into MeNP biosynthesis, Weier (1938) first reported the reduction of Ag to metallic granules in cells of the leaves of *Trifolium repens*. It was discovered that the deposition of such material occurred particularly along the edge of the chloroplasts as well inside them and in the starch granules.

This is also in agreement with the localization of AgNPs in the leaves of the three plant species reported in this study. Ascorbic acid has been proposed as the reducing agent responsible for this process (Weier, 1938). The localization of metallic Ag was later confirmed by Brown et al. (1962), who also hypothesized that other compounds beside ascorbic acid could accomplish Ag reduction, and thus, the process was proposed to be more complex than a single-step reduction reaction.

TEM observations also revealed ultrastructural changes in different cell compartments. These modifications were often observed concomitantly with nanoparticle aggregates. Plant cells could respond to the presence of a high density of nanoparticles by changing their subcellular organization. The main changes concerned cell membranes (plasmalemma, tonoplast, chloroplast thylakoids) as Ag is able to inhibit many enzymes, especially those containing sulfhydryl groups, thereby altering membrane permeability (Koontz and Berle, 1980). We observed that the severity of ultrastructural changes was different in the diverse plant organs. Even though the ICP analyses demonstrated a higher metal concentration in the root tissues of plants, the aerial fractions were more damaged by Ag treatment than the roots.

The limited toxic effects observed in the root tissue are probably due to the ability of the plants to 'block' and store AgNPs at the membrane level. On the other hand, nanosized individuals, translocated to the upper levels of the plant, resulted in a higher toxicity, as already reported for other metal-based nanoparticles (Aubert et al., 2012).

AgNP synthesis in living plants has been demonstrated previously in *B. juncea* and *M. sativa* in hydroponics by Harris and Bali (2008), Haverkamp and Marshall (2009) and Beattie and Haverkamp (2011). Our data confirms their findings. Furthermore, the current paper demonstrates AgNP formation in the live tissues of *F. rubra* which has not been reported previously. Some experimental evidences demonstrated that metal reduction and nucleation (steps both involved in the NP synthesis) can occur in agar/soil-plant system (respectively, Gardea-Torresdey et al., 2003; Manceau et al., 2008). For this reason, we cannot totally exclude that also in our conditions a fraction of AgNPs can be formed due to the release of root metabolites then absorbed by plant roots.

MeNP synthesis, which occurs in plant tissues very quickly, is influenced by environmental conditions. Starnes et al. detected the formation of AuNPs in *M. sativa* and other species as early as 6 h after the start of exposure to $KAuCl_4$. It was also verified that plant growth conditions have an effect on MeNP biosynthesis: variations in temperature, pH and photosynthetically active radiation (PAR) influence the size and shape of growing AuNPs

(Starnes et al., 2010). Theoretically, this suggests the possibility of managing living plants as nanofactories and promoting the synthesis of nanomaterials of desired size and shape.

The most intriguing question about plant MeNP biosynthesis is where and how this phenomenon begins. So far, the steps of this process in living plants have not been completely clarified. Wherever this occurs, it is highly likely that the key factor is the presence of immediately available reducing agents. An investigation by Beattie and Haverkamp (2011) demonstrated that in *B. juncea* the sites of the most abundant reduction of metal salts to NPs were the chloroplasts, in which high reducing sugars (i.e. glucose and fructose) may be responsible for the metal reduction. This might support the hypothesis that plants with the highest concentrations of reducing sugars are the 'nanofactories' *par excellence*.

In our experiment, leaf extracts of the studied species were analyzed to detect the concentrations of two reducing sugars (GLC and FRU) and the antioxidants AA, CA and PP, assuming that possible differences in the concentration of such substances may have some influence on MeNP biosynthesis. If the hypothesis by Beattie and Haverkamp (2011) were true, and given our findings regarding the high concentration of GLC and FRU, among the species studied *F. rubra* should be a very promising species because it also translocated in its leaves very well. To verify this hypothesis would require a demonstration of a quantitative relationship between the concentration of reducing sugars and the amount of AgNPs; however, this was beyond the scope of the present study.

Our data demonstrate that in the leaves of *B. juncea* and *M. sativa* (species used as model plants by several authors in studies on the biosynthesis MeNPs), there are concentrations of AA and PP that are considerably higher than those in *F. rubra*. In contrast, *F. rubra* had a level of reducing sugars much higher than *B. juncea* and *M. sativa*. This leads to the concept that there is no substance that is solely responsible for the process. In fact, currently, it is thought that polysaccharides, proteins, flavonoids and terpenoids, which together promote the total reducing capacity of plant cells, could be involved in the biosynthesis of MeNPs and their stabilization (Park et al., 2011; Gan and Li, 2012 and references therein). On the other hand, it should be considered that MeNP biosynthesis starts in healthy cells, which then rapidly undergo a progressive alteration until they are completely disrupted due to Ag toxicity. Thus, it could be that MeNP biosynthesis is initiated within the chloroplasts in a healthy cell and ends in the cytoplasm of the same cell, which has been damaged.

3.5 Conclusions

The synthesis of AgNPs in living plants was confirmed in *B. juncea* and *M. sativa* and demonstrated for the first time in *F. rubra*. We assessed the subcellular localization of AgNPs in the plant fractions demonstrating that AgNPs had a similar distribution but different sizes.

Regarding promotion agents, the presence of AgNPs within the chloroplasts suggested that primary sugars, at least in the beginning phase, could have a role in the in vivo synthesis of AgNPs. However, while the effects of these substances are usually studied individually, it is very unlikely that they have an exclusive role. On the contrary, given the complexity of plant metabolism, it is most likely that there are synergistic effects between different substances.

We did not verify a clear quantitative relationship between the amount of GLU, FRU, AA and PP and the quantity of AgNPs formed. To evaluate if plants can be efficiently exploited for their ability to synthesize in vivo MeNPs, further experiments are needed not only to define more precisely the mechanism of metal nanoparticle formation in living plants but also to better understand if differences in plant behaviour, due to molecular mechanisms, result in differences in the amount, forms, dimensions and 3-D structures of the in vivo synthesized MeNPs.

frontiers in Plant Science

ORIGINAL RESEARCH
published: 25 November 2015
doi: 10.3389/fpls.2015.01043

Evidence of Phytotoxicity and Genotoxicity *in Hordeum vulgare* L. Exposed to CeO_2 and TiO_2 Nanoparticles

*Alessandro Mattiello[1], Antonio Filippi[1], Filip Pošćić[1], Rita Musetti[1], Maria C. Salvatici[2], Cristiana Giordano[2,3], Massimo Vischi[1], Alberto Bertolini[1] and Luca Marchiol[1]**

[1] Department of Agriculture and Environmental Sciences, University of Udine, Udine, Italy, [2] Centro di Microscopie Elettroniche "Laura Bonzi", Istituto di Chimica dei Composti OrganoMetallici, Consiglio Nazionale delle Ricerche, Firenze, Italy, [3] Tree and Timber Institute, Istituto Per La Valorizzazione del Legno e delle Specie Arboree-CNR, Firenze, Italy

Engineered nanoscale materials (ENMs) are considered emerging contaminants since they are perceived as a potential threat to the environment and the human health. The reactions of living organisms when exposed to metal nanoparticles (NPs) or NPs of different size are not well known. Very few studies on NPs–plant interactions have been published, so far. For this reason there is also great concern regarding the potential NPs impact to food safety. Early genotoxic and phytotoxic effects of cerium oxide NPs ($n$$CeO_2$) and titanium dioxide NPs ($n$$TiO_2$) were investigated in seedlings of *Hordeum vulgare* L. Caryopses were exposed to an aqueous dispersion of $n$$CeO_2$ and $n$$TiO_2$ at, respectively 0, 500, 1000, and 2000 mg l^{-1} for 7 days. Genotoxicity was studied by Randomly Amplified Polymorphism DNA (RAPDs) and mitotic index on root tip cells. Differences between treated and control plants were observed in RAPD banding patterns as well as at the chromosomal level with a reduction of cell divisions. At cellular level we monitored the oxidative stress of treated plants in terms of reactive oxygen species (ROS) generation and ATP content. Again $n$$CeO_2$ influenced clearly these two physiological parameters, while $n$$TiO_2$ were ineffective. In particular, the dose 500 mg l^{-1} showed the highest increase regarding both ROS generation and ATP content; the phenomenon were detectable, at different extent, both at root and shoot level. Total Ce and Ti concentration in seedlings was detected by ICP-OES. TEM EDSX microanalysis demonstrated the presence of aggregates of $n$$CeO_2$ and $n$$TiO_2$ within root cells of barley. $n$$CeO_2$ induced modifications in the chromatin aggregation mode in the nuclei of both root and shoot cells.

Keywords: barley, cerium oxide nanoparticles, titanium oxide nanoparticles, genotoxicity, oxidative stress

OPEN ACCESS

Edited by:
Nelson Marmiroli, University of Parma, Italy

Reviewed by:
Margarita Sánchez-Domínguez, Centro de Investigación en Materiales Avanzados, S.C., Mexico
Jozsef Dudas, Medical University of Innsbruck, Austria

****Correspondence:***
Luca Marchiol
marchiol@uniud.it

Specialty section:
This article was submitted to Functional Plant Ecology, a section of the journal Frontiers in Plant Science

Received: *12 September 2015*
Accepted: *09 November 2015*
Published: *25 November 2015*

4.1 Background

It is estimated that by 2020 about six million people will be employed worldwide in industries that use nanotechnologies, which will have the potential to produce goods for a market of more than 3,000 billion dollars (Roco, 2011). There is therefore a tumultuous development of new materials justified by a rapid growth of technological and commercial applications. Model simulations demonstrated that flows of engineered nanomaterials (ENMs) are able to reach several natural ecosystems (Colman et al., 2013). Cerium oxide nanoparticles (*n*CeO_2) and titanium oxide nanoparticles (*n*TiO_2) are among the top ten most produced ENMs by mass (Keller et al., 2013) and used in cosmetics industries, in solar cells, paints, cements, coatings, in agriculture and the food industry (Gogos et al., 2012; Piccinno et al., 2012; Parisi et al., 2015). *n*CeO_2 and *n*TiO_2 were included in the list of ENMs of priority for immediate testing by the Organization for Economic Cooperation and Development (OECD, 2010). From point sources (e.g. discharges of wastewaters from industries or landfills), such materials will tend to accumulate in sediments and soils, exposing the organisms inhabiting these environments to potential risks (Liu and Cohen, 2014).

Plants are able to assimilate metal nanoparticles (MeNPs) largely depending on the type of plant and the size of MeNPs (Rico et al., 2011). In addition, the primary particle size of MeNPs is relevant for their bioavailability and therefore their toxicity (Van Hoecke et al., 2009), also raising questions on the potential for MeNPs exposure of crops and food safety (Hong et al., 2013). Experimental evidences were reported by Zhang et al (2011). which studied the *n*CeO_2 uptake and translocation in cucumber, reporting an higher Ce assimilation in plants treated with 7 nm Ce than 25 nm ones.

Clément et al. (2013) reported similar results for *n*TiO_2 on rapeseed plantlets treated with 14-25 nm particles. Another functional property that influence the MeNPs plant assimilation is the agglomeration/aggregation status that in turn is influenced directly by the zeta-potential (Navarro et al., 2008). Song et al. (2013a) demonstrated a negative correlation between *n*TiO_2 agglomeration/aggregation and assimilation in tomato. A similar behavior could be hypothesized also for *n*CeO_2.

Although there are potential positive applications of ENMs in agriculture (Parisi et al., 2015), studies on the toxicity of MeNPs have shown early negative consequences on crops due to genotoxic and phytotoxic effects (Miralles et al., 2012; Gardea-Torresdey et al.,

2014). From an ecological point of view, this raises questions about potential risks due to the input of MeNPs in the food chain. Early plant MeNPs toxicity can be measured observing seed germination, root elongation, DNA mutations (López-Moreno et al., 2010a; Atha et al., 2012) or changes in biochemical parameters (Rico et al., 2013; Schwabe et al., 2013).

The aims of this study were to determine the early phytotoxic and genotoxic effects of *n*CeO_2 and *n*TiO_2 on barley (*Hordeum vulgare* L.) plants. The FAO ranks barley 4th in the top 5 cereals in the world ordered based on production tonnage (FAOSTAT, 2014) and the cereal is one of the major crops grown worldwide for human and animal consumption. Suspensions of *n*CeO_2 and *n*TiO_2 were prepared at 0, 500, 1000 and 2000 mg l^{-1}. Phytotoxicity of nanoparticles was determined through percentage of germination and root elongation, ATP and ROS generation in root and leaf cells. Genotoxicity was investigated by the mitotic index and RAPDs. Ce and Ti uptake and translocation within seedling tissues were determined by inductively coupled plasma-optical emission spectroscopy (ICP-OES), while *n*CeO_2 and *n*TiO_2 within plant cells were detected by transmission electronic microscope and energy dispersive x-ray spectrometer (TEM-EDX).

4.2 Materials and Methods

4.2.1 Nanoparticles Characterization

The cerium(IV) oxide (*n*CeO_2) and titanium(IV) oxide anatase (*n*TiO_2) powders with a nominal average particle size < 25 nm were purchased from Sigma-Aldrich (Milwaukee, WI, USA). The specific surface area of the *n*CeO_2 and *n*TiO_2 was measured by the Brunauer–Emmett–Teller (BET) method by using the Surface Area and Pore Size Analyzer SA 3100 plus (Beckman Coulter, USA). The *n*CeO_2 and *n*TiO_2 powders were suspended in deionized water at a concentration of 1000 mg l^{-1} and sonicated at 60 °C for 30 min. The suspensions were characterized for Z-average size, measured as hydrodynamic diameter, zeta potential, via electrophoretic mobility, and polydispersity index (PDI), calculated from the signal intensity, by the dynamic light scattering (DLS) method using the Nano ZS90 (Malvern Instruments, UK). The *n*CeO_2 and *n*TiO_2 powder suspensions at three different concentrations (500, 1000 and 2000 mg l^{-1}) were prepared in MilliQ® water by sonication for 30 min at room temperature and then stirred for 15 min. The range of concentrations (0, 500, 1000 and 2000 mg l^{-1}) was chosen according to Yang and Watts (2005), Lin and Xing (2007) and López-Moreno et al. (2010a).

4.2.2 Seed Germination and Root Elongation

Caryopses of *Hordeum vulgare* L. var. Tunika were provided by S.I.S. Società Italiana Sementi (San Lazzaro di Savena, Bologna, Italy). The caryopses were sterilized by orbital agitation with 70% ethanol for 2 min and then with 5% sodium hypochlorite plus some drops of Tween 80 for 30 min. They were rinsed six times with sterilized MilliQ® water. All caryopses were transferred in sterile conditions into 15 mm Petri dishes containing filter paper (Ø 90 mm Whatman No. 1) soaked with 8 ml of MilliQ® water (control treatment) or 8 ml of *n*CeO_2 or *n*TiO_2 suspensions at different concentrations. The Petri dishes were taped and placed in the dark at 21 °C for 3 d. The germination percentage was calculated as the ratio of germinated seeds out the total seeds of each Petri dish. A second set of caryopses were treated for 7 d in the same conditions to evaluate root elongation and Ce and Ti uptake. The seedlings were photographed and Image J software (Schneider et al., 2012) was used to measure roots length. Root elongation was calculated as the average or the sum of all roots emerged from each seed. The experiments were performed in triplicate.

4.2.3 Mitotic Index

The germinated seedlings with actively growing roots (2.5 cm in length) were placed in the *n*CeO_2 and nTiO_2 suspensions (0, 500, 1000, 2000 mg l^{-1}) for 24 h. After treatment the root tips were fixed in 3:1 alcohol : acetic acid and then, kept in 70% ethanol at 4 °C. The root tips were rinsed in deionized water for 5 min, hydrolyzed in 1N HCl for 8 min at 60 °C, rinsed in deionized water for 5 min, stained in leuco-basic-fuchsine for 45 min and washed in tap water for 5 min. The root tips were then transferred to 45% acetic acid for 1 to 5 min, root caps were removed, and the roots were dissected to release the meristematic cells. Ten tips per treatment were evaluated and each treatment was replicated three times, for a total of about 10,000 cell observations. The mitotic index was evaluated in Feulgen stained preparations as the percentage of dividing cells out of the total number of cells scored.

4.2.4 Random Amplified Polymorphic DNA (RAPD) Analysis

The genotoxicity of *n*CeO_2 and nTiO_2 was investigated by observing the band profile after a random amplified polymorphic DNA (RAPD) assay on 6 replicates per treatment obtained from seedlings exposed as for mitotic index experiment. Plant genomic DNA was extracted from root tips using the DNeasy Plant Mini Kit (QIAGEN®) according to manufacturer's protocol. PCR reactions were performed with 30 ng of genomic DNA as a template using six primer pairs: OPA04 (AATCGGGCTG), OPA10 (GTGATCGCAG),

OPB01 (GTTTCGCTCC), OPB03 (CATCCCCCTG), OPB12 (CCTTGACGCA) and OPB20 (GGACCCTTAC). The PCR conditions consisted of an initial Taq polymerase activation at 95 °C for 5 min, followed by 45 cycles of denaturation (95 °C, 1 min), annealing (35 °C, 1 min) and extension (72 °C, 1 min) with a final extension for 10 min at 72°C. The PCR products were subjected to electrophoresis on 1.6% agarose in TBE 0.5%, for 2 h at 60 V/cm stained with GelRed® and photographed for band scoring.

4.2.5 Evaluation of ATP Content

ATP content was determined by means of the luciferin–luciferase luminometric assay (Lundin, 1984). Root and shoot of each seedling were separated, frozen with liquid nitrogen and ground to a fine powder. Tissue powder (100 ± 20 mg FW) was suspended in 1 ml of 50 mM Tris–HCl (pH 7.5), 0.05% (w/v) Triton X-100 and immediately kept at 95 °C for 3 min to inactivate any possible hydrolytic activity. After cooling, samples were centrifuged to obtain the cellular soluble fraction in the supernatant. The sample assays were performed in a 96-well plate with ATPlite Luminescence ATP Detection Assay System, (PerkinElmer) according to manufacturer's protocol. Aliquots (20 µl) of soluble fraction were mixed with 20 µl of ATPlite buffer in 130 µl of 50 mM Tris–HCl (pH 7.5) and 5 mM $MgCl_2$. Signals were detected by a Multilabel Counter (WALLAC, model 1420, PerkinElmer Waltham, MA, USA). Actual ATP concentration of each experiment (expressed as nmol ATP g^{-1} FW) was calculated by a calibration curve obtained with commercially purchased ATP (Sigma, USA) in a 8–100 nM range.

4.2.6 Reactive Oxygen Species (ROS) Determination

The generation of ROS was monitored by the method of Wang and Joseph (1999), using 2',7'-dichlorodihydrofluorescein diacetate (H_2DCFDA) as a probe. Tissue powder (0.5 g FW) obtained from both roots and shoots was extracted in 2.5 ml cold acetone and incubated for 4 h at 4°C. After centrifugation at 1000 g for 10 min, the pellet was homogenized in 1 ml of 50 mM Tris-HCl (pH 7.5), 0.4 M sucrose and 1 mM EDTA by Turrax device. The sample was again centrifuged for 15 min and the supernatant stored at -80°C until analysis. Aliquots of sample (20 µl) were incubated in 96-well microplate with 5 µM H2DCFDA and 180 µl of 50 mM Tris-HCl (pH 7.5). Detection was performed by fluorimetric assay using Multilabel Counter (WALLAC, model 1420, Perkin-Elmer) with orbital shaking and reading for 1.75 h at 5 min intervals with excitation filter set at 485 ± 10 nm and the emission filter set at 530 ± 10 nm. Values of relative fluorescence (RFU)

were expressed as RFU mg^{-1} protein. Protein concentration was estimated by the Bradford (1976) method.

4.2.7 Cerium and Titanium in Seedling Tissues

The seedlings were washed by agitation with 0.01 M HNO_3 for 30 min and rinsed 3 times by agitation with MilliQ® water for 15 min. The seedling roots and shoots were then oven-dried at 105 °C for 24 h and 0.5 g material was digested using 10 ml of HNO_3 in a microwave oven (CEM, MARS Xpress) according to the USEPA 3052 method (USEPA, 1995).[30] After mineralization, the plant extracts were filtered (0.2 µm PTFE), diluted and analyzed. Total content of Ce and Ti was determined by an ICP-OES (Varian Inc., Vista MPX). The accuracy of the analytical procedure adopted for ICP-OES analysis was checked by running standard solutions every 20 samples. Yttrium was used as the internal standard.

4.2.8 TEM Observations and X-ray Microanalysis

The morphology of nanoparticles was assessed by direct observation of suspension of *n*CeO_2 or *n*TiO_2 nanoparticles under the transmission electron microscope (TEM). Drops of suspensions (prepared as described above) were placed on carbon-formvar coated nickel grids, dried at room temperature and observed under a Philips CM 10 (FEI, Eindhoven, The Netherlands) TEM, operating at 80 kV.

For microscopic analyses in planta, tissues from seedlings treated with *n*CO_2 or *n*TiO_2 at 1000 and 2000 mg l^{-1} were sampled as in the root elongation experiment were sampled. Roots and shoots were excised, cut into small portions (2x3 mm) and fixed for 2 h at 4 °C in 0.1% (w/v) buffered sodium phosphate and 3% (w/v) glutaraldehyde at pH 7.2. They were then post-fixed with 1% osmium tetroxide (w/v) in the same buffer for 2 h, dehydrated in an ethanol series, and embedded in Epon/Araldite epoxy resin (Electron Microscopy Sciences, Fort Washington, PA, USA). For conventional TEM observations, serial ultrathin sections from embedded leaf tissues were cut with a diamond knife, mounted on uncoated 200 mesh copper grids (Electron Microscopy Sciences, Fort Washington, PA, USA), stained in uranyl acetate and lead citrate, and then observed under TEM as reported above. For X-ray microanalysis, unstained ultrathin sections were placed on formvar/carbon-coated 200 mesh nickel grids and dried at room temperature. The nature of nanoparticles observed in plant tissues was determined by a TEM (PHILIPS CM 12, FEI, Eindhoven the Netherlands) equipped with an EDS-X-ray microanalysis system (EDAX, AMETEK

Mahwah NJ, USA, software EDAX Genesis). The images were recorded by a Megaview G2 CCD Camera (Olympus; software iTEM FEI, AnalySIS Image Processing).

4.2.9 Data Analysis

One-way analysis of variance (ANOVA) was conducted to test differences in the plants' behavior. Tukey's Multiple Comparison test at 0.05 p level were used to compare means. Statistical analyses were performed using the SPSS program (SPSS Inc. Chicago, IL, USA, ver. 17). Principal Coordinate Analysis (PCoA) was computed based on the binary genetic distance option in GenAlEx v. 6.501 software (Peakall and Smouse, 2012). Graphics were produced using CoPlot (CoHort ver. 6.204,Monterey, CA, USA).

4.3 Results

4.3.1 Nanoparticles Characterization

The specific surface values obtained by BET measurements were 46.1 m^2 g^{-1} for *n*CeO_2 and 61.6 m^2 g^{-1} for *n*TiO_2. The Z-average sizes of the *n*CeO_2 and *n*TiO_2 suspended in deionized water were 174 ± 1.2 nm and 925 ± 105 nm, respectively, these values result remarkable higher respect the declared producer dimensions. The zeta potentials were 0.027 ± 0.064 mV for *n*CeO2 and 19.9 ± 0.55 mV *n*TiO_2. These parameter values put in evidence their instability, in fact for both nanoparticle types are included in the range of the nanoparticle instability (- 30 mV ÷ + 30 mV) and justify the differences between the declared dimension and the measured ones. The PDI of 212 *n*CeO_2 and *n*TiO_2 were 0.339 ± 0.011 and 0.841 ± 0.173, respectively. These values indicate a narrow dimensional distribution of *n*CeO_2 respect to *n*TiO_2.

4.3.2 Caryopses Germination and Root Elongation

Effects of *n*CeO_2 and *n*TiO_2 on caryopses germination and root growth are shown in Table 1.

Table 1: Germination percentage of seeds, number of seminal roots and root length in barley seedlings treated with 0, 500, 100, and 2000 mg l^{-1} of *n*CeO_2 and *n*TiO_2. Values are mean ± SE (n=3). Different letters indicate statistical difference between treatments at Tuckey's test ($p<0.05$).

	nCeO_2			*n*TiO_2		
Treatment	Germination (%)	Seminal roots (n)	Root length (mm)	Germination (%)	Seminal roots (n)	Root length (mm)
Ctrl	87±1.76 a	5.2 ± 0.18 a	52.7 ± 4.13 a	88 ± 1.20 a	6.6 ± 0.34 a	53.3 ± 3.03 a
500 mg l^{-1}	83 ± 2.03 a	5.5 ± 0.22 a	39.8 ± 2.24 b	87 ± 1.76 a	6.1 ± 0.27 a	45.4 ± 2.85 b
1000 mg l^{-1}	80 ± 2.08 a	5.2 ± 0.26 a	45.8 ± 17.8 ab	85 ± 1.45 a	6.5 ± 0.22 a	53.9 ± 3.13 a
2000 mg l^{-1}	79 ± 1.86 a	4.9 ± 0.25 a	43.8 ± 1.72 ab	87 ± 1.76 a	6.4 ± 0.13 a	58.5 ± 2.97 a

Since there was not a statistically significant effect of concentrations for *n*CeO_2 and *n*TiO_2, our results demonstrate that, even at the highest level of concentration, caryopses germination is not affected by *n*CeO_2 or *n*TiO_2 (Table 1). At the end of our experiment, the barley seedlings had reached coleoptile emergence. At this stage typically has between six and seven seminal roots (Knipfer and Fricke, 2011). In our experiment, the number of seminal roots was not affected by *n*CeO_2 and *n*TiO_2 (Table 1). On the contrary, in both cases the development of root tissues was influenced in a similar manner by the treatments. In fact, there was a significant effect of both *n*CeO_2 ($p<0.05$) and *n*TiO_2 ($p<0.05$) on the average length of the seminal roots. Post hoc comparison tests indicated that root elongation in seedlings treated with 500 mg l^{-1} *n*CeO_2 and *n*TiO_2 was significantly lower than controls (-24.5% and -14.8%, respectively). At higher *n*CeO_2 and *n*TiO_2 concentrations we would have expected to see a further reduction in the development of seminal roots. However, this did not occur since the average length of seminal roots was similar to controls (Table 1).

4.3.3 Cerium and Titanium in Plant Tissues

Although without visible symptoms of phytotoxicity, the concentration of total Ce and Ti in the issues of barley seedlings showed (i) a dose-response and (ii) a different magnitude

of accumulation between Ce and Ti. Table 2 shows the concentration of Ce and Ti in the fractions of barley seedlings.

Table 2: Concentration of total Ce and Ti in roots and shoots of barley seedlings treated with 0, 500, 100, and 2000 mg l^{-1} of *n*CeO_2 and *n*TiO_2. Values are mean ± SE (n=3). Different letters indicate statistical difference between treatments at Tuckey's test

Treatment	Ce roots (mg kg^{-1} DW)	Ce coleoptile (mg kg^{-1} DW)	Ti roots (mg kg^{-1} DW)	Ti coleoptile (mg kg^{-1} DW)
Ctrl	< d.l.	< d.l.	< d.l.	< d.l.
500 mg l^{-1}	579 ± 168 b	38.3 ± 5.77 b	< d.l.	< d.l.
1000 mg l^{-1}	5262 ± 1751 b	98.1 ± 40.2 b	35.2 ± 17.3 b	7.83 ± 3.3 b
2000 mg l^{-1}	20,714 ± 5722 a	622 ± 95.1 a	412 ± 127 a	26.2 ± 8.71 a

As expected Ce and Ti accumulated much more within root tissues than in the shoot ($p<0.05$). Ce concentration in the roots increased significantly ($p<0.05$) as the concentration of *n*CeO_2 in the growth medium increased (Table 2). A statistically significant effect of treatments in Ce accumulation in the shoots ($p<0.001$) was verified. Mean comparisons showed differences among the treatments. Ce concentration in shoots did not significantly differ between the 500 and 1000 mg l^{-1} Ce treatment (38.3 and 98.1 mg Ce kg^{-1} DW, respectively), whereas at 2000 mg *n*CeO_2 l^{-1} a Ce concentration of 622 mg Ce kg^{-1} DW was observed in the shoots, which is significantly different from other values (Table 2).

Titanium concentrations in barley roots and shoots were one-two orders of magnitude lower compared to Ce. However, also in this case a statistically significant dose dependent increase was also observed. With the lowest *n*TiO_2 treatment (500 mg l^{-1}) Ti concentration in roots was negligible and no Ti was detected in shoots (Table 2). At the intermediate *n*TiO_2 treatment (1000 mg l^{-1}) the root tissues had 37.2 mg Ti kg^{-1} DW which is significantly lower ($p=0.0001$) than 413 mg Ti kg^{-1} DW found at highest *n*TiO_2 treatment (Table 2). Finally, we verified that also Ti concentration in the shoots also responded positively to the treatments ($p <0.001$). The mean Ti concentration detected in barley shoots were 7.83 mg kg^{-1} DW and 26.2 mg kg^{-1} DW for 1000 and 2000 mg *n*TiO_2 l^{-1}, respectively (Table 2).

4.3.4 Ce and Ti Nano-aggregates in Plant Tissues

The morphology of *n*CeO_2 and *n*TiO_2 NPs is visible in Figure 1A and 1B, respectively.

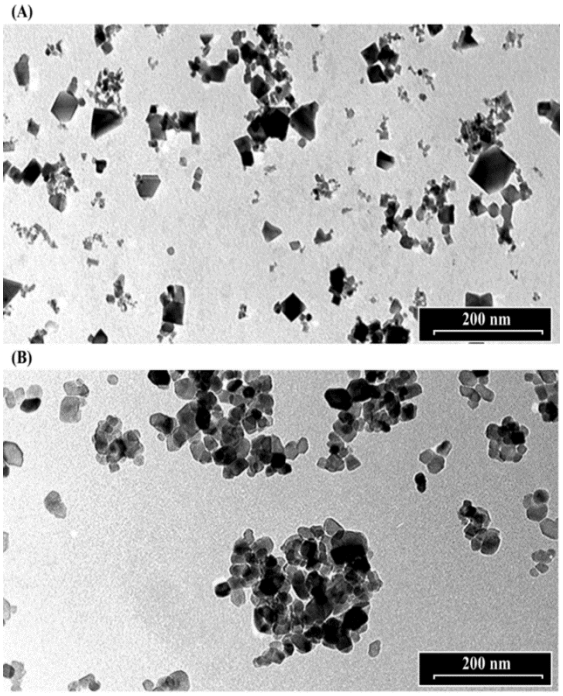

Figure 1: Transmission electron microscope images of 1000 mg l^{-1} suspensions of (A) *n*CeO_2 and (B) *n*TiO_2.

Transmission electron microscopy analysis demonstrated that CeO_2 particles exhibited an approximate equi-axes shape with sharp edges (Figure 1A), while particle sharp edges are less evident in TiO_2. To assess the possible uptake of *n*CeO_2 or *n*TiO_2 from the culture medium to the root tissues and the translocation to the different parts of the plantlets, we performed ultrastructural analyses on roots and shoot tissues. Several clusters of NPs were found in cortical parenchymal tissues of roots, both in the case of *n*CeO_2 (Figure 2A) and *n*TiO_2 treatment, at all concentrations.

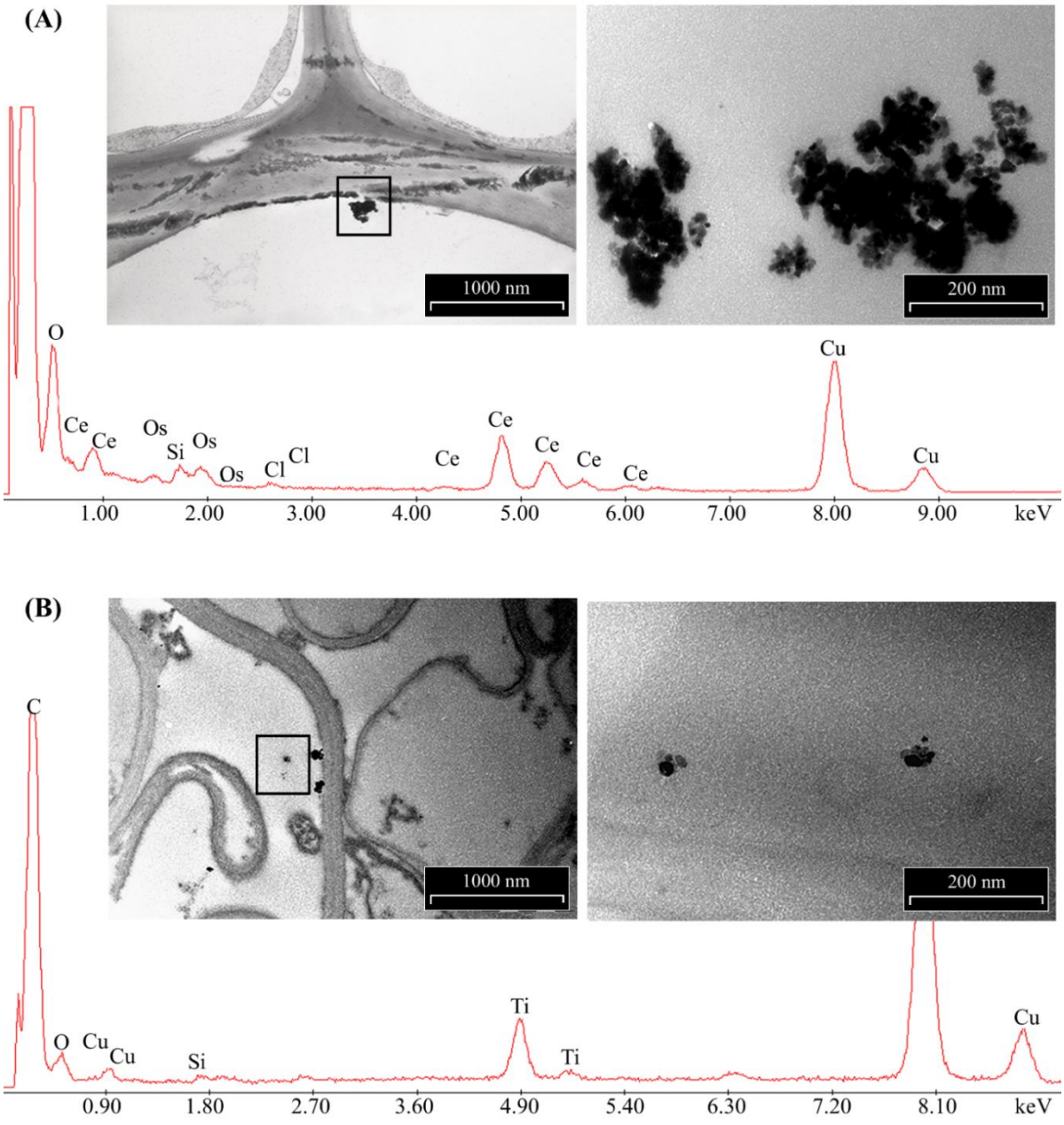

Figure 2: Representative images of electron dense precipitates recovered in root tissues of *Hordeum vulgare* exposed to 1000 mg l^{-1} of (A) *n*CeO_2 and (B) *n*TiO_2 and X-ray spectra of elements recovered in. Insets represent enlarged regions where X-ray microanalyses have been performed. Presence of C, Os were due to sample preparation, Cu to the grids used as section support.

Clusters were also observed in the xylem, even if in to lesser extent (Figure 2B). EDS-X ray microanalysis allowed the identification of the clusters as aggregates of Ce and Ti nanoparticles.

No NPs were detected in the shoots of *n*CeO_2 or *n*TiO_2 treated plantlets. The ultrastructure of all observed tissues appeared preserved. No necrosis or damage to membranes, nor cell modifications were detected. In general, the cell compartments were not significantly

affected by treatments, except for the nuclei of parenchymal cells of root and shoot of seedlings treated with nCeO$_2$ (1000 and 2000 mg l^{-1}), which showed compact chromatin (Figure 3A-D).

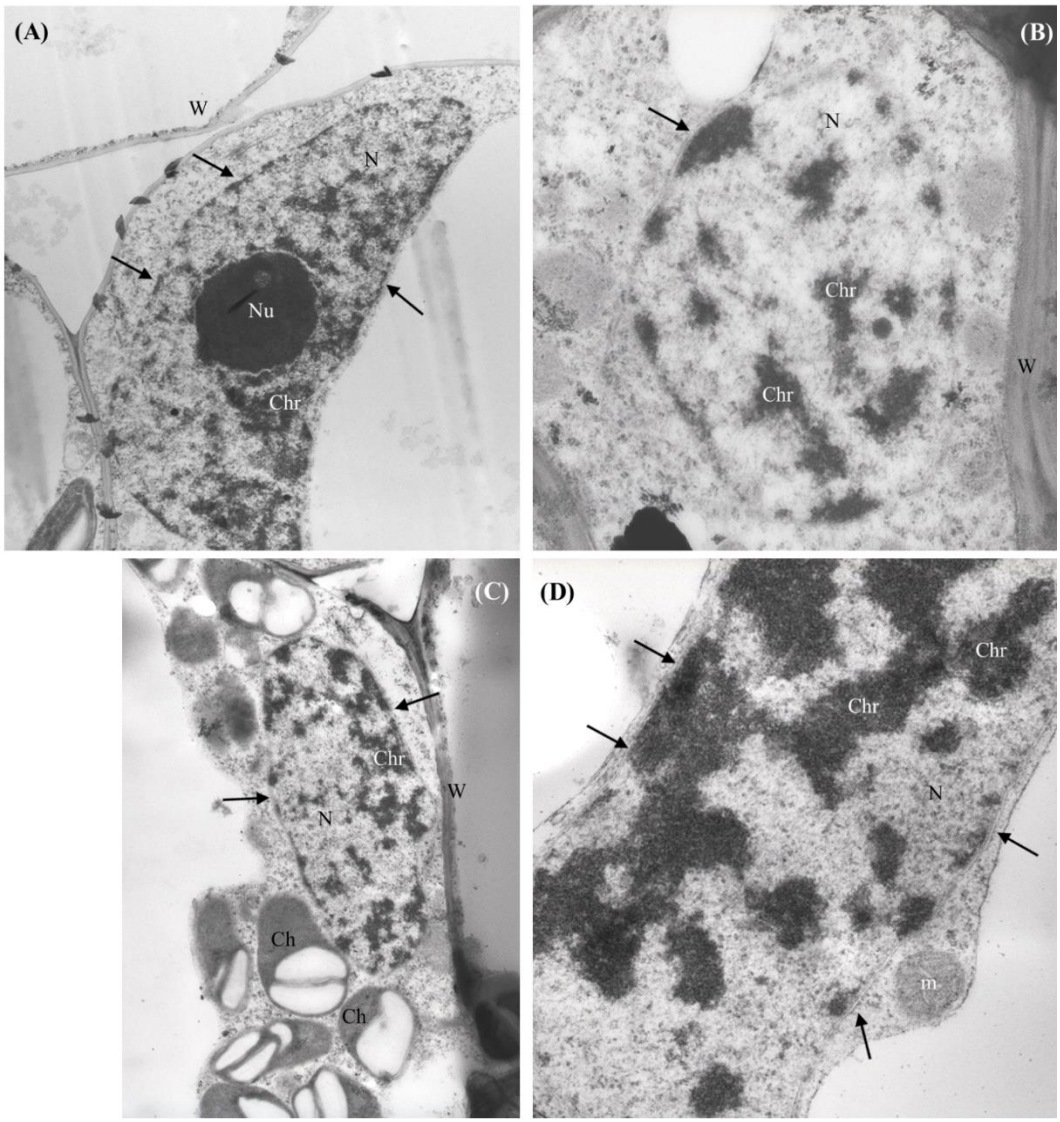

Figure 3: Representative micrographs of nuclei (N) from shoot (A, B and C) and root (D) parenchymal cells of *H. vulgare*. (A) control untreated shoot: nucleus presents regular shape, nuclear membranes are intact (arrows), nucleolus (Nu) and chromatin (Chr) appear normally dispersed. (B-C) 1000 mg nCeO$_2$ l^{-1}- treated shoot and (D), 1000 mg nCeO$_2$ l^{-1}- treated root: nuclei still present normal shape and apparently undamaged membranes, while chromatin shows condensation. (Ch, chloroplasts; m, mitochondrion).

4.3.5 ATP and ROS

The evaluation of ATP concentration aimed to evidence the energetic status in different fractions of barley seedlings exposed to nCeO$_2$ and nTiO$_2$. The different concentrations of

nCeO_2 induced a statistically significant effect (Figure 4), with a trend of values peaking at 500 and 1000 mg l^{-1}, in root and lowering at 2000 mg l^{-1} in shoot samples.

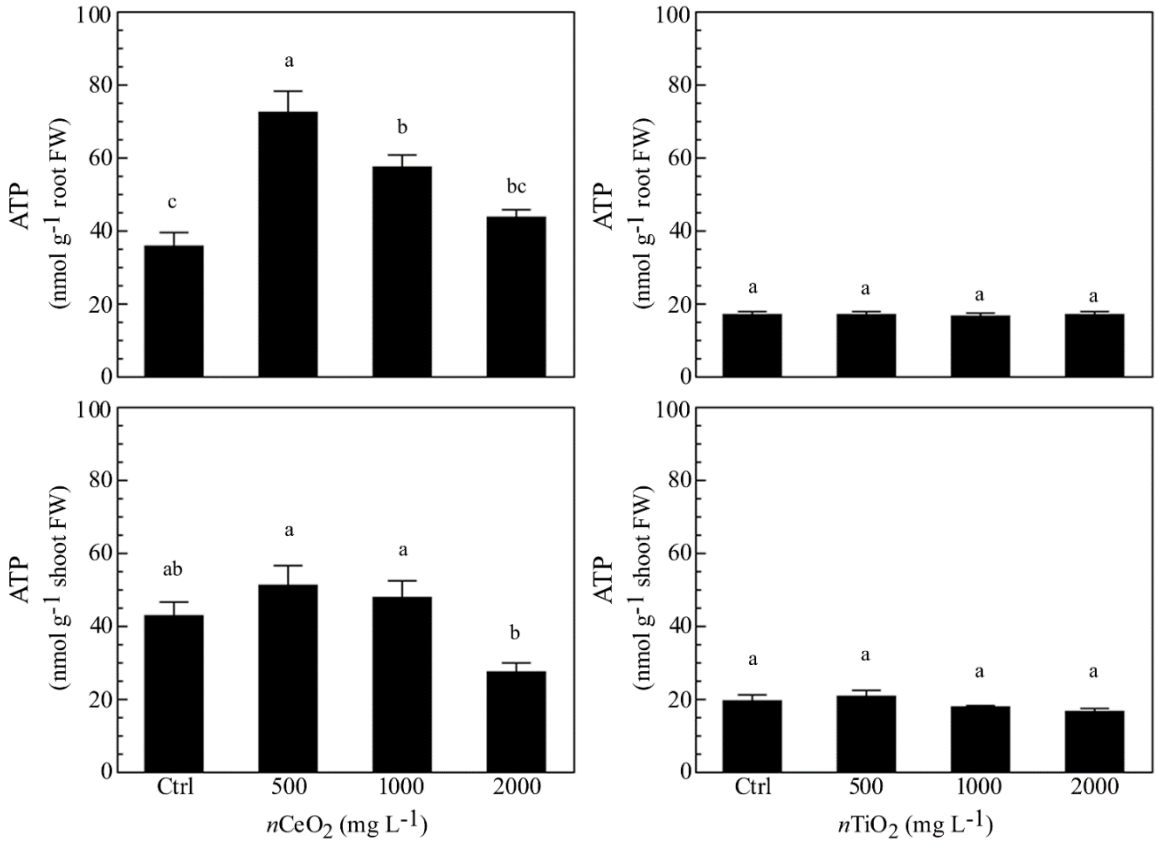

Figure 4: Determination of ATP concentration in extracts obtained from plantlets of barley roots and shoots, grown on wet paper filters, in the presence of different concentrations of *n*CeO_2 and *n*TiO_2.

The highest *n*CeO_2 (2000 mg l^{-1}) reached a low concentration of ATP in roots, statistically comparable to control samples. On the contrary, *n*TiO_2 induce no significant changes of ATP concentration, since different *n*TiO_2 doses were similar to the controls in both roots and shoots (Figure 4). The measurement of ROS was performed as marker for oxidative stress. Similarly to ATP content, *n*CeO_2 were able to induce an increase of a ROS formation at all the concentrations assayed (Figure 5), in comparison with the control, although no statistically significant differences were observed.

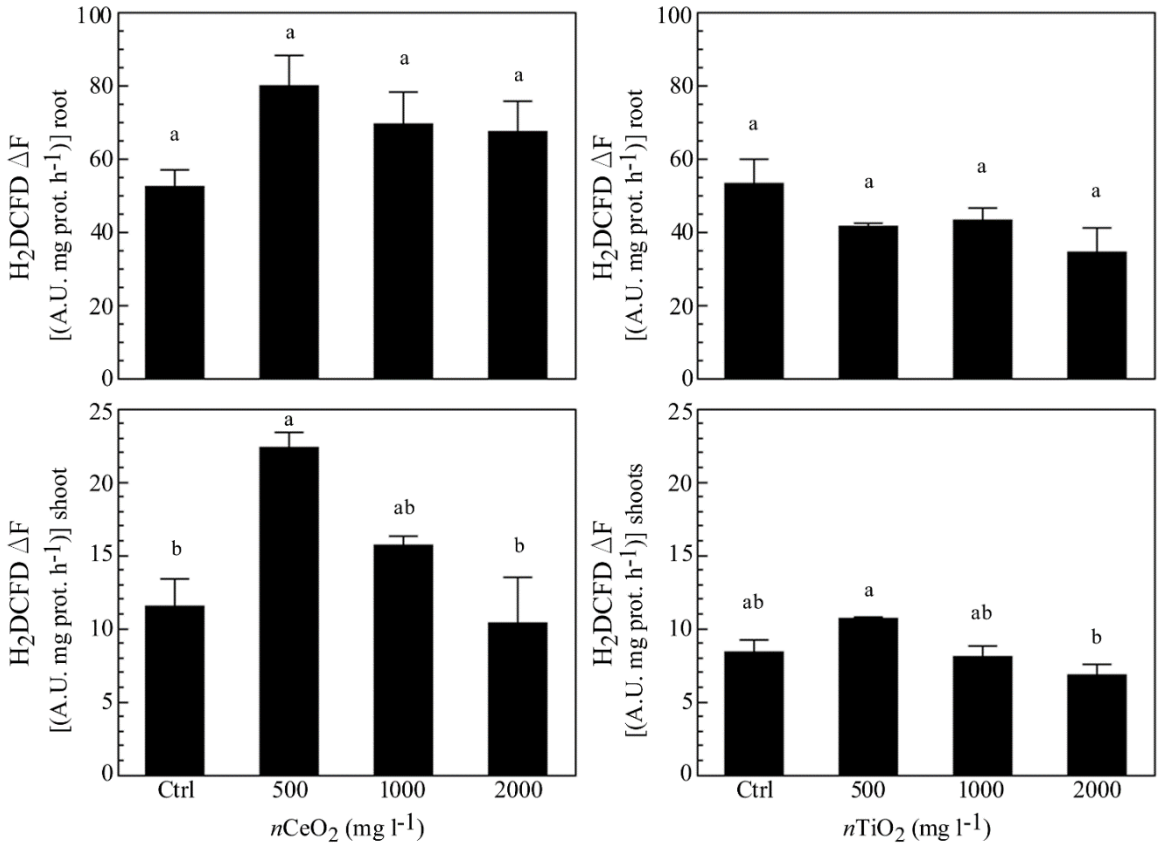

Figure 5: Evaluation of ROS evolution in extracts obtained from plantlets of barley roots and shoots, grown on wet paper filters, in the presence of different concentrations of *n*CeO_2 and *n*TiO_2. The analysis was performed by means of a fluorimetric probe.

Also for this parameter, a trend with a peak at 500 mg l^{-1} was present in both roots and shoots. In the case of *n*TiO_2 (Figure 5), the treatments did not show any difference, if compared with the control in roots, whereas a decrease of ROS level was observed at the higher dose (2000 mg l^{-1}) in shoots.

4.3.6 Mitotic Index and RAPDs

The mitotic index was significantly reduced by *n*CeO_2 2000 mg l^{-1} (from 4 ± 1.2% in the control to 2.4 ± 1.2%). Instead, the *n*CeO_2 500 and 1000 mg l^{-1} treatments with mean values of 4 ± 1.3% were very similar to the control (Figure 6A). The treatments with *n*TiO_2 with values of 6.2 ± 3.2%, 4.6 ± 3.2%, 4.9 ± 2.5% for the concentration at 500, 1000 and 2000 mg l^{-1}, respectively, were not significantly different from the control (4.9 ± 2.8%) (Figure 6A).

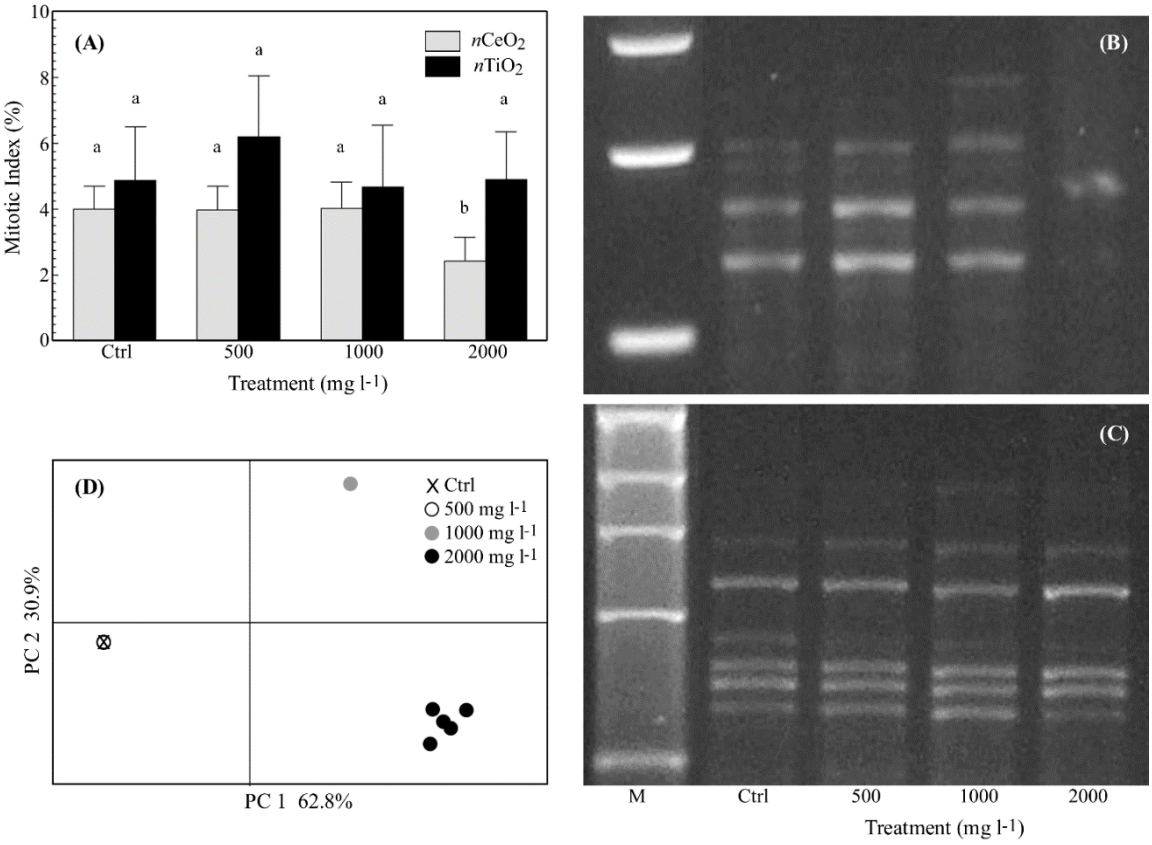

Figure 6: (A) Mitotic index (%) (mean ± SE) observed in root tips of seedlings of barley treated with 0-2000 mg l^{-1} of *n*CeO_2 and *n*TiO_2. Different letters indicate statistical difference between treatments at Tuckey's test ($p<0.05$). (B-C) Representative RAPD profiles from the roots of barley seedlings treated with *n*CeO_2 (B) or nTiO_2 (C) at control, 500-2000 mg l^{-1}. The shown RAPD profiles were generated using primer OPA04 for *n*CeO_2 (it is shown an enlargement around polymorphic zone) and OPB12 for *n*TiO_2. The first line is a 1 kb DNA marker (M). (D) Principal coordinate analysis (PCoA) based on RAPD profiles from the barley roots with *n*CeO_2. Values on axes indicate the variance explained.

The six primers used for the RAPD analysis amplified for a total of 40 representative bands in controls with a variable number of 3 to 9 (9, 5, 6, 3, 9, 8 bands respectively for OPA04, OPB01, OPA10, OPB20, OPB12 and OPB03). Amplification was highly reproducible since the same RAPD profile was observed within control replicates. A concentration effect was observed for the *n*CeO_2 treatments on the RAPD profiles. The same banding pattern as controls was obtained for the *n*CeO_2 500 mg l^{-1} treatment, whereas new profiles at 1000 mg l^{-1} were observed and 3 additional bands appeared and 8 disappeared. Even greater variability was observed at *n*CeO_2 2000 mg l^{-1} with a total of 20 differences (appearing and disappearing bands) in treated plants (Figure 6B-C). The results were summarized by Principal Coordinates Analysis (PCoA), with almost 94% of the total variability explained by the two axes (Figure 6D). The overlap of the control and 500 mg l^{-1} treatments is notable,

while the treatments at 1000 and 2000 mg l^{-1} are well separated in different quadrants. The band polymorphism in the different replicates at the higher concentration (2000 mg l^{-1}) can be noticed by the point cloud (Figure 6D). In a similar way to what was observed fro the mitotic index, the *n*TiO_2 treatments at each concentration have no effect on the RAPD profiles (Figure 6D).

4.4 Discussion

Since plant nanotoxicology is a new field of investigation, specific ecotoxicological methods for the estimation of toxicity of ENPs have not yet been developed (Jośko and Oleszczuk, 2014). According to OECD guidelines, the acute effects of MeNPs on plant physiology are currently investigated by adapting the methods already used for traditional contaminants (Kühnel and Nickel, 2014). Evidence of MeNPs plant uptake and toxicity are still scarce and contradictory (Etheridge et al., 2013). This is likely because, compared to their bulk counterparts, MeNPs show particular properties, which are subjected to transformations (e.g. redox reactions, aggregation or agglomeration and dissolution) according to different environmental factors. These changes might modify the ecotoxicological properties of MeNPs and thus, their interactions with the biota (Nowack et al., 2012; Maurer-Jones et al., 2013). However, despite these limitations, the experimental results obtained so far offer early indications on MeNPs phytotoxicity (Li et al., 2015; Rico et al., 2015a). Our data suggests that also in very simple experimental conditions, *n*TiO_2, as expected taking into account their intrinsic properties, forms bigger agglomerates with a wider dimensional distribution than *n*CeO_2.

4.4.1 *n*CeO_2 and *n*TiO_2 Affects Seed Germination and Seedling Development

Previous studies carried out in controlled conditions reported that the toxicity of MeNPs in the early stages of plant growth is likely due to the following factors: (i) chemical and physical properties which influence the release of ions or the aggregation of particles in more stable forms and (ii) the size and shape of the particles, which determine the specific surface area of MeNPs (Yang and Watts, 2005; Lin and Xing, 2007).

In agreement with Rico et al. (2015b), we found that germination of barley was unaffected by 500-2000 mg l^{-1} *n*CeO_2. This is in contrast with the results provided by López-Moreno et al. (2010a) who reported that suspensions of 2000 mg l^{-1} *n*CeO_2 significantly reduced seed germination in maize, cucumber, tomato, and soybean. Possible explanations could be

the greater Ce tolerance of barley to the treatment if compared to other species and/or to the very small size of Ce nanoparticles they used (7 nm). Another explanation could be related to the chemical and physical properties of *n*CeO_2, in particular his zeta potential value. This parameter is the cause of the agglomeration behavior of the *n*CeO_2 that brings to a low bioavailability and the absence of phytotoxic effects on the treated seeds regards the germination percentage.

Another important issue that plays a role on seed/nanoparticle interaction, is the methodology adopted for seed treatment. In fact, following Lin and Xing (2007), we prepared the barley seeds for germination trials by soaking them in distilled water before starting treatments, whereas López- Moreno et al. (2010a) soaked the seeds directly in the *n*CeO_2 suspensions. This different experimental approach could result in a different exposure of germinating seeds to *n*CeO_2.

As regards Ti, there is a substantial agreement in literature on the fact that suspensions of *n*TiO_2 do not affect seed germination, with few exceptions, as reported by Zheng et al. (2005) and Feizi et al. (2012). Our results are in accordance with those reported by other authors on rice, lettuce, radish, cucumber, tomato and pea (Boonyanitipong et al., 2011; Wu et al., 2012; Song et al., 2013a; Fan et al., 2014).

Besides the germination percentage, we observed a negative influence of the treatments with *n*CeO_2 and *n*TiO_2 on root elongation in barley seedlings. However, this did not occur in seedlings treated with *n*CeO_2 at the highest concentration, in which the root length was very similar to controls. In addition, in this case the literature reports contradictory evidence. López-Moreno et al. (2010a) reported that the root growth in maize and cucumber seedlings was significantly promoted by *n*CeO_2 (up to 4000 mg l^{-1}) whereas the same treatments resulted in a negative effect on root development in alfalfa and tomato. An inhibitory effect of *n*TiO_2 on root elongation in cucumber was reported by Mushtaq. (2011). A decrease in the number of secondary lateral roots in pea seedlings was verified by Fan et al. (2014), whereas Boonyanitipong et al. (2011) did not record any effect on root length in rice seedlings exposed to *n*TiO_2. In our case, the different effect of the *n*CeO_2 and *n*TiO_2 on the root elongation is likely due to their different grade of agglomeration demonstrated by the z-average size and PDI values of *n*TiO_2 that results significantly higher than *n*CeO_2.

It might happen that the quantification analysis of trace metals in plant roots is disturbed by external contamination. In this case, the concentration of the element in the plant tissues could be significantly overestimated due to a fraction of metal, which is not taken up but simply adsorbed onto the external root surface. In our experiment, a concentration of Ce

about 60 times greater than Ti, was found in barley root tissues. This substantial difference indicates that the procedures for preparation of the samples were conducted properly; otherwise, we would also have very high concentrations also for Ti.

Our results showed that the exposure of *H. vulgare* to *n*CeO_2, which are smaller and less aggregated than *n*TiO_2, resulted in a greater total Ce concentration in roots compared to Ti. In can therefore be assumed that, for some still unknown reasons, the model of root uptake of the two elements could differ, depending in part on the intrinsic properties of solubility and agglomeration properties of *n*CeO_2 and *n*TiO_2. On the other hand, this is in agreement with the findings by Zhang et al. (2011), who verified that cucumber roots absorbed higher amounts of 7 nm *n*CeO_2 than 25 nm ones. On the other, some studies pointed out the possibility of interactions between the root metabolism and MeNPs. Lin and Xing (2007) demonstrated that root exudates such as proteins, phenolic acids, and aminoacids have a role in the adsorption of ZnO nanoparticles to the root surface of perennial rye grass. More recently, Schwabe et al. (2015) observed that root uptake of dissolved Ce(III) was promoted by the dissolution of *n*CeO_2 at the medium-root interface in hydroponically growth sunflower and maize. A further confirmation about the role of root exudates on the adsorption of MeNPs was provided by Ma et al. (2015) and Lv et al. (2015), respectively for *n*CeO_2 and *n*ZnO, respectively. However, Lv et al. (2015) reported that a possible access of *n*ZnO to the root tissues could be through the root apex or the meristematic zone to the lateral root system where the Casparian strip is not yet developed.

Root-to-shoot translocation of *n*CeO_2 has been previously described in soybean (Priester et al., 2012), tomato (Wang et al., 2012), cucumber (Zhao et al., 2013) and cotton (Van Nhan et al., 2015) after treatments with *n*CeO_2 suspensions. Different observations have been made on *n*CeO_2 root-to-shoot translocation in graminaceous crops. Schwabe et al. (2013) reported that wheat does not translocate *n*CeO_2 into the aerial tissues, whereas Rico et al. (2013, 2015a) reported the translocation of *n*CeO_2 from roots to rice grains and maize kernels, respectively. According to Rico et al. (2015b), we report evidence of Ce translocation from roots to the aerial part of barley. As regards Ti uptake and translocation, fewer data are available in the literature compared. However, our data are consistent with the findings reported by Song et al. (2013b) on tomato seedlings exposed to Ti at concentrations ranging from 50 to 5000 mg l^{-1}.

Finally, we reported that root length in barley seedlings treated with 500 mg *n*CeO_2 l^{-1} was significantly shorter than controls. This apparent dose-effect was not confirmed at higher *n*CeO_2 concentrations, since the root length was similar to that of controls. Similar evidence

was reported by López-Moreno et al. (2010a). According to Nascarella and Calabrese (Nascarella and Calabrese, 2012) and Bell et al. (2014), such unexpected results might be interpreted as a hormetic effect of *n*CeO_2 on root elongation in barley seedlings.

4.4.2 Plant Stress Induced by Nanoparticle Treatments

Within the plants, nanoparticles may interact with the host cells, causing different effects, ranging from cell death (if the host is sensitive) to not relevant cell modifications (in the case of host tolerance), depending on their type, shape and concentration (Rico et al., 2011; Gardea-Torresdey et al., 2014). The microscopic observations on barley seedlings indicated that both *n*CeO_2 and *n*TiO_2, at the used concentrations used, were able to enter the root tissues, being detected in the parenchymal cells and xylem vessels. Even though we did not observe Ce and Ti crystalline aggregates in the shoots, ICP analyses suggested a root-to-shoot mobilization of Ce and Ti ions. At histological level the accumulation of such elements induced limited injuries. On the contrary, important differences in the effects of treatments were obtained at nuclear level, where only the *n*CeO_2 treatments induced visible modifications in the chromatin aggregation in the nuclei of root and shoot parenchymal cells.

Condensed chromatin and fragmented nuclei are described as part of the programmed cell death (PCD), occurring in response to different environmental stimuli and stresses, induced by pathogens (Lam et al., 2001) and by diverse abiotic factors (White, 1996; Kratsch and Wise, 2000) including the exposition to nanomaterials (Shen et al., 2010). PCD plays an important role in mediating plant adaptation to the environment. In cells that undergo programmed death, chromatin condenses into masses with sharp margins, and DNA is hydrolyzed into a series of fragments (Gladish et al., 2006). Dynamic compaction of chromatin is an important step in the DNA-damage response, because it activates DNA-damage-repair signaling (Burgess et al., 2014) in response to injuries.

The hypothesis of Ce-induced DNA damage in treated seedlings finds further support in the results obtained with the RAPD test. RAPD can potentially detect a broad range of DNA damage and mutations, so it is suitable for studying MeNPs genotoxicity (Atienzar and Jha, 2006). The RAPD modified patterns at high concentrations of *n*CeO_2 (1000-2000 mg l^{-1}) indicated a genotoxic effect, which could directly influence the cell cycle. This is further confirmed by the reduced mitotic index recorded in the samples treated with *n*CeO_2 2000 mg l^{-1}, which clearly demonstrated the negative effect of high *n*CeO_2 concentrations on the cell cycle. Our results are in agreement with López- Moreno et al. (2010b), who

demonstrated *n*CeO_2 genotoxicity on soybean plants subjected to treatments similar to those reported in our work.

It is still far too early to conclude if the observed effects were direct or indirect consequences of the treatments, since *n*CeO_2 were not found in the nucleus. As it is known that increasing oxidative stress leads to DNA damage, the higher presence of ROS in treated samples could cause modification in RAPD patterns. However, as our analysis on ROS indicated a peak at 500 mg *n*CeO_2 l^{-1}, it can be rationalized that lower concentrations triggered an initial oxidative signal, while only higher *n*CeO_2 doses were able to induce damage at nuclear level. The oxidative stress peak at 500 mg l^{-1} dose and could be rationalized by the well-known SOD mimetic activity attributable to *n*CeO_2, which could cause a dismutation of superoxide anions into H_2O_2. Since a similar pattern is also found for ATP measured in *n*CeO_2 treated tissues, it is suggested that the oxidative burst induced by the more effective dose of *n*CeO_2 could be associated to a stimulation of cellular respiration and a consequent increase in ATP production. This could be due to a defense response signal or an increased requirement for energy (Vranová et al., 2002).

On the contrary, the *n*TiO_2 treatments did not influence either the mitotic index or RAPD pattern. This is in contrast to Moreno-Olivas et al. (2014) who observed *n*TiO_2-induced genotoxicity in hydroponically cultivated zucchini. As the size of *n*TiO_2 they reported is comparable to that used in our work, the different results obtained can be explained by (i) the different cultivation systems (Petri dishes vs. full nutrient solution in hydroponics) and (ii) the *n*TiO_2 concentration used by Moreno-Olivas et al. (2014 ten-fold smaller). The latter potentially prevents the formation of big nanoparticle agglomerates, making them more bioavailable.

4.5 Conclusion

Although investigations into the effects of NPs in plants continue to increase, there are still many unresolved issues and challenges, in particular at the biota-nanomaterial interface (Nowack et al., 2015). In this multidisciplinary work, we studied the phytotoxic and genotoxic impact of *n*CeO_2 and *n*TiO_2 cerium and titanium oxide nanoparticle suspensions on the early growth of barley. Seed germination was not affected by the *n*CeO_2 and *n*TiO_2 suspensions, indicating that *n*CeO_2 and *n*TiO_2 are not allowed to enter the seed coatings. However, we verified that the concentration of Ce and Ti in the seedling fractions, as well as the root-to-shoot translocation, were dose-dependent. Then, we found signals of

genotoxicity (RAPD banding patterns and mitotic index) and phytotoxicity in root cells (oxidative stress and chromatin modifications) resulting in a shortage of root elongation.

The different magnitude of bioaccumulation of Ce and Ti suggests a different uptake mechanism, likely due to the different behaviour of *n*CeO_2 and *n*TiO_2,. Recent studies have shown that plant toxic effects of nanomaterials are not merely due to the particle size and concentration of a suspension. Phytotoxicity of metal oxide nanoparticles is related both to the direct adsorption of particles onto the root structures and to the aptitude of the metal ion to dissolve, possibly mediated by binding molecules roduced by plants in the medium-root interface.

Our study had not the objective to investigate the details of the mechanisms by which the NPs entering within the roots. However, we verified the presence of both *n*CeO_2 and *n*TiO_2 into the root cells where an increase in oxidative stress occurred. More research needs to be conducted to verify whether germination can be affected by smaller *n*CeO_2 and *n*TiO_2. In addition, we need to understand if modification of the physical-chemical properties of nanoparticles at the root interface can foster the plant uptake of Ce and Ti forms.

International Journal of
Environmental Research and Public Health

MDPI

Article

Changes in Physiological and Agronomical Parameters of Barley (*Hordeum vulgare*) Exposed to Cerium and Titanium Dioxide Nanoparticles

Luca Marchiol [1,*], Alessandro Mattiello [1,†], Filip Pošćić [1,†], Guido Fellet [1,†], Costanza Zavalloni [1,2], Elvio Carlino [3] and Rita Musetti [1]

1 DI4A—Department of Agriculture, Food, Environment and Animal Sciences—University of Udine, via delle Scienze 206, I-33100 Udine, Italy; alessandro.mattiello@uniud.it (A.M.); filip.poscic@uniud.it (F.P.); guido.fellet@uniud.it (G.F.); czavalloni@csustan.edu (C.Z.); rita.musetti@uniud.it (R.M.)

2 Agriculture Studies Department, California State University Stanislaus, One University Circle, Turlock, CA 95382, USA

3 IOM-CNR Laboratorio TASC, Area Science Park Basovizza, Bld MM, SS 14, Km 163.5, 34149 Trieste, Italy; carlino@iom.cnr.it

* Correspondence: marchiol@uniud.it; Tel.: +39-432-558-611; Fax: +39-432-558-603

† These authors contributed equally to this work.

Academic Editor: Mónica Amorim
Received: 19 January 2016; Accepted: 14 March 2016; Published: 17 March 2016

Abstract: The aims of our experiment were to evaluate the uptake and translocation of cerium and titanium oxide nanoparticles and to verify their effects on the growth cycle of barley (*Hordeum vulgare* L.). Barley plants were grown to physiological maturity in soil enriched with either 0, 500 or 1000 mg· kg^{-1} cerium oxide nanoparticles ($n CeO_2$) or titanium oxide nanoparticles ($n TiO_2$) and their combination. The growth cycle of $n CeO_2$ and $n TiO_2$ treated plants was about 10 days longer than the controls. In $n CeO_2$ treated plants the number of tillers, leaf area and the number of spikes per plant were reduced respectively by 35.5%, 28.3% and 30% ($p \leqslant 0.05$). $n TiO_2$ stimulated plant growth and compensated for the adverse effects of $n CeO_2$. Concentrations of Ce and Ti in aboveground plant fractions were minute. The fate of nanomaterials within the plant tissues was different. Crystalline $n TiO_2$ aggregates were detected within the leaf tissues of barley, whereas $n CeO_2$ was not present in the form of nanoclusters.

Keywords: cerium oxide nanoparticles; titanium oxide nanoparticles; barley; plant growth; food chain

5.1 Background

The useful properties of engineered nanoscale materials (ENMs) have resulted in the rapid development of nanotechnologies and large-scale production of nanoparticles (NPs) or NP-containing products (Tourinho et al., 2012). The increasing use of ENMs may result in the rise in the flux of ENMs discharged into the environment. Water bodies and soil are assumed to be the primary environmental recipients of nanomaterials (Batley et al., 2013). Recent estimates included cerium oxide nanoparticles (nCeO$_2$) and titanium oxide nanoparticles (nTiO$_2$) among the 10 most commonly produced ENMs that are used worldwide. In the cosmetic industry, solar cells, paints, cements and coatings about 10,000 t of nTiO$_2$ are used per year (Piccinno et al., 2012). A number of applications of nTiO$_2$ are in use in the food industry and agriculture, serving as nano-sensors and nano-agents for new delivery systems of plant protection products and fertilizers (Gogos et al., 2012; Liu and Lal, 2015). Also, nCeO$_2$ have a broad range of industrial application as additives in glass and ceramics, fuel-cell materials and the automotive industry (Zhang et al., 2011). On the other hand, nCeO$_2$ and nTiO$_2$ are both included in the list of ENMs for immediate priority testing by the Organization for Economic Cooperation and Development (OECD, 2010). Vascular plants should be of particular concern as they interact closely with the environment and are conduits for bioaccumulation through the food chain (Rico et al., 2011; Miralles et al., 2012; Gardea-Torresdey et al., 2014; Capaldi Arruda et al., 2015).

Even though this subject is of primary importance, to date relatively few studies have been carried out on the responses of plants exposed to metal nanoparticles. Most of the currently available papers have reported data collected from experiments performed in hydroponic conditions (Zhang et al., 2011; OECD, 2010; Rico et al., 2011; Miralles et al., 2012; Gardea-Torresdey et al., 2014; Capaldi Arruda et al., 2015; López-Moreno et al., 2010a; Larue et al., 2012). Such approaches are not able to account for the complexity of the soil-plant system (Liang et al., 2013).

Early studies concerning the relationships between higher plants and nCeO$_2$ were mostly focused on the initial developmental stages of plants. López-Moreno et al. (2010a) observed seed germination and root elongation in cucumber, tomato, alfalfa and corn exposed to 0-4000 mg l^{-1} nCeO$_2$ with contradictory results. Ma et al. (2010) verified that the root growth of cabbage, cucumber, radish, rape, tomato, and wheat were not affected by 2000 mg l^{-1} nCeO$_2$. At the same concentration, the germination of soybean was undisturbed but indications of genotoxicity were reported by López-Moreno et al. (2010b).

The same authors demonstrated significant species-specific differential levels of plant uptake and translocation of Ce in plants exposed to 4000 mg l^{-1} of *n*CeO_2. Differences in root microstructures (e.g. pore size in root hairs) and physical and chemical interactions between *n*CeO_2 and root exudates in the rhizosphere could explain the differences. The movements of nCeO_2 within the morphological structures of soybean plants to the aerial tissues were verified by combining ICP-OES and μ-XANES analysis (Majumdar et al., 2014). More recently it was reported *n*CeO_2 induced compositional modifications in the root xylem in seedlings of rice, wheat and barley (Rico et al., 2015a). Finally, a life cycle study on barley grown in soil amended with 125-500 μg g^{-1} *n*CeO_2, reported both beneficial and harmful effects of nanoceria (Rico et al., 2015b).

The information on the effects of Ti nano-forms are controversial because several papers have demonstrated positive (Hong et al., 2005; Gao et al., 2006; Yang et al., 2007; Linglan et al., 2008; Qi et al., 2013) or negative (Asli and Neumann, 2009; Ruffini et al., 2011; Song et al., 2013) effects of *n*TiO_2 on plants. Recently, Frazier et al. (2014) reported that in plantlets exposed to *n*TiO_2 (range 1000-25,000 ppm) for three weeks the leaf count, root length and plant biomass significantly increased as Ti concentrations were raised. In contrast, Pakrashi et al. (2014) observed a dose-dependent decrease in the mitotic index and an increase in the number of chromosomal aberrations in root tips of *Allium cepa* exposed to 12.5-100 mg *n*TiO_2 ml^{-1}.

Modelling studies have predicted that ENMs released to the environment are likely to be mostly found in water, sediments, and soils (Keller et al., 2013; Liu and Cohen, 2014). Considering the increasing speed of nanotechnology development it is plausible to assume that different ENMS might be present simultaneously in the environmental compartments (water, sediments, soil and biota). Therefore, living organisms could be exposed to a co-occurrence of EMNs. However, this issue was poorly explored in literature and we are still lacking systematic and reliable information (Singh and Kumar, 2014). Moreover, most studies hitherto have only evaluated crop plants to the germination stages, and have not examined the complete developmental cycle.

Currently, nanotechnology is considered as an important tool in agriculture with the potential to provide new strategies to improve crop production for human consumption and animal feeding and promoting a reduction in the use of pesticides (Servin and White, 2016) Since several scientific evidences suggest that nanomaterials may induce harmful environmental effects, it is crucial to investigate on the impact of nanomaterials on crops.

In our study barley was considered as model crop since it is among the world's most important cereal crops (FAOSTAT, 2014).

In the present study, barley plants were grown for the whole crop cycle in a soil enriched with different levels of *n*CeO_2 and *n*TiO_2 and their combination in a fully factorial design. To the authors' knowledge, this is the first study that reports data on plants exposed simultaneously to different metal nanoparticles. We hypothesized that (i) the exposure of barley to *n*CeO_2 and *n*TiO_2 (also combined each other) would influence plant growth; that (ii) nanoparticles would influence plant physiology and that (iii) the concentration of *n*CeO_2 and *n*TiO_2 would affect the uptake of Ce and Ti in roots and the translocation of such elements in the vegetative plant fractions and in seeds.

5.2 Experimental Section

5.2.1 Characterization of *n*CeO_2 and *n*TiO_2

Cerium(IV) oxide nanopowder and titanium(IV) oxide anatase nanopowder both having a nominal average particle size of 25 nm were purchased from Sigma-Aldrich (Saint Louis, MO, USA). Particle characterization was carried out at the Facility for Environmental Nanoscience Analysis and Characterization (FENAC), University of Birmingham (UK).

The specific surface area of the *n*CeO_2 and *n*TiO_2 powders was measured by the Brunauer–Emmett–Teller (BET) method by using the Surface Area and Pore Size Analyser SA 3100 plus (Beckman Coulter, USA). The samples were outgassed at 300 °C for 180 minutes and the nitrogen adsorption-desorption isotherms were recorded at liquid nitrogen temperature (77K). The BET values were 46.1 $m^2 g^{-1}$ and 61.6 $m^2 g^{-1}$ for *n*CeO_2 and *n*TiO_2 respectively.

The size distribution of the *n*CeO_2 and *n*TiO_2 powders were measured by Atomic Force Microscopy (AFM) method using PSIA XE100 (Park System, Korea). The samples were prepared by spreading the *n*CeO_2 and *n*TiO_2 powder over a mica sheet pre-treated with Poly-L-Lysine (Sigma Aldrich, USA). The average height was obtained by measuring at least 100 nanoparticles in non-contact mode. The average height of the *n*CeO_2 and *n*TiO_2 powder were 32.6 ± 20.7 nm and 41.8 ± 24.3 nm, respectively.

Subsequently, the *n*CeO_2 and *n*TiO_2 powders were suspended in deionized water at a concentration of 1000 ppm, sonicated, and simultaneously heated at 60 °C for 30 minutes. The suspensions were characterized for z-average size, measured as hydrodynamic diameter, and zeta potential, via electrophoretic mobility, by dynamic light scattering (DLS) method using the Nano ZS90 (Malvern Instruments, UK).

The z-average size of *n*CeO_2 and *n*TiO_2 powder was 174 ± 1.19 and 925 ± 105 nm, respectively. The zeta potential of the *n*CeO_2 and *n*TiO_2 powders were respectively 0.027 ± 0.064 mV and 19.9 ± 0.55 mV.

Finally, the *n*CeO_2 and *n*TiO_2 powders suspension were characterized also with the Differential Centrifugal Sedimentation (DCS) method using CPS DC24000 UHR (Analytik, UK). The average sizes were 188 ± 5.9 nm and 690 ± 17.5 nm, respectively for *n*CeO_2 and *n*TiO_2.

5.2.2 Addition of Nanoparticles to Soil

The soil used for this study was collected in Udine, Italy (46°04'52'' N, 13°12'13'' E; top 20 cm) air dried at room temperature and sieved through a 2 mm mesh prior to characterization. The soil was classified as clay soil (sand 26%, silt 6.4% and clay 67.6%) with pH 7.4, cation exchange capacity (CEC) of 13.9 (cmol kg^{-1} DM), electrical conductivity (EC) of 1235 (µS m^{-1}) and organic matter (OM) content of 4.4%.

Eight mixtures of soil and *n*CeO_2 and *n*TiO_2 were prepared following the procedure used by Priester et al., (2012) The main treatments were made by adding *n*CeO_2 and *n*TiO_2 directly to the soil and mixing it in a portable concrete mixer previously sealed, to obtain a concentration of 2000 mg kg^{-1} of either *n*CeO_2 and *n*TiO_2. The *n*CeO_2/*n*TiO_2 amended soils were stored in the dark at 10 °C for two weeks. After soil equilibration the final doses of 500 and 1000 mg kg^{-1}, respectively (Ce 500, Ce 1000, Ti 500, Ti 1000) were prepared by serial dilution with soil.

Four additional treatments were obtained by combining the stock soils to achieve the following combinations: *n*CeO_2 500 mg kg^{-1} / *n*TiO_2 500 mg kg^{-1} (Ce 500-Ti 500), *n*CeO_2 500 mg kg^{-1} / *n*TiO_2 1000 mg kg^{-1} (Ce 500-Ti 1000), *n*CeO_2 1000 mg kg^{-1} / *n*TiO_2 500 mg kg^{-1} (Ce 1000-Ti 500) and *n*CeO_2 1000 mg kg^{-1} / *n*TiO_2 1000 mg kg^{-1} (Ce 1000-Ti 1000). The *n*CeO_2 / nTiO_2 -amended soils were stored in the dark at 10°C for two weeks. After the equilibration, five pots per treatment were filled for a total of 45 pots. The control treatment received no nanoparticle amendment.

5.2.3 Plant Growth and Harvest

Eight seeds of spring barley (*Hordeum vulgare* L., cv. Tunika) obtained from the Italian company S.I.S Società Italiana Sementi (San Lazzaro di Savena, Bologna, Italy) were sown in microcosms (4L polyethylene pots) containing the *n*CeO_2 / *n*TiO_2 -amended soils. The trial was carried out in a semi-sealed greenhouse under full sunlight. Two weeks after seed

planting, the seedlings were thinned to four seedlings per microcosm. At tillering, two plants per pot were removed, therefore 90 plants were observed during the experiment (ten plants per treatment). During the growth period the microcosms were irrigated to maintain the soil at 60% of water holding capacity (WHC). During the barley growth cycle the microcosm were singularly weighed and irrigated to compensate for evapotranspiration. Phenological stages were monitored by adapting the Decimal Growth Scale (Zadoks et al., 1974) throughout the growth cycle and were based on 50% of plants within the treatments at each stage. Plants were harvested at physiological maturity. Prior to collecting plants, plant height was measured from soil surface to the flag leaf using a standard meter stick (1 m).The plant shoots were severed at the collar with a razor blade and then separated into stems, leaves, spikes, and grains. Leaf area was measured using a LI-3100C Area Meter (Li-Cor Corporation, Lincoln, NE, USA). Plant samples were thoroughly washed in tap water and rinsed three times with distilled water. In addition, roots were washed in 400 ml of 0.01 M HNO_3 in a shaker bath at 300 rpm for 5 min to remove metal ions adsorbed at the surface. The plant fractions were oven dried at 105° C for 24 h and weighed.

5.2.4 Gas Exchange Parameters

The photosynthetic rate at saturating light intensity (Amax, μmol CO_2 m^{-2} s^{-1}), transpiration rate (Tr, mmol H_2O m^{-2} s^{-1}), and stomatal conductance (gs, mol air m^{-2} s^{-1}) were measured with a portable gas exchange system (LI-6400, LI-COR, Inc., Lincoln, NE, USA) on the youngest fully-expanded leaf of three individual plants per treatment.

The gas exchanges measurements were carried out on the flag leaf at booting, heading and milk maturity on three individual plants per treatment.

The measurements were made after allowing leaves to reach steady-state conditions at saturating photosynthetic active radiation (PAR, 1200 μmol m^{-2} s^{-1}), at a CO_2 concentration of 400 ppm, and at a temperature of 25 °C, and were collected between 9 and 14 h with evaluation of five measurement periods at intervals of 7-8 days.

5.2.5 TEM Observations

A small leaf portion (2x3 mm) was excised close to the central vein of the youngest leaf before the emergence of flag leaves.

The fresh samples were fixed for 2 h at 4°C in 0.1% (wt/vol) buffered sodium phosphate and 3% (wt/vol) glutaraldehyde at pH 7.2. They were then post-fixed with 1% osmium tetroxide (wt/vol) in the same buffer for 2 h, dehydrated in an ethanol series, and embedded

in Epon/Araldite epoxy resin (Electron Microscopy Sciences, Fort Washington, PA, USA). Serial ultrathin sections from each sample were cut with a diamond knife, mounted 100/200 folding grids, and then observed under a Philips CM 10 transmission electron microscope (TEM, FEI, Eindhoven, The Netherlands) operating at 80 kV.

5.2.6 Spectroscopy Analysis

Samples of soils were oven-dried (105°C for 48 h) and digested in 11 ml of a 10 to 1 (v/v) mixture of 96% (v/v) sulphuric acid and 30% (v/v) H_2O_2 in Teflon cylinders for 20 min at 200°C in a microwave (CEM MARS). After digestion, samples were diluted 1 to 20 with milliQ water, filtered through 0.45 µm filters and Ce and Ti were determined with an ICP-OES (Vista MPX, Varian Inc., Palo Alto, CA, USA). Oven-dried plant fractions were acid-digested in 10 mL of a 1 to 4 (v/v) mixture of 65% (v/v) nitric acid and 30% (v/v) hydrogen peroxide in Teflon cylinders for 10 min at 175 °C in microwave oven (CEM MARS Xpress). The plant extracts were filtered with Whatman® PTFE membrane filters (0.45 µm PTFE), diluted, and analysed. Total Ce and Ti in roots, stems, and leaves were determined by an ICP-OES using yttrium as internal standard. The Ce and Ti contents in kernels were quantified using an ICP-MS (Aurora M90, Bruker, Bremen, Germany) with an internal standard solution of ^{72}Ge and ^{89}Y. Quality control for both ICP-OES and ICP-MS was carried out using reagent blank samples, and triplicates reading for each sample. Certified standard reference material (NIST 1573a Tomato leaves) was analysed to validate the protocol.

5.2.7 TEM X-ray Microanalysis

Crystal structure and chemistry of the nanoparticles were studied by using a 2010F UHR TEM/STEM (JEOL, Peabody, MA, USA) equipped with a low spherical aberration coefficient (Cs = 0.47 ± 0.01 mm) objective pole piece and energy dispersive x-ray spectrometer (EDXS). The experiments were performed at an accelerating voltage of 200 kV corresponding to an electron wavelength of 2.5 pm. The EDXS spectra were acquired in scanning transmission electron microscopy (STEM) configuration by rasterizing an electron probe of 0.5 nm within the area of interest imaged by a high angle annular dark field (HAADF) detector to accurately determine the chemical assessment of the investigated nanoparticles. Nanodiffraction were acquired in TEM by illuminating the area of interest with a 50 nm parallel electron probe to study the crystal features of individual nanoparticles (Carlino, 2014).

5.2.8 Data Analysis

The microcosm study was arranged in a completely randomized factorial design with nine treatments (control soil, two levels of *n*CeO_2, two levels of *n*TiO_2 and four *n*CeO_2 / *n*TiO_2 mixtures) and five replicates. Data were tested for homoscedasticity and normality using the Bartlett's test and the Shapiro–Wilk test, respectively. The differences were statistically significant, as determined by one-way and two-way analysis of variance (ANOVA). Tukey's Multiple Comparison test (p=0.05) in case of significant effects were used to analyse individual effects. Statistical analysis was performed using the SPSS program (ver. 16, SPSS Inc. Chicago, IL, USA).

5.3 Results

5.3.1 Phenology and Growth of Barley

A week after sowing, all the plants had germinated, apparently unaffected by the presence of metal oxide nanoparticles in the soil and without early symptoms of phytotoxicity in treated plants.From the 2nd leaf stage we observed that *n*CeO_2 and *n*TiO_2 treated plants had a longer vegetative period than the controls (Figure 1).

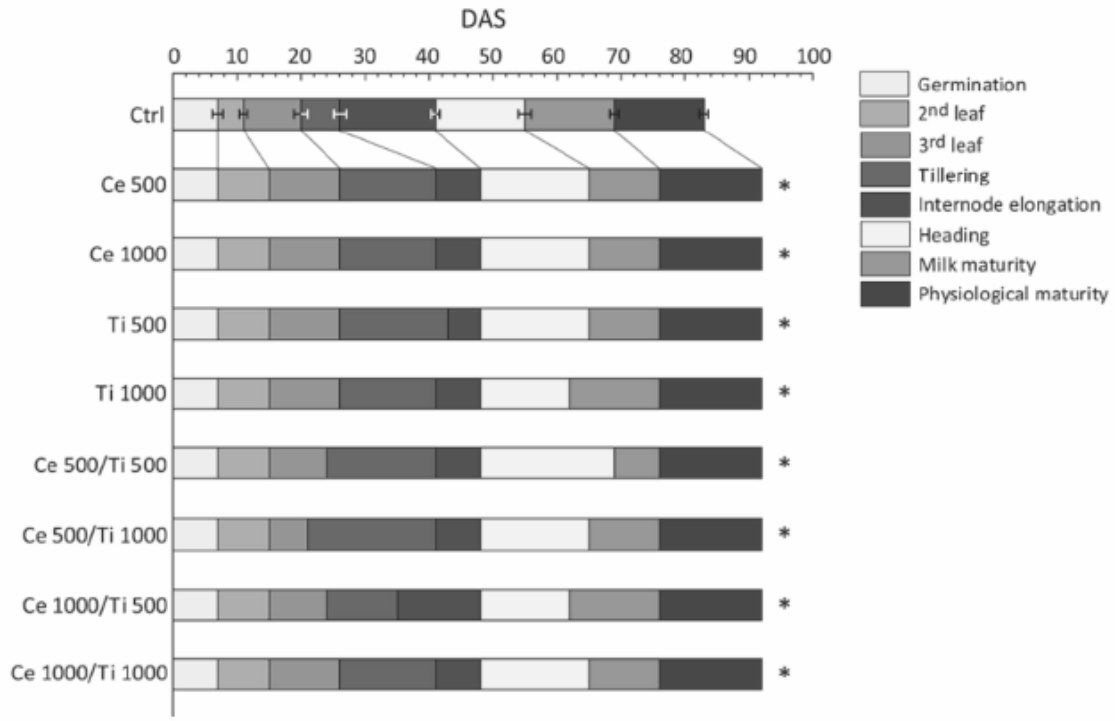

Figure 1: Cumulative contribution of vegetative and reproductive phenophases to the phenology of plants of barley grown in control soil and *n*CeO_2 and *n*TiO_2-amended soil. DAS = days after sowing. Error bars represent ± standard error. * denote significant differences with respect to control ($p \leq 0.05$).

This delay was also verified at the 3rd leaf and tillering stages, even if it was less pronounced for the Ce 500/Ti 1000 treatment. The delay in the nanoparticle-treated plants reached its maximum extent (about ten days) at heading and during the ripening stages (Figure 1). Milk maturity was reached on average 65 days after sowing (DAS) in treated plants. Ti 1000 and Ce 1000/Ti 500 plants were the earliest (62 DAS) and the Ce 500/Ti 500 ones were the latest (69 DAS) at entering physiological maturity (Figure 1).

A two-factor analysis of variance (ANOVA) was performed on the following variables: plant height, number of tillers, leaf area per plant and number of spikes.

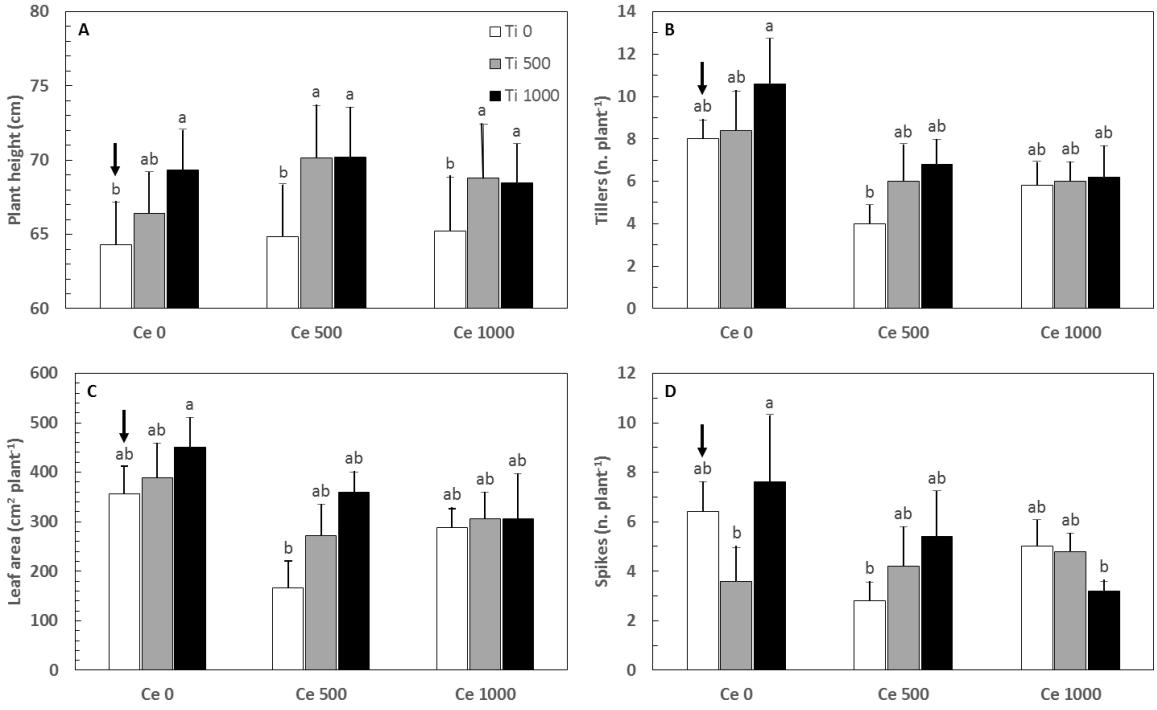

Figure 2: Plant height (A), number of tillers (B), leaf area (C) and number of spikes (D) observed in plants of barley grown in control soil and *n*CeO_2 and *n*TiO_2-amended soil. Bars are mean standard error (n = 5). Arrows indicate the control.

Among the morphological traits that we considered, plant height was the least sensitive to the *n*CeO_2 and *n*TiO_2 treatments. The interaction *n*CeO_2 X *n*TiO_2 was not significant (Figure 2A). The plants treated with *n*TiO_2 were significantly taller than the others (p = 0.0035), whereas there was no statistically significant effect of *n*CeO_2.

The formation of secondary shoots was significantly influenced, but in an opposite way, by the experimental factors. The number of tillers per plant was significantly stimulated by *n*TiO_2 compared to the control (p = 0.009). In fact, in Ce 0 plants *n*TiO_2 1000 promoted, on average, the formation of 2.60 secondary shoots more (+25%) than the control plants (p = 0.032); a more pronounced effect of 2.60 secondary shoots more (+25%) than the control

plants ($p = 0.032$); a more pronounced effect (2.80 tillers more than controls) was recorded in Ce 500 plants ($p = 0.026$) (Figure 2B). In contrast, *n*CeO_2 had a statistically significant ($p < 0.001$) negative effect on tiller formation (Figure 2B). In particular, on average in Ce 500 and Ce 1000 plants the number of secondary shoots was about 35% lower than both control plants ($p = 0.002$) and Ti treated ones (respectively $p = 0.034$, and $p < 0.001$).

The number of tillers and the plants' total leaf area are closely linked. In fact the ANOVA showed a significant effect of both *n*CeO_2 ($p < 0.001$) and *n*TiO_2 ($p = 0.001$). The interaction *n*CeO_2 X *n*TiO_2 was not significant. Multiple comparisons were run for each simple main effect. As noted earlier, in absence of Ti, Ce 500 had a strong negative effect on plant vegetative growth, in fact the average leaf area per plant was about one-half that of the control (166 vs. 356 cm^2 of leaf surface per plant) ($p < 0.001$) (Figure 2C). Such a negative influence of *n*CeO_2 in Ce 500 plants appeared to have been mitigated by *n*TiO_2 which had a positive significant effect ($p < 0.001$) (Figure 2C). In regards to the plant's response to *n*CeO_2 / *n*TiO_2 mixtures, although the interaction was not statistically significant ($p = 0.091$), we assumed that *n*TiO_2 at respectively 500 and 1000 mg per kg of soil was able to remediate the adverse impact on leaf growth of *n*CeO_2 (Figure 2C).

One of the main yield components in barley is the number of spikes per plant. Two way ANOVA revealed a statistically significant effect of the main factor *n*CeO_2 ($p = 0.0016$) and a significant interaction between *n*CeO_2 and *n*TiO_2 ($p = 0.0016$). The effect *n*TiO_2 in this case was not statistically supported, being likely hidden by data variability (Figure 2D). The mean number of spikes in Ce 500 and Ce 1000 plants was 4.2 corresponding to a reduction of 38% than the controls (2D). Regarding interaction, multiple comparisons of the means showed the different main effects of *n*CeO_2 and *n*TiO_2.

In absence of *n*TiO_2 (Ti 0), the number of spikes per plant were negatively affected by *n*CeO_2. There was a statistically significant difference ($p = 0.003$) between Ce 0 and Ce 500 plants (6.4 and 2.8 spikes per plant, respectively; - 56%). The negative influence of *n*CeO_2 was confirmed at the highest dose (Ce 1000) even though it was lighter in magnitude (22% lower than control plants) and not statistically different from Ce 500 (Figure 2D). The same effects were verified also in Ti 1000 plants, where both the levels of *n*CeO_2 determined a reduction of spike number of 32.5% and 60% respectively for Ce 500 ($p = 0.033$) and Ce 1000 ($p < 0.001$). The intermediate dose of *n*TiO_2 (500 mg kg^{-1}) negatively affected the number of spikes in plants (- 43.7% than controls, $p = 0.020$). On the contrary, Ti 1000 plants had 8 spikes each (higher that control plants although not statistically significant). In other words, in terms of spike formation our data suggest that, in absence

of nCeO$_2$, the higher dose of nTiO$_2$ was, at least, harmless to plants. This evidence is in contrast with other growth parameters. Moreover, we detected a negative nTiO$_2$ dose-effect on plant tillers' number and leaf area (Figure 2B-D).

5.3.2 Gas Exchanges

The leaf photosynthetic rate (A_{max}), stomatal conductance (g_s) and transpiration rate (Tr) at three different growth stages (booting, heading, milk maturity) are shown in Table 1.

Because the treatments affected plant development by causing a shift in phenological stages, the gas exchange parameters were evaluated by comparing plants at the same phenological phase.

Both nCeO$_2$ and nTiO$_2$ treatments had a statistically significant effect on the photosynthetic parameters, whereas their interaction was not significant at any of the growth stages. Table 1 reports the data regarding the main factors. At the booting phase, A_{max} and Tr were positively affected by Ce 500 compared to control plants (respectively +26% and + 75%). However, Ce 1000 plants behaved like the controls suggesting that the maximum concentration for a beneficial effect from nCeO$_2$ had been exceeded (Table 1). As expected, in the subsequent phases of the life cycle of barley A_{max} declined, with no evidence of statistically significant differences between treatments and control. At booting Ti 1000 had an overall positive effect compared to the control plants: A_{max}, g_s, and Tr significantly increased by 37, 89, and 92%, respectively. The Ti 500 treatment had an intermediate effect (Table 1).

5.3.3 Plant Uptake and Accumulation of Cerium and Titanium

In Tables 2 and 3 present the concentrations of Ce and Ti in the roots, stems, leaves, and kernels of barley. In general, the concentration of Ce and Ti in the plant tissues showed a dose-response.

A statistically significant dose-response in Ce concentration was recorded in all plant fractions with the exception of kernels. In Ce 500 and Ce 1000 plants, the mean levels of Ce in the roots were 45.3 mg kg^{-1} and 96.9 mg kg^{-1}, respectively (Table 2). The significant dose-dependent response in root Ce accumulation was confirmed also in nCeO$_2$ / nTiO$_2$ treatments.

Ce concentration in stems was significantly different between Ce 500 and Ce 1000 plants both in the case where Ce is individually supplied either when it is associated with the Ti.

The Ce root to shoot translocation percentage in treated plants ranged between 1.24 and 9.1, respectively, for Ce 1000 and Ti 500, indicating that Ce accumulation in the aboveground plant fractions occurred at very low magnitude. The highest Ce concentration in leaves was recorded in Ce 1000 plants (3.03 mg kg^{-1}).

As expected, in the leaves of Ctrl plants and Ti 500 and Ti 1000 ones, lower Ce accumulation values (0.73, 0.77 and 0.84 mg kg^{-1}, respectively) were observed.

Despite the increase in concentration of Ti in the soil ($p = 0.0001$), due to the addition of *n*TiO_2, the Ti uptake and accumulation in the plant fractions did not respond to the treatment. No statistically significant differences in Ti concentration in roots, as well as in stems and leaves, were observed (Table 3). As for Ce, in the case of Ti the root-to-shoot translocation percentage was very low, ranging between 1.42 and 1.91.

Table 1: ANOVA p value for the main factors (nCeO$_2$, nTiO$_2$) and interaction (nCeO$_2$ × nTiO$_2$) for leaf photosynthetic rate at saturating light intensity (Amax, µmol CO_2 m^{-2} s^{-1}), stomatal conductance (gs, mol air m^{-2} s^{-1}) and transpiration rate (Tr, mmol H_2O m^{-2} s^{-1}) recorded at three different phenological stages (booting, heading and milk maturity) in leaves of barley growing in control soil and nCeO$_2$ and nTiO$_2$-amended soil. Values are mean±SE (n=5). Same letters indicated no statistical difference between treatments at Tukey's test. *** $p < 0.001$; ** $p < 0.05$; ns = not significant ($p = 0.05$).

Treatment	Booting			Heading			Milk maturity		
	A_{max}	g_s	Tr	A_{max}	g_s	Tr	A_{max}	g_s	Tr
nCeO$_2$	0.0003***	0.0335	0.0047**	ns	ns	ns	ns	ns	ns
nTiO$_2$	0.0003***	0.0105**	0.0105**	ns	ns	ns	ns	ns	ns
nCeO$_2$ x nTiO$_2$	ns	ns	ns	ns	ns	ns	ns	ns	ns
-	-	-	-	-	-	-	-	-	-
Ctrl	20.4 ± 1.18 b	0.278 ± 0.05 ab	3.064 ± 0.64 b	19.4±1.8 a	0.350±0.06 a	3.24±0.29 a	15.3±1.6 a	0.298±0.05 a	2.95±0.30 a
Ce 500	25.7 ± 1.0 a	0.390 ± 0.05 a	5.36 ± 0.71 a	21.2±1.3 a	0.254±0.02 a	4.33±0.58 a	14.4±1.6 a	0.282±0.04 a	2.53±0.24 a
Ce 1000	19.4 ± 0.9 b	0.249 ± 0.03 b	3.23 ± 0.51 b	19.4±1.7 a	0.220±0.02 a	4.12±0.33 a	17.8±1.1 a	0.349±0.05 a	3.15±0.32 a
-	-	-	-	-					
Ctrl	17.5 ± 1.8 b	0.205 ± 0.06 b	0.205 ± 0.06 b	21.6±1.4 a	0.339±0.04 a	3.79±0.36 a	16.4±1.3 a	0.229±0.03 a	2.29±0.21 a
Ti 500	22.8 ± 1.5 ab	0.287 ± 0.03 ab	0.287 ± 0.03 ab	18.5±1.6 a	0.229±0.03 a	4.04±0.43 a	15.7±1.4 a	0.327±0.05 a	3.05±0.29 a
Ti 1000	23.9 ± 1.0 a	0.387 ± 0.05 a	0.387 ± 0.05 a	18.6±1.9 a	0.230±0.03 a	3.64±0.62 a	16.1±1.8 a	0.357±0.05 a	3.16±0.30 a

Table 2: Ce concentration observed in roots, stems, leaves and kernels of barley grown in control soil and $nCeO_2$ and $nTiO_2$-amended soil. Values are mean ± SE. (n=5). Same letters indicated no statistical difference between treatments at Tukey's test ($p \leq 0.05$).

Treatment	Ce soil (mg kg^{-1})	Ce roots (mg kg^{-1})	Ce stems (μg kg^{-1})	Ce leaves (μg kg^{-1})	Ce kernels (μg kg^{-1})
ANOVA	***	***	***	***	ns
Ctrl	30.9 ± 2.56 c	3.30 ± 0.63 d	642 ± 118 c	734 ± 120 c	0.50 ± 0.19 a
Ce 500	333 ± 6.39 b	45.3 ± 11.6 cd	1383 ± 209 abc	1623 ± 115 bc	0.87 ± 0.57 a
Ce 1000	746 ± 19.5 a	96.9 ± 1.42 bc	1751 ± 295 ab	3027 ± 458 a	0.69 ± 0.36 a
Ti 500	34.2 ± 1.55 c	14.0 ± 0.97 d	862 ± 290 bc	776 ± 114 c	0.98 ± 0.59 a
Ti 1000	30.7 ± 4.10 c	19.1 ± 1.28 d	810 ± 214 bc	844 ± 95 c	1.22 ± 0.73 a
Ce 500/Ti 500	298 ± 8.81 b	58 ± 9.61 cd	1392 ± 243 abc	1424 ± 153 bc	0.34 ± 0.12 a
Ce 500/Ti 1000	376 ± 24.7 b	87 ± 5.60 bc	1692 ± 232 ab	1502 ± 80 bc	1.13 ± 0.52 a
Ce 1000/Ti 500	683 ± 44.4 a	149 ± 19.4 ab	1982 ± 186 a	1760 ± 136 b	0.75 ± 0.41 a
Ce 1000/Ti 1000	726 ± 29.2 a	164 ± 32 a	2010 ± 166 a	1795 ± 171 b	0.03 ± 0.01 a

Table 3: Ti concentration observed in roots, stems, leaves and kernels of barley grown in control soil and $nCeO_2$ and $nTiO_2$-amended soil. Values are mean ± S.E. (n=5). Same letters indicated no statistical difference between treatments at Tukey's test ($p \leq 0.05$). d.l. = detection limit.

Treatment	Ti soil (mg kg^{-1})	Ti roots (mg kg^{-1})	Ti stems (μg kg^{-1})	Ti leaves (μg kg^{-1})	Ti kernels (μg kg^{-1})
ANOVA	***	ns	ns	ns	ns
Ctrl	1797 ± 119 b	77 ± 3.19 a	260 ± 43.5 a	1003 ± 63 a	1.39 ± 1.39 a
Ce 500	1971 ± 156 b	66.5 ± 5.15 a	188 ± 19.5 a	1275 ± 316 a	0.48 ± 0.48 a
Ce 1000	1896 ± 56.3 b	63.9 ± 2.63 a	309 ± 22.3 a	1314 ± 286 a	0.26 ± 0.18 a
Ti 500	2153 ± 119 ab	66.7 ± 7.49 a	284 ± 32 a	1391 ± 352 a	0.71 ± 0.61 a
Ti 1000	2537 ± 56.3 a	81.7 ± 4.96 a	389 ± 56 a	962 ± 89.4 a	< d.l.
Ce 500/Ti 500	2070 ± 140 ab	63.9 ± 4.56 a	201 ± 88 a	1335 ± 315 a	3.62 ± 2.60 a
Ce 500/Ti 1000	2752 ± 113 a	59.4 ± 7 a	215 ± 160 a	1146 ± 273 a	8.14 ± 4.99 a
Ce 1000/Ti 500	1945 ± 106 ab	69.1 ± 7.92 a	223 ± 69 a	1073 ± 216 a	1.34 ± 1.3 a
Ce 1000/Ti 1000	2537 ± 138 ab	68.4 ± 5.41 a	186 ± 39 a	895 ± 115 a	< d.l.

Barley grains are used as food for humans and animals, as well as for other markets (e.g. malting and flour). Thus it is appropriate to examine whether nanoparticles are able to reach the kernels during ripening (Tables 2-3). No statistically significant differences among the treatments were recorded. In absolute values, the content of both elements in the kernels was three-four orders of magnitude lower than those recorded in plant leaves (Ce 0.718 μg kg^{-1} and Ti 1.77 μg kg^{-1}, respectively in Tables 2 and 3).

5.3.4 Ultrastructural Analyses

To verify the root uptake and subsequent translocations of *n*CeO_2 and *n*TiO_2 from roots to aerial plant fractions, ultrastructural analyses on plant leaf tissues were carried out. Nanoparticles were not present in untreated control leaf tissues, which presented well preserved ultrastructure and organelles (Figures 3A-5A). Rare clusters of nanoparticles were found in leaves sampled from plants grown in soil enriched with the different combinations of *n*CeO_2 and *n*TiO_2, at both concentrations (Figure 3).

Nanoparticles were observed in parenchyma leaf tissues, in the stroma of the chloroplast and in the vacuoles, (Figure 3B-D). Despite the presence of *n*CeO_2 and *n*TiO_2, the chloroplasts appeared normal, with preserved ultrastructure, and, in general, the cell compartments of the chlorophyll parenchyma did not appear affected by the treatments (Figure 3B). This evidence was in agreement with phenotypical/morphological analyses, as we did not observe macroscopic cell death at the tissue level after the *n*CeO_2 and *n*TiO_2 treatments. Nevertheless, at the vascular tissue, some ultrastructural modifications were visible, especially those affecting the cellular organelles: some nuclei showed condensed chromatin, mitochondria swollen cristae (Figure 4B,C). Only in Ce 1000 and Ti 1000 leaf tissues, few secondary veins showed irregular-shaped cells with contorted walls (Figure 5B).

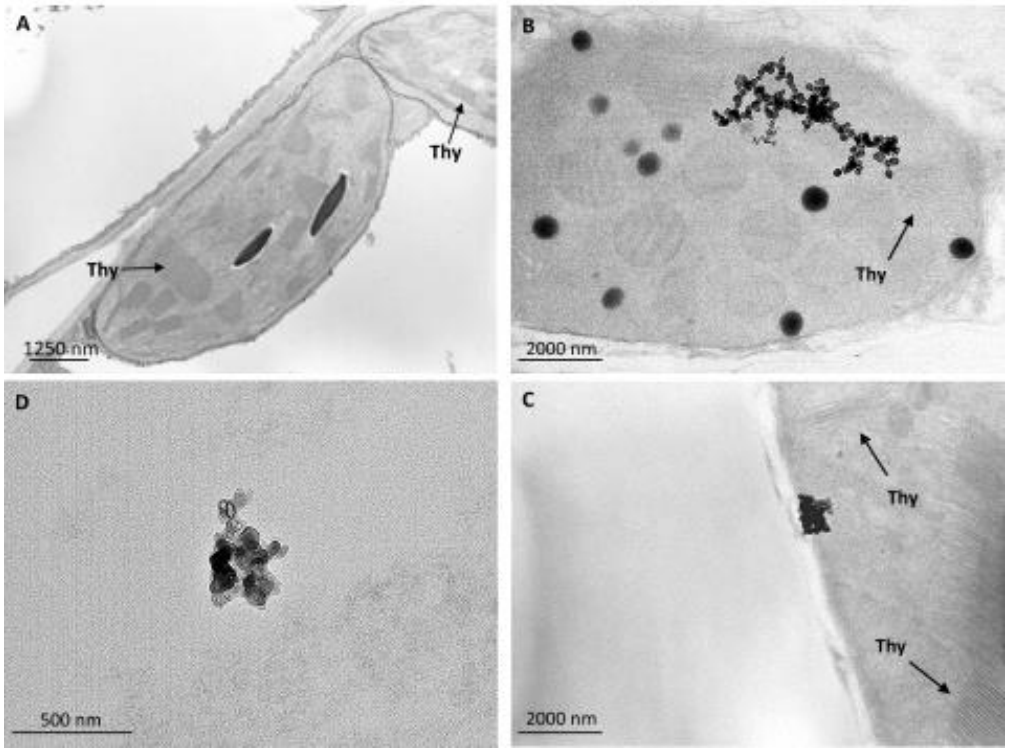

Figure 3: Representative TEM micrographs of leaf tissues from barley plants. In control untreated leaf tissues (A) nanoparticles are absent and chloroplast ultrastructure is well preserved. In plants grown in *n*CeO_2 and *n*TiO_2-amended soil clusters of nanoparticles are visible in the stroma of the chloroplasts (B, Ce 1000; C, Ti 1000) and in the vacuoles of parenchymal cells (D, Ce 1000). Chloroplast structure seems not affected by nanoparticle treatment (arrows in A, B and C indicate thylakoids).

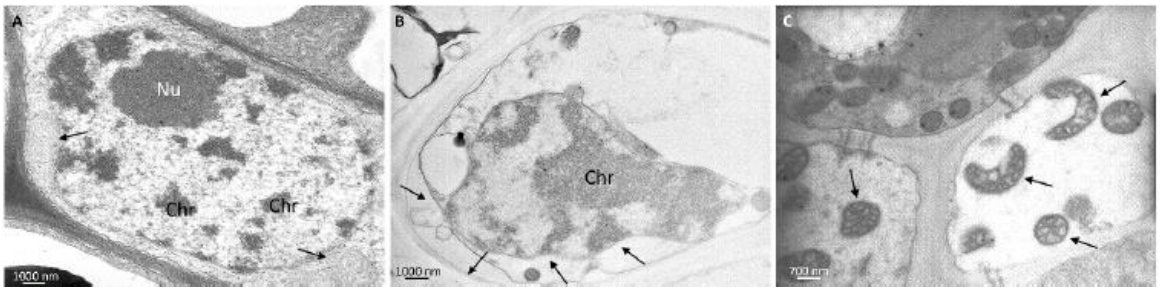

Figure 4: Representative TEM micrographs of leaf tissues from barley plants. (A) In control untreated vascular parenchyma cells mitochondria (arrows) and nuclei appear well preserved with regular shape and intact membranes. Nucleolus (Nu) is recognizable and chromatin (Chr) is normally dispersed. In plants grown in *n*CeO_2 and *n*TiO_2-amended soil vascular parenchyma cell has detached plasma membrane (arrows) and nucleus presents lobed shape and condensed chromatin (Chr) (B, Ce 1000). Mitochondria have disorganized, swollen christae (arrows in C, Ce 1000).

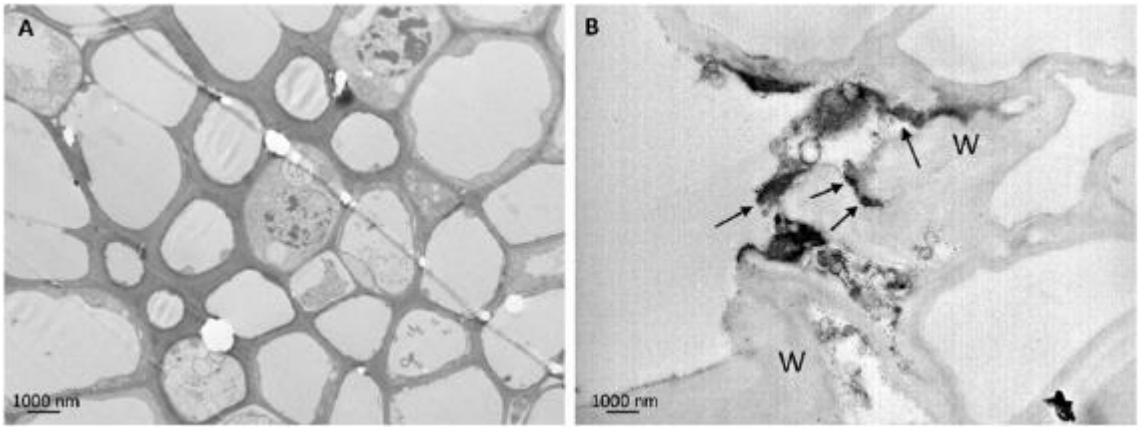

Figure 5: Representative TEM micrographs from secondary vein tissues of barley plants. (A) Control untreated vein tissues appear well structured, cell walls are regular in shape and thickness; (B) Ti 1000: secondary veins showed cells with contorted cell walls (W) associated with little dark precipitates (arrows).

5.3.5 Nanostructures in Leaf Tissues

After verifying the root-to-leaves translocation of Ce and Ti, STEM EDXS observations were carried out to detect the presence of *n*CeO_2 and *n*TiO_2 within the leaf tissues. Regarding *n*CeO_2, several nanostructure aggregates were observed, with sizes ranging from a few nanometers to some hundreds of nanometers. Interestingly, nanodiffraction measurements revealed an amorphous structure in most of cases. The compositional analysis by EDXS reported in Figure 6 did not show Ce in such aggregates so Ce was unlikely to be present in the form of nanoclusters within the leaf tissues of barley.

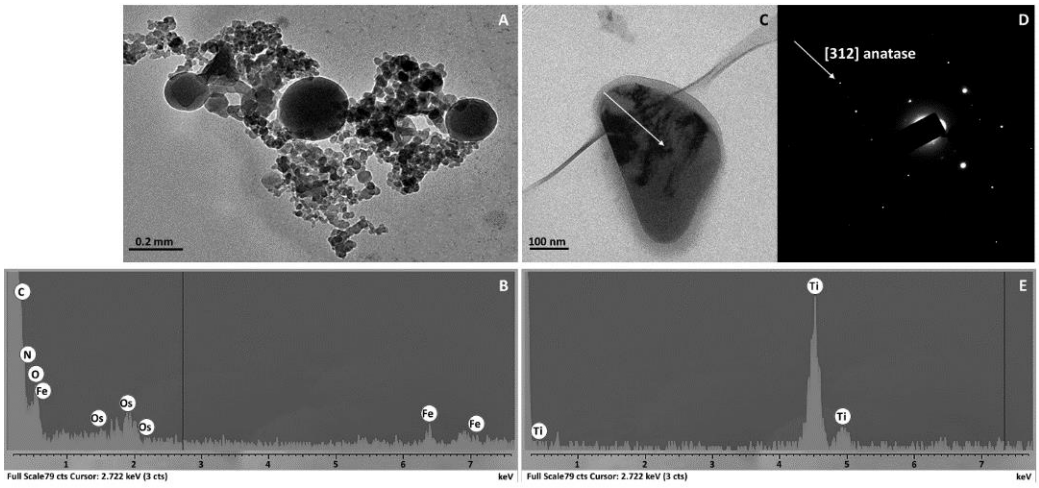

Figura 6: (A) Brightfield TEM image of representative nanostructures observed in Ce 1000 leaves; (B) EDXS spectrum as acquired in the particle area shown in brightfield mode. (C) Brightfield TEM image of Ti nanostructures in Ti 1000 leaves; (D) Nanodiffraction pattern as acquired on individual nanostructures indicated by the arrow in the brightfield image (see text); (E) EDXS spectrum as acquired on the region indicated in the brightfield image.

In Figure 6A, a bright field image shows a typical aggregate of clusters with large size dispersion.

No Bragg's peaks were observed in the relevant nanodiffraction and the EDXS spectrum showed no evidence of Ce characteristic X-rays, but only those of light elements (Figure 6B). Even though we lack direct experimental evidence, it is very likely that the small amount of Ce in leaves (Table 2) is aggregated in ionic form to organic molecules. It is also worthwhile mentioning that during extensive TEM/STEM sessions, isolated crystalline *n*CeO_2 were observed in only two cases. Therefore, we conclude that *n*CeO_2 induces a massive formation of amorphous clusters of light elements rather than nanometer-scale clusters of CeO_2. Such aggregates were abundant in the leaves of Ce 1000 plants but absent in control ones (Figure 5).

Several aggregates of nanoparticles were observed in the leaves exposed to *n*TiO_2.

In Figure 6C-E, a representative result of the chemical and structural analysis performed on a Ti aggregate is shown. Figure 6D shows a brightfield image of several dark aggregates. The nanodiffraction pattern acquired demonstrates the crystalline nature of the aggregates (Figure 6D). The measured lattice spacing is compatible with TiO_2 crystals. Indeed, the diffraction intensities belong to TiO_2 nanocrystallites with different orientation with respect to the primary electron beam. As an example, the arrow in the pattern points to the systematic reflection of a TiO2 anatase particle oriented close to the [312] zone axis (Figure 6D). To identify the chemical signature of the element contained in the nanostructures, the EDXS spectrum was acquired in the same area of the nanodiffraction, and the emission of characteristic fluorescence X-rays of Ti atoms was recorded (Figure 6E). In conclusion, we report the presence of TiO_2 nanoclusters in parenchyma leaf tissues—particularly inside the chloroplasts—of barley plants exposed to *n*TiO_2.

5.4 Discussion

Model simulations have demonstrated that flows of ENMs are currently able to reach natural ecosystems (Colman et al., 2013).

For this reason, questions are rising about the consequences of the interaction of ENMs with biota. Plant phenological traits and growth parameters always respond to the physical environment, so they can be used to assess the adaptive behaviours of the plants and evaluate their relationships to the ecosystem where they grow.

It was reported that ENMs have the potential to influence the growth of some crops with enhancing or inhibitory effects on plant growth according to their composition, size and physical and chemical properties (Gardea-Torresday et al., 2014; Priester et al., 2012; Yoon et al., 2014).

Studying the phenological stages of barley plants, according to the findings of Rico et al. (2015b) and Yoon et al. (2014), we verified that *n*CeO_2 and *n*TiO_2 treated plants had a longer vegetative period than the controls. This fact per se may not be negative. In fact, a longer vegetative phase may promote higher biomass and grain yield because plants are allowed to produce more photosynthetically active leaves and therefore more photosynthates (Dofing, 1995).

Our data showed that *n*TiO_2 were associated with effects opposite to those induced by *n*CeO_2. First, we observed an *n*TiO_2 dose-response effect on vegetative growth. Second, the compensation of the adverse effects of *n*CeO_2 observed in plants grown in *n*CeO_2 / *n*TiO_2-treated soils was probably due to the beneficial effects of *n*TiO_2 on plant metabolism. Several evidences obtained in different experimental conditions support this hypothesis. Studies carried out on *Spinacia olearacea* have demonstrated that *n*TiO_2 promote plant photosynthesis increasing light absorbance and transformation of light energy (Yang et al., 2006) and enhancing Rubisco activity (Gao et al., 2006). Also, it was demonstrated that *n*TiO_2, could significantly improve CO_2 fixation by plants, where it enhances absorption and transmission of the solar energy into the chain electron transport in chloroplasts (Morteza et al., 2013). Our data support such evidences, even though we cannot provide a physiological explanation. On the other hand, working with *Cucurbita pepo* grown in soil containing 400-800 mg kg^{-1} of *n*CeO_2, Zhao et al. (2013) did not observe any differences in the photosynthetic rate between treated plants and controls. Such different responses suggest that, at least at the intermediate level of concentration, different interactions with metabolism occur in various species exposed to metal nanoparticles. However, we still lack a systematic study on the effects on basic metabolism of plants induced by different nanomaterials and different levels of exposition.

At the end of the plant life cycle we studied a number of biometric variables observing some differences between treated plants and the controls. Recently, observations made on plants of barley grown for the entire life-cycle in a soil amended with 125-250-500 mg kg^{-1} *n*CeO_2 were reported (Rico et al., 2015b).

Thus, we can compare part of our data with those presented in that paper. In general, our results regarding the effects induced by *n*CeO_2 on plant growth are in contrast with Rico et

al. (2015b). One of the most relevant differences was that in our case all the plants were able to reach the reproductive stage, whereas Rico et al. (2015a) did not observe the formation of spikes in *n*CeO_2 500 mg kg^{-1} treated plants. Moreover, they observed that *n*CeO_2 500 mg kg^{-1} increased the height of barley plants and the accumulation of dry matter in the shoots, whereas in our case the vegetative growth was not stimulated by any level of *n*CeO_2. If we consider studies carried out on other crop species, our data partially agree with the findings of Priester et al. (2012) in *Glycine max*, whereas Zhao et al. (2013) did not observe statistically significant differences in biometric parameters in plants of *Cucumis sativum* between control plants and those treated with *n*CeO_2.

With regard to Ce and Ti accumulation in the plant tissues, it must be emphasized that both DLS and DCS analyses, carried out for the higher *n*CeO_2 and *n*TiO_2 test suspension (1000 ppm), indicate agglomeration of nanoparticles. Therefore, the actual bioavailability of nanomaterials may be lower than expected. For this reason, we believe that the concentrations of Ce and Ti in the plant tissues were underestimated. In addition, similarly to what happens in the case of conventional contaminants, soil pH, OM, texture and CEC have an important influence on the fate of nanomaterials in soil, (Cornelis et al., 2014; Schlich and Hund-Rinke, 2015) and particularly with respect to those, which release ions, such as *n*CeO_2 (Schwabe et al., 2015).

It was demonstrated that after root uptake, Ce was able to reach the plant leaves by moving through the vascular system (Zhao et al., 2013). We verified that Ce did not translocate easily since only a small fraction of the element moved from the roots to the aerial biomass of plants. Our findings and data agree with those obtained in similar studies respectively on soybean, cucumber, and wheat (Zadoks et al., 1974; Zhao et al., 2013; Rico et al., 2014). The increase in Ti concentration in the roots of Ce 500 and Ce 1000 plants could be due to a stimulatory effect of Ce on root growth and the formation of adventitious roots (Zhang et al., 2013). Therefore, *n*CeO_2 treated plants were able to explore a greater volume of soil, accumulating more Ti and Ce compared to the controls. This raises interesting questions about the bioavailability of Ti, which occurs in the soil as *n*TiO_2 from anthropogenic sources. It was previously observed that an increase in root assimilation and translocation of Ti after exposure to *n*TiO_2 would mean that the nano formulation of Ti makes it more bioavailable (Foltête et al., 2001). Other studies have shown that plants could translocate *n*TiO_2 into their aerial fractions. Titanium nanoparticles of 5 nm in diameter were found in leaves of *Arabidopsis thaliana* (Kurepa et al., 2010), in addition both the uptake and translocation of 100 nm *n*TiO_2 to the leaves of *Nicotiana tabacum* were observed (Ghosh

et al., 2010). However, the soil environment is very different and much more complex than artificial conditions. In our case, we observed very different results.

Macro- and micro-morphological observations indicate that under our conditions *n*CeO_2 and *n*TiO_2 induced limited cell injuries, at least in the parenchyma tissues. Inside the tissues, metal nanoparticles, depending on their type, shape and concentration may cause either cell death or other side effects (Sohaebuddin et al., 2010). Alternatively, metal nanoparticles can be well tolerated by the cells; however, this does not mean that nanoparticles do not affect cellular pathways (Panariti et al., 2012). The primary ultrastructural alteration we detected in leaf tissues of plants treated with metal oxide nanoparticles was the condensed chromatin in the nuclei and swollen mitochondria of vascular parenchyma cells. Condensed chromatin and fragmented nuclei, as well as swollen mitochondria, are described in programmed cell death (PCD), reported in cell response to different environmental stimuli and stresses, induced by pathogens (Lam et al., 2012) and abiotic factors as salinity, cold stress, waterlogging, or hypoxia (White, 1996; Kratsch and Wisw, 2000).

Referring to the literature findings (Asli and Neumann, 2009; Zhao et al., 2012; Hernandez-Viezcas et al., 2013) we would have expected to find crystalline forms of both elements in the plant tissues. Several nanostructures were observed in the leaf tissues of *n*CeO_2 treated plants; however, microanalysis did not confirm the presence of Ce in such aggregates. This is in contrast with Zhao et al. (2012) which verified the presence of *n*CeO_2 aggregates within vascular tissues of corn, thus demonstrating that Ce nanoparticles migrate through the xylem under transpiration. In studies on soybean plants grown in *n*CeO_2 amended soil, it was observed that most of the Ce stored in the pods was in the form of *n*CeO_2 (Hernandez-Viezcas et al., 2013).

We have not investigated the speciation of Ce and Ti in plant tissues, however this evidence constitutes a rather strong indication of Ce biotransformation. The biotransformation of ceria nanoparticles in plant tissues was demonstrated in soybean (López-Moreno et al., 2010) and in cucumber (Zhang et al., 2012; Ma et al., 2015a). In our case we hypothesized that the formation of the amorphous clusters could be related to the presence of intracellular Ce and, a defensive mechanism against Ce-cytotoxicity, as previously demonstrated (Horie et al., 2009). To the contrary, Ti nanoparticles were able to cross biological barriers in plant tissues. In fact, we report the presence of Ti nanoclusters in parenchymatic cells of barley leaves. Early evidence of root to shoot translocation of *n*TiO_2 was found in hydroponically grown cucumber seedlings, using micro X-ray fluorescence (μ-XRF) and micro X-ray

absorption spectroscopy (μ-XANES) (Servin et al., 2012). Subsequently, the same evidence was confirmed in older cucumber plants growing in *n*TiO_2-enriched soil, as well (Servin et al., 2013). Our work undertaken with the same method agrees with these findings. Furthermore, unlike what was observed for Ce, we did not observe evidence of biotransformation, confirming the literature findings (Servin et al., 2013).

5.5 Conclusions

ENMs are currently considered as an emerging class of environmental contaminants and thus, as mentioned above, neither (i) potential interactions with other pollutants (Balbi et al., 2014; Ribas Ferreira et al., 2014) and/or (ii) the possibility of co-occurrence of ENMs in the environment can be excluded (Kumar et al., 2014). In other words, there exists a chance of simultaneously exposure of target organisms to different types of ENMs. This implies that the horizon of knowledge gaps on the relationships between ENM and biota has to be moved farther. According to Kumar et al. (2014) "to properly incorporate exposure of more than one type of ENM, data on toxicity due to mixture of ENMs for a given target organ are required".

With regard to plants, it is very likely that several research groups are currently working on this topic. However, in literature we found only one paper reporting evidence of stimulating effects on germination and early growth of *Glycine max* induced by a mixture of *n*SiO_2 and *n*TiO_2 (Lu et al., 2002). Therefore, we reiterate that this paper is the first to report data on the effects of a co-exposure to different metal oxide nanoparticles on a worldwide important crop. Moreover, our data were collected at the end of the life-cycle of soil grown barley plants.

Data available on the effects of ENMs in humans, crop plants, and livestock are not enough to allow for a thorough evaluation of their potential and of their safety. With respect to the aims of this study, although no visual symptoms of toxicity have been detected in plants, we demonstrated that the phenology and growth of barley were affected by *n*CeO_2 and *n*TiO_2. All plants concluded their life cycle producing seeds. However, in treated plants we verified differences in some biometric parameters compared to the control ones. In particular, *n*CeO_2 at the lower concentration were associated with a reduction in the leaf area, the number of tillers and spikes per plant, and for this reason the number of kernels per plant. It can be assumed that this will lead to a reduction in crop production. An attenuation of such adverse effects was observed in plants treated with the higher dose of

nCeO_2. Titanium nanoparticles were associated with positive effects on plants. First, we observed *n*TiO_2 positive dose-response effect on vegetative growth. Second, in plants co-exposed to *n*CeO_2 and *n*TiO_2, it is likely that the beneficial effects of Ti on plant metabolism have more than compensated for the adverse effects of Ce. Lacking literature data, at this moment we cannot discuss further these results and this part of our experiments should be considered simply exploratory. However, we demonstrated that the co-occurrence of *n*CeO_2 or *n*TiO_2 in soil determined in barley plants effects other than those observed in plants exposed separately to nanomaterials. It is likely that the study on this issue will be further dealt in the near future, through developing appropriate experimental protocols to study the physiological bases of plant response to ENMS co-occurrence.

From an ecological point of view, our data suggest that the fate of *n*CeO_2 and *n*TiO_2 could be different. In both cases, their bioaccumulation in plants is minute. Cerium nanoparticles inside plant tissues seem to dissolve into the ionic form that most likely undergoes a subsequent biotransformation. Titanium oxide nanoparticles are found in crystalline form in the leaves of barley and also in the seeds, although in small concentrations, so in this form the *n*TiO_2 may be able to continue on through the food chain. Further research should be carried out on the intricate relationships that exist in the soil-plant system with respect the fate of nanomaterials.

6 Cerium and Titanium Oxide Nanoparticles in Soil Differently Affect Nutrient Composition of Barley (Hordeum vulgare L.) Kernels

Filip Pošćić[(1)], Alessandro Mattiello[(1)], Guido Fellet[(1)], Costanza Zavalloni[(1)], Fabiano Miceli[(1)], Luca Marchiol[(1)]

[(1)] Department of Agriculture and Environmental Sciences, Via delle Scienze 206, 33100 University of Udine, Italy

Submitted to International Journal of Environmental Research and Public Health on 1st April 2016

Abstract

The implications of engineered nanoparticles in many food crops it is still unknown. The purpose of this study was to evaluate effects of cerium oxide nanoparticles (*n*CeO_2) and titanium oxide nanoparticles (*n*TiO_2) in soil at 0, 500 and 1000 mg kg^{-1} on barley (*Hordeum vulgare*) kernels. Mineral nutrients, amylose, β-glucan, amino acid and crude protein (CP) concentrations in barley (*Hordeum vulgare*) kernels were measured. Kernels were analyzed by ICP-AES/MS, HPLC and Elemental CHNS Analyzer.

Results have shown that Ce and Ti accumulation were not enhanced by MeNPs trereatments. However, *n*CeO_2 and *n*TiO_2 impacted the nutritional quality of barley kernels in contrasting ways. Both MeNPs reduced amylose and increased amino acid and CP content. Potassium and S were both negatively impacted by MeNPs, while B only under 500 mg *n*CeO_2 kg^{-1}. On the contrary Zn and Mn concentrations were improved under 500 mg *n*TiO_2 kg^{-1} and Ca at both *n*TiO_2 treatments.

6.1 Background

Nanotechnology is expected to be in widespread use by 2020 promoting a market of three trillion dollars' worth of nanotechnology-based products with six million workers (Roco, 2010). The applications of nanotechnologies in medicine, consumer goods, heavy industry, information and communication technologies, electronic devices, and environmentally-friendly energy systems are developing at a much faster pace than our knowledge of their impact (Nadeau et al., 2013). Several questions were raised about the fate of nanomaterials (defined as materials with at least one dimension comprised between 1 and 100 nm) (ISO, 2010) used in the agro-environment and those resulting from uncontrolled or accidental flows such as MeNPs. For this reason, Food and Agriculture Organization of the United Nations (FAO) as well as many countries adhering to the Organization for Economic Co-operation and Development (OECD) recognized the need of early consideration of the existing gaps in knowledge on toxicity of nanoparticles, their bioaccumulation, oral exposure and risks by ingestion of target organisms, which are the key factors needed for risk assessment on nanomaterials (Gruère, 2012; Takeuchi et al., 2014).

Human diets obtain primarily minerals from grains. On the other hand, uptake of nutrients by plant roots is affected by abiotic and biotic stressors and so the mineral storage in plant organs (Marschner, 1995). Therefore, it is appropriate to examine whether MeNPs in soil are able to influence mineral accumulation in grains of food-crops. However, little information about accumulation of MeNPs in edible tissues and how MeNPs affect grain quality can be found in the literature. Vascular plants and especially crops are of special concern as they could be exposed to risks of MeNPs bioaccumulation and their subsequent entry into the food chain (Zhu et al., 2008; Miralles et al., 2012). The effects of MeNPs on plants will depend, among others, on the soil type and plant species (Zhao et al., 2012), and indeed contrasting results are reported among dicot and monocot plants (Rico et al., 2013; Schwabe et al., 2013; Peralta-Videa et al., 2014; Rico et al., 2014; Zhao et al., 2014; Zhao et al., 2015; Rico et al., 2015).

Cerium oxide nanoparticles (*n*CeO_2) and titanium oxides nanoparticles (*n*TiO_2) are both included in the list of engineered nanomaterials of priority for immediate testing (OECD, 2010). A number of papers report data collected in the course of short experiments exposing plants to *n*CeO_2 or *n*TiO_2 carried out on seedlings in petri-dishes (López-Moreno et al., 2010; López-Moreno et al., 2010; Gomez-Garay et al., 2014; Mattiello et al., 2015), in hydroponic solutions or perlite-containing pots (Schwabe et al., 2013; Hong et al., 2005;

Zheng et al., 2005; Asli et al., 2009; Zhang et al., 2011; Larue et al., 2012; Jacob et al., 2013; Zhang et al., 2015), and in nutrient medium in agar (Dehkourdi and Mosavi, 2013; Cui et al., 2014). On the other hand other scientists worked on experiments in pots with plants being sprayed on leaves with *n*TiO_2 (Hong et al., 2005; Gao et al., 2006; Yang et al., 2007; Gao et al., 2008; Linglan et al., 2008). Finally, Wang et al. (2012) and the group of Gardea-Torresdey published research on *n*CeO_2 and *n*TiO_2 effects on yield of different plant species in soil experiments (Schwabe et al., 2013; Zhao et al., 2015; Rico et al., 2015). This paper reports the observations made on barley (*Horedum vulgare*) kernels produced by plants grown in *n*CeO_2 or *n*TiO_2 amended soil. Barley is among the world's most important crops being the fourth cereal after maize, rice and wheat for global grain production in 2013 (FAOSTAT, 2015). Due to its adaptation, N uptake and utilization efficiency (NUtE) barley is widely cultivated on more than 49 million hectares (FAOSTAT, 2015; Delogu et al., 1998). It has relevant economic importance for animal feed, malting and brewing and it is used as an important food in some parts of the world (FAOSTAT, 2015). Barley plants were selected also because their seeds contain an high starch concentration approximately 65 to 75% of their dry weight. Amylose and amylopectin are the two components of starch. Barley can be classified into normal type (25-27% amylose), waxy type (below 5% amylose) and high-amylose type (> 35% amylose) (Shu and Ramussen, 2014). The barley material (cv. Tunika) was released as a two-row spring barley, and marketed in Italy for malt or feed production, as its high-amylose and moderate β-glucan traits are functional for both purposes. In general, the high-amylose trait in cereals is connected to resistant starch, which in turn has a positive rule in human nutrition (Berry, 1986).

The main aims of our experiment were: (i) to evaluate the bioaccumulation of Ce and Ti in kernels, (ii) to verify the concentration in mineral nutrients in kernels compared to that of control plants, and (iii) to monitor the changes if any in seed quality parameters.

6.2 Materials and Methods

6.2.1 Soil Characterization

The soil used in our pot experiment was collected from the first top 40 cm of an agricultural field at the University of Udine, Italy (46° 04' 53'' N, 13° 12' 34'' E). The soil was air dried and sieved through a 2-mm sieve. For the soil characterization, samples (5 replicates) were furthermore oven-dried at 40°C for 48 h. Soil samples were then analyzed according

to Pansu and Gautheyrou (2006) for particle size distribution (Bouyoucos hydrometer method), pH (potentiometric measurements in a 1 to 2.5 of soil and Milli-Q® water suspension), electrical conductivity (EC, conductometric measurements in a 1 to 5 of soil and Milli-Q® water suspension), cation exchange capacity (CEC), available P (sodium bicarbonate extractable P at pH 8.5, Olsen method) and equivalent carbonate (calcimeter method). Total organic carbon (TOC) and total nitrogen (TN) contents were determined through an Elemental CHNS Analyzer (Vario Micro Cube, Elementar Analysensysteme GmbH, Germany) using up to 10 mg fine powder of grounded soil. Carbonates from the soil were previously removed by adding drops of hydrochloric acid (18%). The soil was classified as sandy clay loam and its characteristics are reported in Table 1.

Table 1: Characteristics of soil used in this study (n = 5).

Parameter	Mean ± SE
Clay (%)	26 ± 0.0
Silt (%)	6.4 ± 0.4
Sand (%)	67.6 ± 0.4
pH	7.44 ± 0.01
EC (µS cm^{-1}) at 25°C	1235 ± 194
CEC (cmol+ kg^{-1} dw)	13.87 ± 0.3
Available P (µg g^{-1} dw)	61.3 ± 8.4
Total carbonate (g kg^{-1})	72 ± 14.3
Total organic C (%)	2.22 ± 0.27
Total N (%)	0.17 ± 0.01

6.2.2 Nanoparticles Addition

Cerium(IV) oxide nanoparticles (*n*CeO_2) and Titanium(IV) oxide anatase nanoparticles (*n*TiO_2) were purchased from Sigma-Aldrich (Milwaukee, WI, USA) (respectively, ID product 544841 and 637254) which described them having mean diameters of <25 nm (BET). Further characterization studies (to be published in detail elsewhere) showed that nCeO2 and nTiO2 are of different shapes mainly rhombus and disks with respectively an average size obtained after 100 random observations (± SE) of 22.7 ± 1.3 nm and 24.1 ± 0.7 nm (TEM), 32.6 ± 2.1 nm and 41.8 ± 2.4 nm (AFM), and of 174.3 ± 0.1 nm and 924.7 ± 10.5 nm in deionized water (DLS). The specific surface area of *n*CeO_2 and *n*TiO_2 resulted to be 46.1 m^2/g and 61.6 m^2/g (BET) respectively.

Nanoparticles were added to the soil before sowing. Four mixtures of soil with *n*CeO_2 or *n*TiO_2 were prepared. The procedure consisted of preparing a 2000 mg kg^{-1} either *n*CeO_2 or *n*TiO_2 in soil by adding nano-powder directly into the soil and mixing it in a portable

concrete mixer which was properly closed. These mixtures were stored in the dark at room temperature for one week. After this period the final concentration of MeNPs corresponding to 1000 and 500 mg MeNPs kg^{-1} were prepared by serial dilution with source soil. For equilibration purposes MeNPs amended soils were stored once more in dark at room temperature for three days. Finally, five polyethylene pots (4 l each) per treatment were prepared (a total of 25 pots were used). The control treatment received no MeNPs.

6.2.3 Plant Growth and Yield Parameters

A greenhouse experiment was initiated at the experimental farm of the University of Udine (Italy) on 9 April 2014. Seeds of a two-row spring barley (*Hordeum vulgare* L., var. Tunika) obtained from S.I.S. S.p.A. (San Lazzaro di Savena, Bologna, Italy) were sown in pots containing soil amended or not with nanoparticles as above. The pots were irrigated to maintain the soil at 60% of water holding capacity (WHC). During growth pots were singularly weighed and irrigated on a weekly base to compensate for evapotranspiration. At Zadoks growth stage 92 (Ripening, kernel is hard and can no longer be dented by thumb-nail) (Zadoks et al., 1974) kernels were harvested, counted and weighted for 100-caryopses weight and grain yield estimation. Flag leaf area was measured using a LI-3100C Area Meter (Li-Cor Corporation, Lincoln, NE, USA). Finally, kernels from the main shoot were separated for the below analysis. A subsample of kernels were oven-dried at 105°C for 48 h for ICP-AES analysis while for the other analysis kernels were oven-dried at 60°C for 48 h and grinded to fine powder.

Amylose and β-glucan Concentrations Analysis. Amylose and β-glucan concentrations were determined by using the enzyme-specific amylose/amylopectin kit and the mixed linkage β-glucan assay kit, both from Megazyme (Megazyme International Ltd., Bray, Ireland).

6.2.4 Amino Acid and Crude Protein Analysis

Acid hydrolysis with HCl at 110°C for 22-24 h was used for total amino acids except for sulphur amino acids and tryptophan. For sulphur amino acid performic acid oxidation for 16 h followed by acid hydrolysis with HCl was used. For tryptophan alkaline hydrolysis with sodium hydroxide was performed at 100°C for 4 h. After extraction, samples were derivatized at 55°C for 10 min with 20 µl of AccQ-Fluor reagent (6-aminoquinolyl-N-hydroxysuccinimidyl carbamate) and injected in HPLC (Bosch et al., 2006). All reagents were of HPLC grade. Amino acid analysis was performed using a LC 200 Perkin Elmer

pump fitted with an ISS-100 auto sampler (20 µl loop) and a fluorimetric detector (Perkin Elmer, Norwalk, Connecticut, USA), λ excitation of 250 nm and λ emission of 395 nm. Separation was achieved by using one AccQ-Tag amino acid analysis column (Waters Corporation Milford, MA, USA) and one Waters pre-column filter. The column was thermostatted at 37°C and the flow rate was 800 µl min^{-1} (Liu et al., 1995). Mobile phase A consisted of acetate-phosphate aqueous buffer, mobile phase B was acetonitrile 100% and eluent phase C was Milli-Q® water. L-α-amino-n-butyric acid was used as internal standard. For the analysis of cysteine, methionine and tryptophan it was necessary in some occasions to mix two or three samples to obtain sufficient material for analysis.

Total content of N was determined through an Elemental CHNS Analyzer (Vario Micro Cube, Elementar Analysensysteme GmbH, Germany) using up to 2.5 mg fine powder of grounded samples. Finally, crude protein (CP) was estimated by multiplying the nitrogen content by 5.45 (Mariotti et al., 2008).

6.2.5 Elemental Concentrations Analysis

About 300 mg of material were digested in 10 ml of a 1 to 4 (v/v) mixture of 37% (v/v) HCl and 65% (v/v) HNO_3 in Teflon cylinders for 10 min at 175°C in microwave oven (CEM, MARS Xpress). After mineralization plant extracts were filtered (0.45 µm PTFE) and diluted. Total content of B, Ca, Cu, Fe, K, Mg, Mn, Na, Ni, P, and Zn were determined by an ICP-AES (Varian Inc., Vista MPX) with an internal standard solution of Y. Total content of Ce and Ti were determined by an ICP-MS (Aurora M90, Bruker) with an internal standard solution of 72Ge and 89Y. The accuracy of the analytical procedure adopted for ICP-AES analysis was checked by running standard solutions every 20 samples. Quality control for both ICP-AES and ICP-MS was carried out using reagent blank samples, and triplicates reading for each sample. Certified standard reference material (tomato leaves 1573a from the National Institute of Standards and Technology, USA) was treated as the samples (n = 3). The recovery of the elements in the standard material was on average 97% of the certified values with an RSD average of 1.3%.

Total content of S was determined through an Elemental CHNS Analyzer (Vario Micro Cube, Elementar Analysensysteme GmbH, Germany) using up to 2.5 mg fine powder of grounded samples.

6.2.6 Statistical Analysis

The greenhouse experiment was set up as a completely randomized design and each week pots were randomly reallocated. Each analysis consisted of five replicates per treatment, unless otherwise stated. Two-way mixed effect analysis of variance (ANOVA) (Sokal and Rohlf, 2010) were performed for all the data after verification of normality (Kolmogorov-Smirnov test) (Sokal and Rohlf, 2010) and homogeneity of the variance (Hartley's Fmax-test) (Sokal and Rohlf, 2010). The multiple comparisons of means were based on the minimum significant difference (MSD) method obtained from the T statistic for equal replicates or from the T' statistic for not equal replicates in the case of cysteine, methionine and tryptophan analysis (Sokal and Rohlf, 2010). Pearson's product-moment correlation coefficients and significance were calculated between Ce or Ti content in kernels and all the other measured parameters (Sokal and Rohlf, 2010).

6.3 Results and Discussion

6.3.1 Barley Biometric and Yield Parameters

Flag leaf area and 100-kernels weight were unaffected by the presence of CeO_2 nanoparticles ($n$$CeO_2$) and TiO_2 nanoparticles ($n$$TiO_2$) in the soil (Table 2).

Table 2: Biometric and yield parameters of barley plants in soil treated with none (control), 500 mg $n$$CeO_2$ kg^{-1}, 1000 mg $n$$CeO_2$ kg^{-1}, 500 mg $n$$TiO_2$ kg^{-1} and 1000 mg $n$$TiO_2$ kg^{-1}

Treatment	Flag leaf area (cm^2)	Kernels (n. $plant^{-1}$)	Grain yield (g $plant^{-1}$)	100-kernels weight (g)
Control	13.36 ± 1.1 a	117 ± 13.2 a	4.4 ± 0.6 a	3.76 ± 0.19 ab
500 mg $n$$CeO_2$ kg^{-1}	10.75 ± 2.21 a	53.2 ± 6 b	2.4 ± 0.3 b	4.6 ± 0.08 a
1000 mg $n$$CeO_2$ kg^{-1}	10.55 ± 2.98 a	90.6 ± 7.5 ab	3.7 ± 0.3 ab	4.13 ± 0.31 ab
500 mg $n$$TiO_2$ kg^{-1}	15.43 ± 2.79 a	66.2 ± 10.6 b	2.1 ± 0.4 b	3.04 ± 0.26 b
1000 mg $n$$TiO_2$ kg^{-1}	14.31 ± 1.75 a	129.8 ± 18.3 a	5.1 ± 0.6 a	4.04 ± 0.37 ab

[a]Values are means ± SE (n = 5). Different letters indicate significant differences between treatments ($p \leq 0.05$, T test) for each yield parameter separately.

With reference to kernel quantity and grain yield, nanoparticles treatments did impact plants. However, for these traits the dose-responses are unclear (Table 2). In both $n$$CeO_2$ and $n$$TiO_2$ treatments the 500 mg kg^{-1} level did impair kernel quantity and plant grain yield related to control; conversely, the 1000 mg kg^{-1} treatments did not cause any significant limitation and although not significant a beneficial effect can be envisaged for the 1000 mg $n$$TiO_2$ kg^{-1} treatment (Table 2). Regarding $n$$CeO_2$ treated plants, a parallel effect on source-

and sink-organs could be in place: the apparent reduction of flag leaf area is tentatively mirrored by a severe drop of sinks volume (kernel quantity). The severe reduction of kernel quantity, as an effect of 500 mg *n*CeO_2 kg^{-1} treatment (and to a lesser extent of 1000 mg *n*CeO_2 kg^{-1} one), is associated to an increase of 100-kernels weight, but the compensation is not sufficient and plant grain yield resulted negatively affected. Our results are partially in agreement with those obtained by Rico et al. (2015) which observed a reduced spike production in barley exposed to 0, 125, 250 and 500 mg *n*CeO_2 kg^{-1}. Remarkably authors observed that plants exposed at 500 mg *n*CeO_2 kg^{-1} did not form grains (Rico et al., 2015).

6.3.2 Amylose and β-glucans Concentrations in Kernels

The effects of *n*CeO_2 and *n*TiO_2 on amylose and β-glucans concentrations in barley kernels are displayed in Table 3.

Table 3: β-Glucans and Amylose concentrations in barley kernels at ripening from main shoot grown in soil treated with none (control), 500 mg *n*CeO_2 kg^{-1}, 1000 mg *n*CeO_2 kg^{-1}, 500 mg *n*TiO_2 kg^{-1} and 1000 mg *n*TiO_2 kg^{-1}

Treatment	β-glucans (% dw)	Amylose (% dw)
Control	5.1 ± 0.19 a	52.14 ± 1.34 a
500 mg *n*CeO_2 kg^{-1}	4.8 ± 0.19 a	43.85 ± 2.1 b
1000 mg *n*CeO_2 kg^{-1}	4.52 ± 0.11 a	39.74 ± 1.19 b
500 mg *n*TiO_2 kg^{-1}	4.54 ± 0.13 a	39.59 ± 2.08 b
1000 mg *n*TiO_2 kg^{-1}	4.94 ± 0.17 a	41.49 ± 1.65 b

[a]Values are means ± SE (n = 5). Different letters indicate significant differences between treatments ($p \leq 0.05$, T test) for each element separately.

MeNPs treatments had a significant effect over starch composition, as the amylose concentration significantly decreased (till 21% on average) compared to control. However, there were no specific responses across the different MeNPs treatments. Indeed a decrease of amylose as a response of abiotic stress has been in place in our barley experiment. Amylose content has been tagged as the most sensitive parameter to heat stress in Japonica rice, maize and wheat (Beckles and Thitisaksul, 2013), while there was no conclusive evidence for consistent changes in amylose content in barley grains exposed to high temperatures (Kiseleva et al., 2003).

Consistent with our results, Rico et al. (2013) observed a lowered starch content in grain from rice treated with 500 mg *n*CeO_2 kg^{-1} although significantly only in two of the three analyzed varieties. On the contrary, Zhao et al. (2014) did not observe significant differences in starch content in cucumber fruit after growing plants in soil amended with

nCeO_2 at concentrations similar to ours. However, beside they analyzed a different species, they determined starch content in the full cucumber fruit and not separated for skin, pulp and seeds (Zhao et al., 2014).

The variation in the amounts of amylose can affect the physicochemical and functional properties of starch, which may turn affect its utilization in food products or industrial applications (Kobayashi et al., 1986; Yan et al., 1993).

Finally, no significative differences on β-glucans concentration between control and MeNPs-treated plants were found.

6.3.3 Amino Acid Concentration in Kernels

The effects of *n*CeO_2 and *n*TiO_2 in the soil on amino acid concentration and crude protein (CP) concentration in kernels from main shoot are displayed in Table 4.

Table 4: Amino acid (mg g^{-1}) and crude protein (CP, g 100 g^{-1}) concentration in barley kernels at ripening from main shoot grown in soil treated with none (control), 500 mg *n*CeO_2 kg^{-1}, 1000 mg *n*CeO_2 kg^{-1}, 500 mg *n*TiO_2 kg^{-1} and 1000 mg *n*TiO_2 kg^{-1}

Parameter	Control	500 mg *n*CeO_2 kg^{-1}	1000 mg *n*CeO_2 kg^{-1}	500 mg *n*TiO_2 kg^{-1}	1000 mg *n*TiO_2 kg^{-1}
Alanine	5.65 ± 0.23 c	6.06 ± 0.12 bc	6.71 ± 0.31 ac	7.35 ± 0.47 a	6.75 ± 0.07 ab
Arginine	7.55 ± 0.59 a	8.72 ± 0.33 a	8.51 ± 0.32 a	9.26 ± 0.25 a	9.12 ± 0.37 a
Aspartic acid	7.18 ± 0.3 b	8.28 ± 0.35 ab	8.5 ± 0.37 a	8.58 ± 0.29 ab	9.09 ± 0.22 a
Cysteine[b]	6.85 ± 0.06 b	8.7 ± 0.17 a	8.04 ± 0.15 a	8.07 ± 0.00 a	8.42 ± 0.16 a
Glutamic acid	31.98 ± 1.6 b	38.97 ± 2.1 a	39.79 ± 1.08 a	40.75 ± 1.67 a	43.05 ± 0.82 a
Glycine	5.98 ± 0.2 c	6.07 ± 0.24 c	6.79 ± 0.29 bc	7.74 ± 0.13 ab	8.01 ± 0.19 a
Histidine	3.14 ± 0.23 b	3.54 ± 0.19 ab	3.46 ± 0.15 ab	3.66 ± 0.08 ab	3.89 ± 0.08 a
Isoleucine	5.29 ± 0.21 b	6.03 ± 0.29 ab	6.02 ± 0.2 ab	6.42 ± 0.16 a	6.77 ± 0.11 a
Leucine	9.4 ± 0.33 b	10.78 ± 0.52 ab	10.81 ± 0.31 ab	11.24 ± 0.36 a	11.7 ± 0.19 a
Lysine	3.67 ± 0.14 c	5.02 ± 0.23 b	5.34 ± 0.21 ab	5.85 ± 0.15 ab	5.98 ± 0.2 a
Methionine	2.39 ± 0.06 b	2.72 ± 0.11 ab	2.87 ± 0.09 a	3.08 ± 0.00 a	3 ± 0.09 a
Phenylalanine	7.48 ± 0.42 b	8.68 ± 0.53 ab	8.66 ± 0.22 ab	9.12 ± 0.29 ab	9.37 ± 0.2 a
Proline	14.85 ± 0.75 b	19.23 ± 1.29 a	20.16 ± 0.55 a	20.44 ± 1.36 a	21.44 ± 0.63 a
Serine	5.84 ± 0.24 b	6.57 ± 0.38 ab	6.71 ± 0.16 ab	6.78 ± 0.16 ab	6.84 ± 0.08 a
Threonine	4.31 ± 0.14 c	4.7 ± 0.22 bc	5.12 ± 0.14 ab	5.11 ± 0.16 ab	5.35 ± 0.04 a
Tryptophan	1.15 ± 0.3 a	0.89 ± 0.19 a	0.94 ± 0.26 a	0.53 ± 0.00 a	0.74 ± 0.08 a
Tyrosine	3.36 ± 0.19 b	3.39 ± 0.18 b	3.78 ± 0.16 ab	4.34 ± 0.09 a	4.22 ± 0.16 a
Valine	7.04 ± 0.22 b	7.8 ± 0.35 ab	7.8 ± 0.24 ab	8.29 ± 0.29 a	8.68 ± 0.18 a
Total	133.22 ± 5.01 b	155.98 ± 6.81 a	160.17 ± 4.01 a	166.58 ± 4.77 a	172.46 ± 2.36 a
CP	12.08 ± 0.45 b	13.34 ± 0.65 ab	14.55 ± 0.3 a	14.3 ± 0.64 a	15.17 ± 0.3 a

[a]Values are means ± SE (n = 5 except for Cysteine, Methionine and Tryptophan were n = 2 or 3). Different letters indicate significant differences between treatments ($p \leq 0.05$, T or T' test) for each amino acid separately. [b]Cysteine is expressed as cysteic acid.

Overall, glutamic acid, proline and leucine were the most abundant amino acids in kernels with concentration intervals of 32-43, 15-21 and 9-12 mg g^{-1} respectively (Table 4), a ranking consistent with other barley kernel composition studies (Pomeranz et al., 1976; Newman and Newman, 2008).

More in details, *n*CeO_2 and *n*TiO_2 did not significantly modify concentrations of arginine and tryptophan but they significantly and similarly increased cysteine, glutamic acid lysine and proline concentrations in all treatments in respect to control. Aspartic acid concentration was unaffected at 500 mg kg^{-1} of both *n*CeO_2 and *n*TiO_2 treatments while significantly and similarly increased at 1000 mg kg^{-1} of both *n*CeO_2 and *n*TiO_2 treatments. The other amino acid responses varied depending on which MeNPs were added in soil. In particular, *n*CeO_2 treatments did not modify concentrations of alanine, glycine, histidine, isoleucine, leucine, phenylalanine, serine, tyrosine and valine. On the contrary, methionine and threonine significantly increased only at the highest *n*CeO_2 treatment. Both *n*TiO_2 treatments significantly increased concentrations of alanine, glycine, isoleucine, leucine, methionine, threonine, tyrosine and valine. Conversely, only the highest *n*TiO_2 treatment significantly increased histidine, phenylalanine and serine concentrations. However, in most amino acids the largest concentration was consistently measured at 1000 mg *n*TiO_2 kg^{-1} treatment.

In general, a total of 18 amino acids have been identified in barley proteins: with respect to animal growth requirements, lysine and threonine are the first and second most limiting amino acids, with methionine and tryptophan in third and fourth positions, respectively (Newman and Newman, 2008). Since lysine is the first limiting amino acid in cereal grain protein, an improvement in the level of lysine results in an improved nutritional quality.

However, high lysine strains and mutants (as Hiproly barley, found in the world barley collection in 1969) have been found to be associated with reduced grain weight, and lower yields. Also the threonine increasing resulted in an improvement of nutritional quality of the kernel. However, these increments of limiting aminoacids are not sufficient to reach the concentrations required for human nutrition (Newman and Newman, 1992).

The barley cultivar Tunika is principally employied in malt production for brewing scope, these increments of aminoacid, related with decreasing of amylose content resulted in a quality decreasing of kernels for beer production.

As for proline, a positive correlation between proline in leaves and plant stress is supported by a large body of data. Besides acting as an excellent osmolyte, proline plays different roles during stress, as a metal chelator, an antioxidative defense molecule and a signaling

molecule (Hayat et al., 2012). An overproduction of proline, which in turn imparts stress tolerance by maintaining cell turgor or osmotic balance, is a common observation in stressful environments. We did not follow proline in leaf tissues, however, MeNPs-treated plants on average added 37% more proline in kernels compared to controls, which is the second largest increase, after the 51% increase of lysine. Therefore, MeNPs-treatments are supposedly operating as abiotic stressors on barley plants, and observed proline increase in kernels could be related to the in-season proline evolution in green tissues.

Differently from our observations, Rico et al. (2014, 2015) reported contrasting results for different amino acids in both barley and wheat exposed to 0, 125, 250 and 500 mg *n*CeO_2 kg^{-1}.

Finally, CP in kernels was significantly increased by approximately 19% in MeNPs-treated plants compared to control (Table 4). The increased CP is in line with the increased total amino acids concentrations under MeNPs-treatments (Table 4), on average 23% higher related to controls (Table 4). Apart for tryptophan, similar effects were observed for each amino acid separately. Indeed, the magnitude of MeNPs-treatments over CP, total amino acid and single amino acids concentrations were comparable.

6.3.4 Elemental Concentrations in Kernels

The effects of *n*CeO_2 and *n*TiO_2 in the soil on Ce and Ti, macronutrient and Na, and micronutrient concentrations in barley kernels from main shoot are displayed in Table 5, Table 6, and Table 7 respectively.

Table 5: Cerium and Titanium concentrations in barley kernels at ripening from main shoot grown in soil treated with none (control), 500 mg *n*CeO_2 kg^{-1}, 1000 mg *n*CeO_2 kg^{-1}, 500 mg *n*TiO_2 kg^{-1} and 1000 mg *n*TiO_2 kg^{-1}

Treatment	Ce (mg kg^{-1} dw)	Ti (mg kg^{-1} dw)
Control	0.5 ± 0.2 a	2.19 ± 1.19 a
500 mg *n*CeO_2 kg^{-1}	1.03 ± 0.84 a	1.27 ± 0.29 a
1000 mg *n*CeO_2 kg^{-1}	0.7 ± 0.37 a	0.85 ± 0.12 a
500 mg *n*TiO_2 kg^{-1}	1.08 ± 0.54 a	1.7 ± 0.53 a
1000 mg *n*TiO_2 kg^{-1}	1.16 ± 0.61 a	8.72 ± 4.76 a

[a]Values are means ± SE (n = 5). Different letters indicate significant differences between treatments ($p \leq 0.05$, T test) for each element separately.

Table 6: Concentration of macro-nutrients, Na, and Na/K and Na/Ca ratios in barley kernels at ripening from main shoot grown in soil treated with none (control), 500 mg *n*CeO_2 kg^{-1}, 1000 mg *n*CeO_2 kg^{-1}, 500 mg *n*TiO_2 kg^{-1} and 1000 mg *n*TiO_2 kg^{-1}.

Treatment	Ca (mg kg^{-1} dw)	K (mg kg^{-1} dw)	Mg (mg kg^{-1} dw)	Na (mg kg^{-1} dw)	P (mg kg^{-1} dw)	S (mg kg^{-1} dw)	Na/K	Na/Ca
Control	377 ± 21 c	4570 ± 105 a	1881 ± 59 a	187 ± 22 a	4549 ± 335 a	4758 ± 199 a	0.04 ± 0.01 a	0.5 ± 0.05 a
500 mg *n*CeO_2 kg^{-1}	387 ± 11 bc	3792 ± 82 b	1756 ± 22 a	150 ± 31 a	4519 ± 110 a	4162 ± 266 ab	0.04 ± 0.01 a	0.38 ± 0.07 ab
1000 mg *n*CeO_2 kg^{-1}	426 ± 19 bc	3755 ± 75 b	1765 ± 57 a	133 ± 18 a	4511 ± 312 a	3620 ± 144 bc	0.04 ± 0.01 a	0.32 ± 0.05 ab
500 mg *n*TiO_2 kg^{-1}	661 ± 81 a	4187 ± 157 ab	1983 ± 124 a	152 ± 17 a	4867 ± 234 a	3148 ± 80 c	0.04 ± 0.005 a	0.24 ± 0.04 b
1000 mg *n*TiO_2 kg^{-1}	543 ± 8 ab	3762 ± 77 b	1736 ± 39 a	95 ± 26 a	4359 ± 314 a	3194 ± 220 c	0.03 ± 0.01 a	0.18 ± 0.05 b

[a]Values are means ± SE (n = 5). Different letters indicate significant differences between treatments ($p \leq 0.05$, T test) for each element separately.

Table 7: Concentration of micro-nutrients in barley kernels at ripening from main shoot grown in soil treated with none (control), 500 mg *n*CeO_2 kg^{-1}, 1000 mg *n*CeO_2 kg^{-1}, 500 mg *n*TiO_2 kg^{-1} and 1000 mg *n*TiO_2 kg^{-1}.

Treatment	B (mg kg^{-1} dw)	Cu (mg kg^{-1} dw)	Fe (mg kg^{-1} dw)	Mn (mg kg^{-1} dw)	Ni (mg kg^{-1} dw)	Zn (mg kg^{-1} dw)
control	8.64 ± 1.02 ab	8.91 ± 1.33 a	38.81 ± 6.51 a	18.8 ± 0.64 b	0.44 ± 0.14 a	55.74 ± 5.36 b
500 mg *n*CeO_2 kg^{-1}	15.12 ± 4.73 a	8.01 ± 0.8 a	37.52 ± 2.61 a	21.87 ± 1.17 ab	0.34 ± 0.07 a	54.07 ± 2.55 b
1000 mg *n*CeO_2 kg^{-1}	3.32 ± 1.37 b	6.99 ± 0.31 a	28.49 ± 1.67 a	19.84 ± 0.68 b	0.39 ± 0.04 a	56.69 ± 1.18 b
500 mg *n*TiO_2 kg^{-1}	8.01 ± 1.7 ab	7.52 ± 1.16 a	34.25 ± 2.17 a	25.1 ± 1.06 a	0.75 ± 0.17 a	69.63 ± 2.61 a
1000 mg *n*TiO_2 kg^{-1}	6.02 ± 1.58 ab	8.24 ± 0.28 a	38.35 ± 4.47 a	21.59 ± 1.23 ab	0.32 ± 0.08 a	59.59 ± 1.34 ab

[a]Values are means ± SE (n = 5). Different letters indicate significant differences between treatments ($p \leq 0.05$, T test) for each element separately.

We did not observe significant differences among the treatments for Ce and Ti concentrations in kernels, as reported by our previous observations in vitro (Mattiello et al., 2015) and other authors who studied different species under *n*CeO_2 (Rico et al., 2014; Zhao et al., 2015; López-Moreno et al., 2010), or under *n*TiO_2 exposition in soil (Klingenfuss, 2014). However, other authors observed that *n*CeO_2 treatments largely increased Ce concentration in fruits and seeds of different species (Rico et al., 2013; Wang et al., 2012; Priester et al., 2012), among which is also barley (Rico et al., 2015). It was also observed a root to fruit translocation of *n*TiO_2 in cucumber after plant exposition to *n*TiO_2 in soil (Servin et al., 2013).

Our results suggest that translocation of manufactured *n*CeO_2 and *n*TiO_2 (at least of nominal sizes of 25 nm) into barley kernels is hardly possible, as Ce and Ti concentrations in kernels of treated plants were not significantly different from that of the control plants (Table 5).

Regarding nutrient concentrations, *n*CeO_2 treatments did not significantly modify several macro-nutrient concentrations (Ca, Mg, and P), Na (a beneficial nutrient) and all micronutrients except B. As for the affected macro-nutrients, K was significantly lowered under both *n*CeO_2 treatments, while S was significantly lowered only by 1000 mg *n*CeO_2 kg^{-1} treatment. Potassium is the most abundant cation in cytoplasm, actively maintaining osmotic potential and stabilizing pH between 7 and 8, the optimum range for most enzyme activities. Being also necessary for protein synthesis and other metabolic processes (Marschner, 1995), its reduction at both *n*CeO_2 levels and at 1000 mg *n*TiO_2 kg^{-1} treatment (see below) could have a negative impact on enzyme activities (and kernel quality). Sulfur is a structural constituent of coenzymes and secondary plant products containing amino acids cysteine and methionine and can also act as a functional group directly involved in metabolic reactions (Marschner, 1995). Therefore the reduction of S which occurred also at both *n*TiO_2 treatments (see below) could theoretically affect glutathione synthesis and the antioxidant capacity of kernels. However, the expected reduction in cysteine and methionine was not observed: conversely they were enhanced (Table 4). We speculate that even if S translocation to the kernels was lowered, the amount of available S was anyway effectively directed to the protein synthesis and avoiding its use for other purposes like precursors for syntheses of glutathione (GSH), co-factors (like iron–sulfur clusters, heme, siroheme, molybdenum centers, lipoate), essential vitamins (as biotin, thiamine), sulfur esters (coenzyme A) and sulfur derivatives (Beinert 2000; Leustek et al. 2000; Saito 2000; Marquet 2001; Gerber and Lill 2002; Mendel and Hänsch 2002; Noctor et al. 2002).

Under 1000 mg *n*CeO_2 treatment, B concentration was significantly lowered, approximately by 62% compared to the control, the severe reduction of B concentration could indicate a restricted permeation of B due to *n*CeO_2 presence. However, the mechanisms of *n*CeO_2 restriction to B permeation remain unclear.

Other authors reported contrasting data and only partially in agreement with our results. For example, similarly to our results Rico et al. (2013) observed no changes in concentrations of most of the nutrients in grain from three rice varieties grown in soil with 500 mg *n*CeO_2 kg^{-1} compared to control. Notable exceptions regarded Al, Fe, K, Na and S which varied differently in the three analyzed varieties, which indicates not only a dose effect but also a variety response. Also wheat grown on soil exposed at *n*CeO_2 concentrations lower than 500 mg kg^{-1} showed no change in kernel nutrients except for S and Mn (Rico et al., 2014). Sulfur and Mn had an inverse hormetic response, that is at low *n*CeO_2 treatments, S and Mn were significantly lowered while at 500 mg *n*CeO_2 kg^{-1} S and Mn were not different from control (Rico et al., 2014).

Rico et al. (2015b) observed significant increase in both macro- and micro-nutrients in grains from barley plants exposed to *n*CeO_2 at different levels which is in disagreement with our observations on the same species. Peralta-Videa et al. (2014) reported no effects on S and K content in pods from soybean plants grown at *n*CeO_2 treatments close to ours. Different results were obtained also by Zhao et al. (2014) which analyzed mineral content of cucumber fruit from plants grown at comparable *n*CeO_2 concentrations to ours. Authors did not observe any significant differences between treated and control plants in all elements concentrations. Finally, under *n*CeO_2 treatments comparable to ours, significant increases of K and Mn at 800 mg *n*CeO_2 kg^{-1} treatment were observed in undeveloped corn cobs but not in developed ones (Zhao et al., 2015).

Although such a large variation of responses in different species exposed to *n*CeO_2 treatments, it is safe to say that nanoparticles are influencing nutrients concentration of seeds and fruits. This can indicate a breakdown of nutrient homeostasis, due to abiotic stress induced by nanoparticles exposition.

Regarding *n*TiO_2 treatments, Ca was significantly increased and S significantly lowered under both *n*TiO_2 treatments, while K was lowered only by 1000 mg *n*TiO_2 kg^{-1} treatment. Calcium is a messenger between environmental factors and plant responses in terms of growth and development (Marschner, 1995). The high levels of Ca could be linked to the higher yield grain under *n*TiO_2 treatments. *n*TiO_2 (or the released ionic form) could potentially have a beneficial effect enhancing absorption and translocation of Ca (Alcaraz-

Lopez et al., 2003). Moreover, other authors showed that seeds immersed in *n*TiO_2 solution and sprayed with *n*TiO_2 over shoots, could enhance plant growth through several mechanisms including the enhancement of photosynthesis, enzyme activity and even by a supposed new N_2 fixation mechanism in the air (Gao et al., 2006; Yang et al., 2007; Gao et al., 2008; Linglan et al., 2008; Su et al., 2009). However, in our experiment we include *n*TiO_2 into the soil and the observed benefits could be explained by translocation of *n*TiO_2 in shoots, at least of minimum amounts.

As for micronutrients, only Mn and Zn reached significantly higher concentrations at 500 mg *n*TiO_2 kg^{-1} but not at 1000 mg *n*TiO_2 kg^{-1} treatment: again a hormetic response.

Contrary to the *n*CeO_2 only Servin et al. (2013) reported data from a full mineral analysis in cucumber fruit. There was no substantial effect on macro- and micro-nutrients in fruits, apart for P and K in which a hormetic effect was detected. On the other hand and according to our results, Klingenfuss (2014) reported no significant differences in P concentrations in wheat grains after exposition of plants in soil exposed to a range of *n*TiO_2 varying from 1 to 1000 mg *n*TiO_2 kg^{-1}. However, these results could indicate a species-specific response and possibly diverse effects on mineral concentrations in eudicots and monocots, with the latter more affected.

The Na/K and Na/Ca ratios are useful indicators of plant response to the stress and can indicate the kernels quality as well. In all the treatments the Na/K ratio was unaffected indicating no major metabolic disorders (Table 6) (Brady et al., 1984). On the contrary, Na/Ca ratio was significantly affected under both *n*TiO_2 treatments with the ratio reduced of 2.4 folds on average (Table 6). This is suggesting an increased competitive inhibition between absorption of Na and Ca which can possibly mitigate eventually harmful effects of Ti – similarly to what was observed for rice under *n*CeO_2 exposition (Rico et al., 2013). Alternatively, as Na concentrations did not change significantly from the control whereas Ca concentrations increased significantly under *n*TiO_2 treatments this can be due to a beneficial effect of *n*TiO_2 which can enhance Ca absorption and translocation as observed above. In kernels under *n*TiO_2 treatments, the reduction in Na/Ca ratio and the increased concentration of Ca can be beneficial for human nutrition from one side but can also affect negatively the eating quality of kernels on the other side.

6.3.5 Pearson's Product-moment Correlation

Pearson's product-moment correlation coefficients had shown that only Mn ($r = 0.859$, $df = 13$, $p < 0.001$) concentration was positively and significantly correlated with Ce

concentration in kernels from different concentrations of *n*CeO_2 in soil. Therefore, *n*CeO_2 interfered with Mn demonstrating the tendency of Mn accumulation at increasing levels of Ce in kernels. With respect to the few published articles about Ce correlation with other elements in grains of barley and other species, we did not find any evidence of correlation between other elements and Ce (Rico et al., 2013; Rico et al., 2014; Rico et al., 2015a).
Finally, there were no significant correlation between Ti concentration in kernels and all the other measured parameters under *n*TiO_2 treatments.
A separate comment need to be given for the contrasting data reported in the only one barley full life cycle study performed (Rico et al., 2015b). A compromised barley production from plants cultivated at 500 mg *n*CeO_2 kg^{-1} in soil and an enhanced storage in grains of macro- and micro-nutrients and only a partial increase in amino acid content (among which there was no lysine) in lower treatments were observed (Rico et al., 2015b). Besides the fact that authors cultivated a different variety of barley in another soil, the contrasting results obtained by our experiments can be tentatively explained by different *n*CeO_2 sizes (8 nm vs. 22.7 nm) and the methodology used to apply MeNPs into the soil. In fact, Rico et al. (2015b) sonicated a *n*CeO_2 solution prior diluting it into soil and mixing, thus possibly making *n*CeO_2 more bioavailable. It is also possible that a large ionic Ce quantity was released in this solution which is toxic to plants (Zhang et al., 2015; Cui et al., 2014).
In conclusion, bioaccumulation results showed a low translocation of Ce and Ti into kernels of comparable level to the control treatment. Results had shown that among macro-nutrients K and S can represent a threat to food chain if their content is reduced. On the contrary Ca in kernels was enhanced by *n*TiO_2 treatments. Among the MeNPs treatments some significant effects (on kernel numbers and 100-kernels weight, Zn, and Mn concentrations) were visible only on lower concentration while not at higher concentration (hormetic response). Therefore, different nanoparticles can influence negatively or positively different nutritional values. Although the observed differences between 500 and 1000 mg MeNPs kg^{-1} treatments might be due to MeNPs interactions (agglomeration and/or association) with soil constituents, at higher concentrations this hypothesis remains to be tested. Indeed, toxicity of MeNP could be closely related to their chemical composition, structure, particle size and surface area. Substantial research on MeNP size, their physico-chemical characteristics and interactions with soil components is largely needed.
Both MeNPs impacted negatively the amylose content of kernels with a reduction in grain yield. This was associated to the increase of CP and of most amino acids. Interestingly,

lysine, the essential and largely deficient amino acid in cereal grains, showed the largest percent increase.

In terms of MeNPs impact on barley food production, our data are far from being exhaustive; however, a possibly negative impact over kernel energy content, K and S concentrations might be counterbalanced by CP and lysine increase. Moreover, *n*TiO_2 treatments increased also Ca, Mg and Zn kernel concentrations.

Our findings demonstrate that *n*CeO_2 and *n*TiO_2 are acting differently on the nutritional quality of barley kernels. Generally, barley kernels resulted more negatively affected by *n*CeO_2 while *n*TiO_2 can potentially have a beneficial effect. This study provides the first proof that *n*CeO_2 and *n*TiO_2 NPs can have significant and contrasting impacts on the composition and nutritive value of barley kernels.

7 Conclusions and Future Perspectives

The majority of green chemistry research has the synthesis of metal nanoparticles (MeNPs) by plants extracts (ex-planta) as the principal objective while only a little part of them study the MeNPs formation inside the tissue of the living plants (in-planta). This tendency is due to the applicative purpose of the experiments. In fact in the majority of paper, researcher obtain MeNPs by changing the reaction conditions. Subsequently MeNPs are characterized in order to verify their physical-chemical characteristics and whether the methods are reproducible.

From these assumptions, we decided to investigate the green synthesis of MeNPs in planta because their mechanism formation and the organic molecules involved in the process are less studied.

The results demonstrate the plant capacity to synthetize MeNPs but among the organic molecules analyzed none of them resulted as the principal actor for the MeNPs formation. For this reason further experiments are needed to investigate this aspect.

The clarification of metabolic processes involved in MeNPs synthesis in vivo could open new insight in synthetizis of MeNPs.

One intriguing possibility is screening of metallophyte species for high amount of organic molecule or class of organic molecules involved in the MeNPs formation.

The selected metallophyte species could then be used for a double purpose: phytoremediation intervention and also MeNPs synthesis.

Regarding the toxic effects caused from the interaction between NPs and plants, the obtained results demonstrate the genotoxic and phytotoxic effects of NPs in the early stages and phenologic and morphologic effects along the plant entire life cycle but in this case the parameters analyzed were affected both in a negative and in a positive way. The effects of this interaction was also verified at the level of kernels obtained from the plants treated for the entire life cycle. The kernels chemical composition was modified both in this case in a positive and in a negative way. In conclusion the effects could be related to the element of which is composed the NPs but also on the base of their concentration. In fact, some parameters resulted more affected by the treatment at the lowest concentration than the highest ones, this concentration effect could be related to the peculiar NPs characteristics which differ from their bulk counterpart and consequently the NPs could be more toxic at lower concentrations respect to the higher ones.

This could bring a new kind of issue, as the majority of works done in last years were conducted in the presence of high concentration of NPs, and it would be interesting to verify what could happen whether the plants grow in presence of low NPs concentration in the media and for a period longer than a generation. Moreover, the seeds obtained in this way could be studied in order to check how they are affected by these way of treatments in terms of germinability.

On the contrary to the observed toxic effects, the uptake and translocation showed a dose response in all experiments. At increase of NPs present in the media the NPs element concentration in plant tissues increase as well. For this aspect the NPs behave like their bulk counterpart. This effect rising another lack about NPs in their legislation. At the present day there are not any European directives which regulate or fix a limit of this new kind of material in the environment and more specifically into the soil.

In the last decade the number of agricultural products based on NPs are increased and they will increase more in the next years. Therefore, a prompt action by legislation in order to regulate the NPs emissions would be desired.

Another aspect which is not well studied is how the NPs behave in a complex system, as the majority of the experiments were conducted in hydroponic system or in petri dishes. For this reason the experiment set up along the entire life cycle were conducted in soil spiked with NPs in order to see how they behave in a complex environment. More precisely what is happening once the NPs reach the soil and they start to interact with the organic matter or the inorganic matrix was studied. The difficult part to achieve this aim is linked with the nature of NPs, in particular it is still quite difficult to detect them in a complex

environment like the soil and also itself complexity make the investigation quite difficult. Hence it could be useful to find some methods to analyze the NPs in a complex matrix.

Another aspect which needs to be elucidate is related with the "corona" concept. The "corona" is the evolving collection of protein or biomolecule associated with NPs which confers to them a well define biological/ecological identity. This identity is the combination of NPs material-intrinsic properties and the "corona" of a given biological or ecological compartment that determine the interactions of NPs with cell and tissues.

The "corona" could be subdivide in hard and soft "corona", the tightly bound proteins that remained associated with the NPs even following extensive centrifugation and washing steps represent the hard "corona" whereas more loosely bind protein associated with the hard "corona" represent the soft "corona". The soft "corona" is in dynamic exchange with the surrounding protein while the hard "corona" remain associated for sufficiently long timescale that it is the NPs-corona complex that interacts with living system and it is what cell "sees". When the NPs enter in the environment they go through different types of transformation as chemical (photooxidation or photoreduction), physical (agglomeration, aggregation or dissolution), biological (oxidation and carboxylation) and interaction with biomolecules including natural organic macromolecules (NOM), all of which influence the NPs persistence, bioavailability/biouptake, reactivity and toxicity.

Biomolecule can be any macromolecule produced via biological processes and acquire by NPs as it interacts with living systems. An ecomolecule can be any macromolecule formed and acquired by the NPs in the environment, generally NOM or secreted biomolecules. Two most important types of NOM are humic substances (HS) and polysaccharides (and their residues). The NOM in the nanoscale size range and their concentration are orders of magnitude higher than the modeled concentration of NPs and so are likely to modify the properties and behaviors of NPs.

From this purposes part of the research was focused on how the NPs o are influenced by the ecomolecule nce in the environment and how the secreted biomolecules affect the NPs properties and consequently their biovailability. For this purpose, experiments with barley plants were grown in a hydroponic system in presence of low cerium nanoparticles (*n*CeNPs) because from the previous works (Mattiello et al., 2015) some parameters were more affected at the lowest concentrations than the highest and in presence of gum arabic (GA) and because not many studies in the last years have investigated the behavior of NPs when they enter in contact with polysaccharides. The experiments were conducted in the first seven months of my third year of research at the Facility for Environmental

Nanoscience Analysis and Characterization (FENAC) laboratory of School of Geography Earth and Environmental Science (GEES) in Birmingham University. There I learnt how to use instruments for the NPs characterization like Dynamic Light Scattering (DLS) system, Differential Centrifugal Sedimentation (DCS) system, Atomic Force Microscopy (AFM), Transmission Electron Microscopy (TEM) and Brunauer-Emmett-Teller (BET) instrument. I utilized these instruments for the *n*CeO_2 characterization not and in contact with plants exudates at different time in order to analyze if the *n*CeO_2 properties change or not between them.

The obtained data are not display in this thesis because they are still in elaboration but the preliminary data show some differences between the *n*CeO_2 were not in contact with plants and the *n*CeO_2 in contact with them.

8 Abbreviations Used

AA = ascorbic acid

AFM = Atomic Force Microscopy

AgNPs = silver nanoparticles

BET = Brunauer Emmett Teller method

CA = citric acid

DLS = Dynamic Light Scattering method

FRU = fructose

GLC = glucose

ICP-OES = inductively coupled plasma optical emission spectroscopy

MeNPs = metallic nanoparticles

nCeO_2 = Cerium Oxide Nanoparticles

nTiO_2 = Titanium Oxide Nanoparticles

PAR = photosynthetically active radiation

PP = polyphenols

TEM = transmission electron microscope

9 Acknowledgments

These works were in part supported by a project funded by DISA – Department of Agriculture and Environmental Sciences, University of Udine, through Grant n.64 dd. 08-09.2014 (RANDOLPH – Relazioni tra nanoparticelle metalliche e piante superiori). The

authors acknowledge Francesco Bertolini and Nicola Zorzin for their relevant contribution to the work, Anastasios Papadiamantis for technical assistance in the use of BET. The authors also thank Giorgio Angelo Lucchini (Dipartimento di Scienze Agrarie e Ambientali – Produzione, Territorio, Agroenergia, Università degli Studi di Milano, Italy) for ICP-MS analyses, Barbara Piani (Department of Agricultural and Environmental Sciences, University of Udine, I) for HPLC analysis, Marta Fontana (Department of Agricultural and Environmental Sciences, University of Udine, I) for CHNS, amylose and β-glucan analysis, and Iseult Lynch (The School of Geography, Earth and Environmental Sciences, Facility for Environmental Nanoscience Analysis and Characterization, University of Birmingham, UK) for providing nanoparticles characterizations facilities.

References

Aaron Wold, Photocatalytic Properties of TiO_2. Chem Mater 1993, 5:280-283

Adriano DC (2001). Trace Elements in Terrestrial Environments Biogeochemistry, Bioavailability, and Risks of Metals, New York, New York: Springer.

Aeschlimann M, Bauer M, Bayer D, (2009). Ultrafast Phenomena, Berlin, Germany: Springer.

Ahmad N, Sharma S, Rai R, Rapid green synthesis of silver and gold nanoparticles using peels of Punica granatum. Adv Mat Lett 2012, 3:376-380.

Alcaraz-Lopez C, Botia M, Alcaraz CF, Riquelme F, Effects of foliar sprays containing calcium, magnesium and titanium on plum (*Prunus domestica* L.) fruit quality. J Plant Physiol 2003, 160:1441-1446.

Alivisatos AP, Gu W, Larabell C, Quantum dots as cellular probes. Annu Rev Biomed Eng 2005, 7:55-76.

Al-Salman HS, Abdullah MJ, Structural, optical, and electrical properties of Schottky diodes basedon undoped and cobalt-doped ZnO nanorods prepared by RF-magnetron sputtering. Mat Sci Eng B-Solid 2013, 178:1048-1056.

Anderson CWN, Brooks RR, Chiarucci A, LaCoste CJ, Leblanc M, Robinson BH, Simcocke R, Stewart RB, Phytomining for nickel, thallium and gold. J Geochem Explor 1999, 67:407-415.

Antisari LV, Carbone S, Gatti A, Vianello G, Nannipieri P, Uptake and translocation of metals and nutrients in tomato grown in soil polluted with metal oxide (CeO_2, Fe_3O_4, SnO_2, TiO_2) or metallic (Ag, Co, Ni) engineered nanoparticles. Environ Sci Pollut Res 2015, 22:1841-1853.

Arepalli S, Nikolaev P, Holmes W, Files BS, Production and measurements of individual single-wall nanotubes and small ropes of carbon. Appl Phys Lett 2001, 78:1610-1612.

Armendariz V, Herrera I, Peralta-Videa JR, Yacaman MJ, Troiani H, Santiago P, Gardea-Torresdey JL, Size controlled gold nanoparticle formation by Avena sativa biomass: Use of plants in nanobiotechnology. J Nanopart Res 2004, 6:377-382.

Ascencio JA, Mejia Y, Liu HB, Angeles C, Canizal G, Bioreduction synthesis of Eu-Au nanoparticles. Langmuir 2003, 19:5882-5886.

Asli S, Neumann M, Colloidal suspensions of clay or titanium dioxide nanoparticles can inhibit leaf growth and transpiration via physical effects on root water transport. Plant Cell Environ 2009, 32:577-584.

Atha DH, Wang H, Petersen EJ, Cleveland D, Holbrook D, Jaruga P, et al., Copper oxide nanoparticle mediated DNA damage in terrestrial plant models. Environ Sci Technol 2012, 46:1819-1827.

Atienzar FA and Jha AN, The random amplified polymorphic DNA (RAPD) assay and related techniques applied to genotoxicity and carcinogenesis studies: a critical review. Mutat Res 2006, 613:76-102.

Aubert T, Burel A, Esnault M-A, Cordier S, Grasset F, Cabello-Hurtado F, Root uptake and phytotoxicity of nanosized molybdenum octahedral clusters. J Haz Mat 2012, 219-220:111-118.

Babu S, Velez A, Wozniak K, Szydlowska J, Seal S, Electron paramagnetic study on radical scavenging properties of ceria nanoparticles. Chem Phys Lett 2007, 442:405-408.

Balbi T, Smerilli A, Fabbri R, Ciacci C, Montagna M, Grasselli E, Brunelli A, Pojana G, Marcomini A, Gallo G, et al., Co-exposure to n-TiO_2 and Cd^{2+} results in interactive effects on biomarker responses but not in increased toxicity in the marine bivalve M. galloprovincialis. Sci Total Environ 2014, 493:355-364.

Bamwenda GR, Arakawa H, Cerium dioxide as a photocatalyst for water decomposition to O-2 in the presence of Ce-aq(4+) and Fe-aq(4+) species. J Mol Catal A-Chem 2000, 161:105-113.

Bankar A, Joshi B, Kumara AR, Zinjarde S, Banana peel extract mediated novel route for the synthesis of silver nanoparticles. Colloids and Surfaces Colloids Surf, A 2010, 368:58-63.

Batley G, Kirby JK, McClaughlin MJ, Fate and risks of nanomaterials in aquatic and terrestrial environments. Acc Chem Res 2013, 46:854-862.

Beattiew IR, Haverkamp RG, Silver and gold nanoparticles in plants: Sites for the reduction to metal. Metallomics 2011, 3:628-632.

Beckles DB, Thitisaksul M, How environmental stress affects starch composition and functionality in cereal endosperm. Starch-Stärke 2013, 65:1-14.

Beinert H, A tribute to sulfur. Eur J Biochem 2000, 267:5657-5664.

Bekyarova E, Fornasiero P, Kašpar J, Graziani M, CO oxidation on $Pd/CeO_2 \pm ZrO_2$ catalysts. Catal Today 1998, 45:179-183.

Bell IR, Ives JA, Jonas WB, Non linear effects of nanoparticles: biological variability from hormetic doses, small particle sizes, and dynamic adaptive interactions. Dose Response 2014, 12: 202-232.

Bergmeyer HU, Bernt E, Schmidt F, Stork H (1974). Methods of Enzymatic Analysis, New York, New York:Academic; 1974:1196-1201.

Berndt M, Rohmer M, Ashall B, Schneider C, Aeschlimann M, Zerulla D, Polarization selective near-field focusing on mesoscopic surface patterns with threefold symmetry measured with PEEM. Opt Lett 2009, 34:959-961.

Berry CS, Resistant starch: formation and measurement of starch that survives exhaustive digestion with amylolytic enzymes during the determination of dietary fibre. J Cereal Sci 1986, 4:301-314.

Bhaduri SB, Chakraborty A, Rao RM, Method of fabrication ceria-stabilized tetragonal zirconia polycrystals. J Am Ceram Soc 1988, 71:C410-C411.

Bhatt I, Tripathi BN, Interaction of engineered nanoparticles with various components of the environment and possible strategies for their risk assessment. Chemosphere 2011, 82:308-317.

Binns C, Nanocluster deposited on surfaces. Surf Sci Rep 2001, 44:149.

Blake DM, Maness P-C, Huang Z, Wolfrum EJ, Huang J, Jacoby WA, Application of the photocatalytic chemistry of titanium dioxide to disinfection and the killing of cancer cells. Separ Purif Method 1999, 28:1-50.

Boonyanitipong B, Kositsup B, Kumar P, Baruah S, Dutta J, Toxicity of ZnO and TiO_2 nanoparticles on germinating rice seed *Oryza sativa* L. Int J Biosci Biochem Bioinform 2011, 1:282-285.

Borker P, Salker AV, Solar assisted photocatalytic degradation of Naphthol Blue Black dye using $Ce_{1-x}Mn_xO_2$. Mater Chim Phys 2007, 103:366-370.

Bosch L, Alegria A, Farrè R, Application of the 6-aminoquinolyl-N-hydroxysuccinimidyl carbamate (AQC) reagent to the RP-HPLC determination of amino acids in infant foods. J Chromatogr B, 2006, 831:176-183.

Bradford M, A rapid and sensitive method for the quantitation of microgram quantities of protein utilizing the principle of protein-dye binding. Anal Biochem 1976, 72:248-254.

Brady CJ, Gibson TS, Barlow EWR, Speirs J, Wyn Jones RG, Salt-tolerance in plants. I. Ions, compatible organic solutes and the stability of plant ribosomes. Plant Cell Environ 1984, 7:571-578.

Brant JA, Lecoanet H, Hotze M, Wiesner MR., Comparison of electrokinetic properties of colloidal fullerenes (n-C60) formed using two procedures. Environ Sci Technol 2005, 39:6343-6351.

Brar SK, Verma M, Tyagi RD, Surampalli RY, Engineered nanoparticles in wastewater and wastewater sludge – Evidence and impacts. Waste Manage 2010, 30:504-520.

Breierová E, Vajcziková I, Sasinková V, Stratilová E, Fišera M, Gregor T, Šajbidor J, Biosorption of cadmium ions by different yeast species. Z Naturforsch C Bio Sci 2002, 57c:634-639.

Brooks RR, Chambers MF, Nicks LJ, Robinson BH, Phytomining. Trends Plant Sci 1998, 3:359-362.

Brown WN, Molhenhauer H, Johnson C, An electron microscope study of silver nitrate reduction in leaf cells. Am J Bot 1962, 49:57-63.

Brust M, Kiely CJ, Some recent advances in nanostructure preparation from gold and silver nanoparticles: A short topical review. Colloid Surf A: Physicochem Eng Asp 2002, 202:175-186.

Burda C, Chen X, Narayanan R, El-Sayed MA, Chemistry and properties of nanocrystals of different shapes. Chem rev 2005, 105:1025-1102.

Burgess RC, Burman B, Kruhlak MJ, Misteli T, Activation of DNA damage response signaling by condensed chromatin. Cell Rep 2014, 9:1703-1717.

Burke DJ, Zhu S, Pablico-Lansigan MP, Hewins CH, Samia ACS, Titanium oxide nanoparticle effects on soil microbial communities and plant performance. Biol Fert Soil 2014, 50:1169-1173.

Buzea C, Pacheco-Blandino II, Robbie K, Nanomaterials and nanoparticles: Sources and toxicity. Biointerphases 2007, 2:MR17-MR172.

Capaldi Arruda SC, Silva AL, Galazzi RM, Azevedo RA, Arruda MA, Nanoparticles applied to plant science: a review. Talanta 2015, 131:693-705.

Carlino E, (2014). Transmission Electron Microscopy Characterization of Nanomaterials, Berlin, Deutschland:Springer.

Carp O, Huisman CL, Reller A, Photoinduced reactivity of titanium dioxide. Prog Solid State Ch 2004, 32:33-177.

Cassee FR, van Balen EC, Singh C, Green D, Muijser H, Weinstein J, Dreher K, Exposure, health and ecological effects review of engineered nanoscale cerium and cerium oxide associated with its use as a fuel additive. Crit Rev Toxicol 2011, 41: 213–229.

Chen H-I, Chang H-Y, Synthesis and characterization of nanocrystalline cerium oxide powders by two-stage non-isothermal precipitation. Solid State Commun 2005, 133:593-598.

Chen M, von Mikecz A, Formation of nucleoplasmic protein aggregates impairs nuclear function in response to SiO2 nanoparticles. Exp Cell Res 2005, 305:51-62.

Chug K-H, Park D-C, Water photolysis reaction on cerium oxide photocatalysts. Catal Today 1996, 30:157-162.

Clément L, Hurel C, Marmier N, Toxicity of TiO2 nanoparticles to cladocerans, algae, rotifers and plants–effects of size and crystalline structure. Chemosphere 2013,90:1083-1090.

Colman BP, Arnaout CL, Anciaux S, Gunsch CK, Hochella MF Jr, Kim B, Lowry GV, McGill BM, Reinsch BC, Richardson CJ, Unrine JM, Wright JP, Yin L, Bernhardt ES, Low concentrations of silver nanoparticles in biosolids cause adverse ecosystem responses under realistic field scenario. PLoS ONE 2013, 8:e57189.

Corma A, Atienzar P, García H, Chane-Ching J-Y, Hierarchically mesostructured doped CeO_2 with potential for solar-cell use. Nature Mater 2004, 3:394-397.

Cornelis G, Hund-Rinke K, Kuhlbusch T, van den Brink N, Nickel C, Fate and bioavailability of engineered nanoparticles in soils: A review. Crit Rev Env Sci Tec 2014, 44:2720−2764.

Corredor E, Testillano PS, Coronado M-J, González-Melendi P, Fernández-Pacheco R, Marquina C, Ibarra MR, de la Fuente JM, Rubiales D, Pérez- de-Luque A, Risueño MC, Nanoparticle penetration and transport in living pumpkin plants: in situ subcellular identification. BMC Plant Biol 2009, 9:45.

Cruz D, Falé P, Mourato A, Vaza PD, Serralheiro ML, Lino ARL, Preparation and physicochemical characterization of Ag nanoparticles biosynthesized by Lippia citriodora (Lemon Verbena). Colloids Surf, B 2010, 81:67-73.

Cui D, Zhang P, Ma Y, He X, Li Y, Zhang J, Zhao Y, Zhang Z, Effect of cerium oxide nanoparticles on asparagus lettuce cultured in an agar medium. Environ Sci Nano 2014, 1:459-465.

Dagley S (1974). Methods of Enzymatic Analysis, New York, New York:Chemie.

Dai ZR, Pan ZW, Wang ZL, Novel nanostructures of functional oxides synthesized by thermal evaporation. Adv Funct Mater 2003, 13:9-24.

Daniel MC, Astruc D, Gold nanoparticles: Assembly, supramolecular chemistry, quantum-size-related properties, and applications toward biology, catalysis, and nanotechnology. Chem Rev 2004, 104:293-346.

Darlington TK, Neigh AM, Spencer MT, Nguyen OT, Oldenburg SJ, Nanoparticle characteristics affecting environmental fate and transport through soil. Environ Toxicol Chem 2009, 28:1191-1199.

Das M, Patil S, Bhargava N, Kang J-F, Riedel LM, Seal S, Hickman JJ, Auto-catalytic ceria nanoparticles offer neuroprotection to adult rat spinal cord neurons. Biomaterials 2007, 28:1918-1925.

Dehkourdi EH, Mosavi M, Effect of anatase nanoparticles (TiO2) on parsley seed germination (Petroselinum crispum) in vitro. Biol Trace Elem Res 2013, 155:283-286.

Delogu G, Cattivelli L, Pecchioni N, De Falcis D, Maggiore T, Stanca AM, Uptake and agronomic efficiency of nitrogen in winter barley and winter wheat. Eur J Agron 1998, 9:11-20.

Derfus AM, Chan WCW, Bhatia SN, Probing the cytotoxicity of semiconductor quantum dots. Nano Lett 2004, 4:11-18.

Dietz KJ, Herth S, Plant nanotoxicology. Trends plant Sci 2011, 16:582-589.

Dimpka CO. McLean JE, Britt DW, Anderson AJ, Bioactivity and biomodification of Ag, ZnO, CuO nanoparticles with relevance to plant performance in agriculture. Ind Biotechnol 2012, 8:344-357.

Dofing SM, Phenological development–yield relationships in spring barley in a subarctic environment. Can J Plant Sci 1995, 75:93-97.

Elsila JE, de Leon NP, Plows FL, Buseck PR, Zare RN, Extracts of impact breccia samples from Sudbury, Gardnos, and Ries impact craters and the effects of aggregation on C60 detection. Geochim cosmochim Ac 2005, 69:2891-2899.

Etheridge ML, Campbell SA, Erdman AG, Haynes CL, Wolf SM, McCullough J, The big picture on nanomedicine: the state of investigational and approved nanomedicine products. Nanomed Nanotechnol Biol Med 2013, 9:1-14.

Evelyn A, Mannick S, Sermon PA, Unusual carbon-based nanofibers and chains among diesel-emitted particles. Nano Lett 2002, 3:63-64.

Fan R, Huang YC, Grusak MA, Huang CP, Sherrier DJ, Effects of nano-TiO(2) on the agronomically-relevant Rhizobium-legume symbiosis. Sci Total Environ 2014, 466-467:503-512.

FAOSTAT (2014). Food and Agricultural Commodities Production: Commodities by Regions. Available at: http://faostat3.fao.org/faostat-gateway/go/to/browse/ranking/commodities_by_regions/E [accessed Sept 4, 2015]

FAOSTAT (2016). Food and Agriculture Organization of the United Nations. Available at: http://faostat3.fao.org/download/Q/QC/E [accessed Feb 20, 2016].

Feizi H, Moghaddam PR, Shahtahmassebi N, Fotovat A, Impact of bulk and nanosized titanium dioxide (TiO_2) on wheat seed germination and seedling growth. Biol Trace Elem Res 2012, 146:101-106.

Ferry JL, Craig P, Hexel C, Sisco P, Frey R, Pennington PL, Fulton MH, Scott IG, Decho AW, Kashiwada S, Murphy CJ, Shaw TJ, Transfer of gold nanoparticles from the water column to the estuarine food web. Nat Nanotechnol 2009, 4:441-444.

Feynman PR, "Plenty of room at the bottom", American Physical Society, Pasadena, December 1959.

Fierro JLG, Soria J, Sanz J, Rojo JM, Induced changes in ceria by thermal treatments under vacuum or hydrogen. J Solid State Chem 1987,

Foltête A-S, Masfaraud J-F, Bigorgne E, Nahmani J, Chaurand P, Botta C, Labille J, Rose J, Férard J-F, Cotelle S, Environmental impact of sunscreen nanomaterials: Ecotoxicity and genotoxicity of altered TiO2 nanocomposites on *Vicia faba*. Env Poll 2001, 159:2515-2522.

Frazier TP, Burklew CE, Zhang B, Titanium dioxide nanoparticles affect the growth and microRNA expression of tobacco (*Nicotiana tabacum*). Funct Integr Genomics 2014, 14:75-83.

Frens G, Particle size and sol stability in metal colloids. Colloid Polym Sci 1972, 250:736-741.

Fujishima A, Honda K, Electrochemical photolysis of water at a semiconductor electrode. Nature 1972, 238:37-38.

Fujishima A, Rao TN, Tryk DA, Titanium dioxide photocatalysis. J Photochem Photobiol C 2000, 1:1-21.

Fujishima A, Zhang X, Tryk DA, TiO_2 photocatalysis and related surface phenomena. Surf Sci Rep 2008, 63:515-582.

Galata SF, Evangelou EK, Panayiotatos Y, Sotiropoulos A, Dimoulas A, Post deposition annealing studies of lanthanum aluminate and ceria high-k dielectrics on germanium. Microelectron Reliab 2007, 47:532-535.

Gan PP, Li SFY, Potential of plant as a biological factory to synthesize gold and silver nanoparticles and their applications. Rev Environ Sci Biotechnol 2012, 11:169-206.

Gao F, Hong F, Liu C, Zheng L, Su M, Wu X, Yang F, Wu C, Yang P, Mechanism of nano-anatase TiO_2 on promoting photosynthetic carbon reaction of spinach: inducing complex of rubisco-rubisco activase. Biol Trace Elem Res 2006, 111:239-253.

Gao F, Liu C, Qu C, Zheng L, Yang F, Su M, Hong F, Was improvement of spinach growth by nano-TiO_2 treatment related to the changes of Rubisco activase? Biometals 2008, 21:211-217.

Gardea-Torresdey JL, Gomez E, Peralta-Videa JR, Parsons JG, Troiani H, Yacaman MJ, Alfalfa sprouts: A natural source for the synthesis of silver nanoparticles. Langmuir 2003, 19:1357-1361.

Gardea-Torresdey JL, Parsons JG, Gomez E, Peralta-Videa J, Troiani HE, Santiago P, Yacaman MJ, Formation and growth of Au nanoparticles inside live alfalfa plants. Nano Lett 2002, 2:397-401.

Gardea-Torresdey JL, Rico CM, White JC, Trophic transfer, transformation and impact of engineered nanomaterials in terrestrial environments. Environ Sci Technol 2014, 48:2526-2540.

Gelesky MA, Umpierre AP, Machado G, Correia RRB, Magno WC, Morais J, Ebeling G, Dupont J, Laser-induced fragmentation of transition metal nanoparticles in ionic liquids. J Am Chem Soc 2005, 127:4588-4589.

Gerber J and Lill R, Biogenesis of iron–sulfur proteins in eukaryotes: components, mechanism and pathology. Mitochondrion 2002, 2:71-86.

Ghosh M, Bandyopadhyay M, Mukherjee A, Genotoxicity of titanium dioxide (TiO_2) nanoparticles at two trophic levels: Plant and human lymphocytes. Chemosphere 2010, 81:1253-1262.

Gladish DK, Xu J, Niki T, Apoptosis-like programmed cell death occurs in procambium and ground meristem of Pea (*Pisum sativum*) root tips exposed to sudden flooding. Ann Bot 2006, 97:895-902.

Gogos A, Knauer K, Bucheli TD, Nanomaterials in plant protection and fertilization: Current state, foreseen applications, and research priorities. J Agric FoodChem 2012, 60:9781-9792.

Goharshadi EK, Samiee S, Nancarrow P, Fabrication of cerium oxide nanoparticles: Characterization and optical properties. J Colloid Interface Sci 2011, 356:473-480.

Gomez-Garay A, Pintos B, Manzanera JA, Lobo C, Villalobos N, Martín L, Uptake of CeO_2 nanoparticles and its effect on growth of *Medicago arborea* in vitro plantlets. Biol Trace Elem Res 2014, 161:143-150.

Grätzel M, Mesoporous oxide junctions and nanostructured solar cells. Curr Opin colloid In 1999, 4:314-321.

Grätzel M, Photoelectrochemical cells. Nature 2001, 414:338-344.

Grätzel M, Solar energy conversion by dye-sensitized photovoltaic cells. Inorg Chem 2005, 44:6841-6851.

Gruère GP, Implications of nanotechnology growth in food and agriculture in OECD countries. Food Policy 2012, 37:191-198.

Guerinot ML, Salt DE, Fortified foods and phytoremediation. Two sides of the same coin. Plant Physiol 2001, 125:164-167.

Günter Schmid (2004). Nanoparticles: From Theory to Application, Weinheim, Germany: WILEY-VCH.

Ha J, Cordova CD, Yoon TH, Spormann AM, Brown GE, "Microbial reduction of hematite: Effects of particle size and exopolysaccharides", American Chemical Society, San Francisco September 2006.

Hall JL, Cellular mechanism for heavy metal detoxification and tolerance. J Exp Bot 2002, 53:1-11.

Hall JL, Williams LE, Transition metal transporters in plants. 2003, 54:2601-2613.

Hamdy AS, Advanced nano-particles anti-corrosion ceria based sol gel coatings for aluminum alloys. Mater Lett 2006, 60:2633-2637.

Handy RD, Owen R, Valsami-Jones E, The ecotoxicology of nanoparticles and nanomaterials: Current status, knowledge gaps, challenges, and future needs. Ecotoxicology 2008, 17:315-325.

Hao YF, Meng GW, Ye CH, Zhang LD, Controlled synthesis of In_2O_3 octahedrons and nanowires. Cryst Growth Des 2005, 5:1617-1621.

Hardman R, A toxicologic review of quantum dots: Toxicity depends on physicochemical and environmental factors. Environ Health Persp 2006, 114:165-172.

Harris AT, Bali R, On the formation and extent of uptake of silver nanoparticles by live plants. J Nanopart Res 2008, 10:691-695.

Hasanzadeh M, Shadjou N, Eskandani M, Soleymani J, Jafari F, de la Guardia M, Dendrimer-encapsulated and cored metal nanoparticles for electrochemical nanobiosensing. Trends Anal Chem 2014, 53:137-149.

Hashimoto K, Irie H, Fujishima A, TiO_2 photocatalysis: A historical overview and future prospects. Jpn J Appl Phys 2005, 44:8269-8285.

Haverkamp RG (2011). Handbook of Phytoremediation, New York New York:Nova.

Haverkamp RG, Agterveld DV, Marshall AT, Pick your carats: nanoparticles of gold-silver copper alloy produced in vivo. J Nanopart Res 2007, 9:697-700.

Haverkamp RG, Marshall AT, The mechanism of metal nanoparticle formation in plants: limits on accumulation. J Nanopart Res 2009, 11:1453-1463.

Hayat S, Hayat Q, Alyemeni MN, Wani AS, Pichtel J, Ahmad A, Role of proline under changing environments. Plant Signal Behav 2012, 7:1456-1466.

Hernández-Alonso MD, Hungría AB, Martínez-Arias A, Fernández-García M, Coronado1 JM, Conesa JC, Soria J, EPR study of the photoassisted formation of radicals on CeO_2 nanoparticles employed for toluene photooxidation. Appl Catal B-Environ 2004, 50:167-175.

Hernández-Viezcas JA, Castillo-Michel H, Andrews JC, Cotte M, Rico CM, Peralta-Videa JR, Ge Y, Priester JH, Holden PA, Gardea-Torresdey JL, *In situ* synchrotron X-ray fluorescence mapping and speciation of CeO(2) and ZnO nanoparticles in soil cultivated soybean (*Glycine max*). ACS Nano 2013, 7:1415−1423.

Herrera-Becerra R, Zorrilla C, Ascencio JA, Production of iron oxide nanoparticles by a biosynthesis method: An environmentally friendly route. J Phys Chem C 2007, 111:16147-16153.

Hilaire S, Wanga X, Luoa T, Gorte RJ, Wagner J, A comparative study of water-gas-shift reaction over ceria supported metallic catalysts. Appl Catal A-Gen 2001, 215:271-278.

Hirano M, Kato E, Hydrothermal synthesis of cerium(IV) oxide. J Am Ceram Soc 1996, 79:777-780.

Holbrook RD, Murphy KE, Morrow JB, Cole KD, Trophic transfer of nanoparticles in a simplified invertebrate food web. Nat Nanotechnol 2008, 3:352-355.

Hong F, Yang F, Liu C, Gao Q, Won Z, Gu F, Wu C, Ma Z, Zhou J, Yang P, Influences of nano-TiO_2 on the chloroplast aging of spinach under light. Biol Trace Elem Res 2005, 104:249-260.

Hong F, Zhou J, Liu C, Yang F, Wu C, Zheng L, Yang P, Effect of nano-TiO_2 on photochemical reaction of chloroplasts of spinach. Biol Trace Elem Res 2005, 105:269-279.

Hong J, Peralta-Videa JR, Gardea-Torresdey JL, (2013). Sustainable nanotechnology and the environment: Advances and achievements, Washington DC, Maryland:American Chemical Society.

Horie M, Nishio K, Fujita K, Endoh S, Miyauchi A, Saito Y, Iwahashi H, Yamamoto K, Murayama H, Nakano H, Nanashima N, Niki E, Yoshida Y, Protein adsorption of ultrafine metal oxide and its influence on cytotoxicity toward cultured cells. Chem Res Toxicol 2009, 22:543-553.

Hoshino A, Fujioka K, Oku T, Suga M, Sasaki YF, Ohta T, Yasuhara M, Suzuki K, Yamamoto K, Physicochemical properties and cellular toxicity of nanocrystal quantum dots depend on their surface modification. Nano Lett 2004, 4:2163-2169.

Hubenthal F, Nanoparticles and their tailoring with laser light. Eur J Phys 2009, 30:S49-S61.

Hulkoti NI, Taranath TC, Biosynthesis of nanoparticles using microbes—A review. Colloids Surf, B 2014, 121:474-483.

Inaba H, Tagawa H, Ceria-based solid electrolytes. Solid State Ionics 1996, 83:1-16.

International Organization for Standardization (ISO) ISO/TS 80004-1:2010(en). Nanotechnologies-Vocabulary-Part 1: Core terms. Geneva, Switzerland, 2010.

Iravani S, Green synthesis of metal nanoparticles using plants. Green Chem 2011, 13:2638-2650.

Jacob DL, Borchardt JD, Navaratnam L, Otte ML, Bezbaruah AN, Uptake and translocation of Ti from nanoparticles in crops and wetland plants. Int J Phytoremediat 2013, 15:142-153.

Jew AD, Rogers SB, Rytuba JJ, Spormann AM, Brown JGE, "Bacterially mediated breakdown of cinnabar and metacinnabar and environmental implications", American Geophysical Union, San Francisco, December 2006.

Jha AK, Prasad K, Prasad K, A green low-cost biosynthesis of Sb_2O_3 nanoparticles. Biochem Eng J 2009, 43:303-306.

Jia L, Zhang Q, Li Q, Song H, The biosynthesis of palladium nanoparticles by antioxidants in Gardenia jasminoides Ellis: Long lifetime nanocatalysts for p-nitrotoluene hydrogenation. Nanotechnology 2009, 20:1-10.

Jiang J, Oberdörster G, Biswas P, Characterization of size, surface charge, and agglomeration state of nanoparticle dispersions for toxicological studies. J Nanopart Res 2009, 11:77-89.

Jiang M, Wood NO, Komanduri R, On the chemo-mechanical polishing (CMP) of Si3N4 bearing balls with water based CeO_2 slurry. J Eng Mater Tech 1998, 120:304-312.

Jin, RC, Cao YW, Mirkin CA, Kelly KL, Schatz GC, Zheng JG, Photoinduced conversion of silver nanospheres to nanoprisms. Science 2001, 294:1901-1903.

Jośko I and Oleszczuk P, Phytotoxicity of nanoparticles-problems with bioassay choosing and sample preparation. Environ Sci Pollut Res 2014, 21:10215-10224.

Ju-Nam Y, Lead JR, Manufactured nanoparticles: An overview of their chemistry, interactions and potential environmental implications. Sci Total Environ 2008, 400:396-414.

Kasthuri J, Kathiravan K, Rajendiran N, Phyllanthin-assisted biosynthesis of silver and gold nanoparticles: A novel biological approach. J Nanopart Res 2009, 11:1075-1085.

Kaushik N, Thakkar MS, Snehit S, Mhatre MS, Rasesh Y, Parikh MS, Biological synthesis of metallic nanoparticles. Nanomedicine: NBM 2010, 6:257-262.

Kaviya S, Santhanalakshmi J, Viswanathan B, Muthumary J, Srinivasan K, Biosynthesis of silver nanoparticles using citrus sinensis peel extract and its antibacterial activity. Spectrochim Acta Mol Biomol Spectrosc 2011, 79:594-598.

Kawazoe Y, Meech JA (2005). Intelligence in a Small Materials World, Lancaster, United Kingdom:DSEtech.

Keller A, McFerran S, Lazareva A, Suh S, Global life cycle releases of engineered nanomaterials. J Nanopart Res 2013, 15:1692.

Keller T, Schwager H, Air pollution and ascorbic acid. Eur J Forestry Pathol 1977, 7:338-350.

Kesharwani P, Jain K, Jain NK, Dendrimer as nanocarrier for drug delivery. Prog Polym Sci 2014, 39:268-307.

Kharissova OV, Dias HVR, Kharisov BI, Pérez BO, Pérez VMJ, The greener synthesis of nanoparticles. Trends Biotechnol 2013, 31:240-248.

Kharissova OV, Rasika Dias HV, Kharisov BI, Olvera Pérez B, Jiménez Pérez VM, The greener synthesis of nanoparticles. Trends Biotechnol 2012, 31:240-248.

Kiseleva VI, Tester RF, Wasserman LA, Krivandin AV, Popov AA, Yuryev VP, Influence of growth temperature on the structure and thermodynamic parameters of barley starches. Carbohyd Polym 2003, 51:407-415.

Kittelson DB, "Recent measurements of nanoparticle emissions from engines", Current Research on Diesel Exhaust Particles Japan Association of Aerosol Science and Technology, Tokyo, January 2001.

Klaine SJ, Alvarez PJJ, Batley GE, Fernandes TF, Handy RD, Lyon DY, Mahendra S, McLaughlin MJ, Lead JR, Nanomaterials in the environment: behavior, fate, bioavailability, and effects. Environ Toxicol Chem 2008, 27:1825-1851.

Klein DA, Striffler WD, Tellner HL (1975). National Hail Research Expt, Fort Collins, Colorado:Colorado State University.

Klingenfuss F, Testing of TiO_2 nanoparticles on wheat and microorganisms in a soil microcosm. Master thesis dissertation, University of Gothenburg, Sweden, July 2014.

Knipfer T and Fricke W, Water uptake by seminal and adventitious roots in relation to whole-plant water flow in barley (*Hordeum vulgare* L.). J Exp Bot 2011, 62:717-733.

Kobayashi S, Schwartz SJ, Lineback DR, Comprison of the structures of amylopectins from different wheat varieties. Cereal Chem 1986, 63: 71-74.
Konstantinou IK, Albanis TA, TiO_2-assisted photocatalytic degradation of azo dyes in aqueous solution: Kinetic and mechanistic investigations a review. Appl Catal B-Environ 2004, 49:1-14.

Koontz HV, Berle KL, Silver uptake, distribution, and effect on calcium, phosphorus, and sulfur uptake. Plant Physiol 1980, 65:336-339.

Kowshik M, Ashataputre S, Kharrazi S, Kulkarni SK, Paknikar KM, Vogel W, Urban J, Extracellular synthesis of silver nanoparticles by a silver-tolerant yeast strain MKY3. Nanotechnology 2003, 14:95-100.

Kratsch HA, Wise RR: The ultrastructure of chilling stress. Plant Cell Environ 2000, 23:337-350.

Kroto HW, Heath JR, O'Brien SC, Curl RF, Smalley RE, C60: Buckminsterfullerene. Nature 1985, 318:162-163.

Kühnel D and Nickel C, The OECD expert meeting on ecotoxicology and environmental fate—Towards the development of improved OECD guide lines for the testing of nanomaterials. Sci Tot Environ 2014, 472:347-353.

Kulacki KJ, Cardinale BJ, Keller AA, Bier R, Dickson H, How do stream organisms respond to, and influence, the concentration of titanium dioxide nanoparticles? A mesocosm study with algae and herbivores. Environ Toxicol Chem 2012, 31:2414-2422.

Kumar A, Kumar P, Anandan A, Fernandes TF, Ayoko GA, Biskos G, Engineered nanomaterials: Knowledge gaps in fate, exposure, toxicity, and future directions. J Nanomater 2014.

Kumar R, Khare N, Temperature dependence of conduction mechanism of ZnO and Co-doped ZnO thin films. Thin Solid Films 2008, 516:1302-1307.

Kumar R, Roopan SM, Prabhakarn A, Khanna VG, Chakroborty S, Agricultural waste Annona squamosa peel extract: Biosynthesis of silver nanoparticles. Spectrochim Acta Mol Biomol Spectrosc 2012, 90:173-176.

Kumar S, Kumar R, Singh DP, Swift heavy ion induced modifications in cobalt doped ZnO thin films: Structural and optical studies. Appl Surf Sci 2009, 255:8014-8018.

Kumar V, Yadav SK, Plant-mediated synthesis of silver and gold nanoparticles and their applications. J Chem Technol Biotechnol 2009; 84:151-157.

Kurepa J, Paunesku T, Vogt S, Arora H, Rabatic BM, Lu J, Wanzer MB, Woloschak GE, Smalle JA, Uptake and distribution of ultrasmall anatase TiO_2 Alizarin red S nanoconjugates in *Arabidopsis thaliana*. Nano Letters 2010, 10:2296-2302.

Lam E, Kato N, Lawton M, Programmed cell death, mitochondria and the plant hypersensitive response. Nature 2001, 411:848-853.

Lamprecht B, Leitner A, Aussenegg FR, SHG studies of plasmon dephasing in nanoparticles. Appl Phys B 1999, 68:419-423.

Lan Y, Lub Y, Ren Z, Mini review on photocatalysis of titanium dioxide nanoparticles and their solar applications. Nano energy 2013, 2:1031-1045.

Larsen MR, Thingholm TE, Jensen ON, Roepstorff P, Jørgensen TJD, Highly selective enrichment of phosphorylated peptides from peptide mixtures using titanium dioxide microcolumns. Mol Cell Proteomics 2005, 4:873-886.

Larue C, Castillo-Michel H, Sobanska S, Trcera N, Sorieul S, Cécillon L, Ouerdane L, Legros S, Sarret S, Fate of pristine TiO_2 nanoparticles and aged paint-containing TiO_2 nanoparticles in lettuce crop after foliar exposure. J Haz Mat 2014, 273:17-26.

Larue C, Laurette J, Herlin-Boime N, Khodja H, Fayard B, Flank A-M, Brisset F, Carriere M, Accumulation, translocation and impact of TiO_2 nanoparticles in wheat (*Triticum aestivum* spp.): influence of diameter and crystal phase. Sci Total Environ 2012, 431:197-208.

Lee J,. Fortner J, Hughes JB, Kim JH, Photochemical production of reactive oxygen species by C60 in the aqueous phase during UV irradiation. Environ Sci Technol 2007, 41:2529-2535.

Leustek T, Martin MN, Bick JA and Davies JP, Pathways and regulation of sulfur metabolism revealed through molecular and genetic studies. Ann Rev Plant Physiol Plant Mol Biol 2000, 51:141-165.

Li K-E, Chang Z-Y, Shen C-X., Yao N (2015). Nanotechnology and Plant Sciences, Cham, Switzerland: Springer International Publishing.

Liang Y, Bradford SA, Simunek J, Heggen M, Vereeken H, Klumpp E, Retention and remobilization of stabilized silver nanoparticles in an undisturbed loamy and soil. Environ Sci Technol, 2013, 47:12229-12237.

Lin C, Basil JDC, Hunia RM, Bihuniak PP, US Patent 1994, 5316854.

Lin D and Xing B, Phytotoxicity of nanoparticles: Inhibition of seed germination and root growth. Environ Pollut 2007, 150:243-250.

Linak WP, Miller CA, Wendt JO, Comparison of particle size distribution and elemental partitioning from the combustion of pulverized coal and residual fuel oil. J Waste Manag Assoc 2000, 50:1532-1544.

Linglan M, Chao L, Chunxiang Q, Sitao Y, Jie L, Fengqing G, Fashui H, Rubisco Activase mRNA expression in spinach: Modulation by nanoanatase treatment Biol Trace Elem Res 2008, 122:168-178.

Linse S, Cabaleiro-Lago C, Xue W-F, Lynch I, Lindman S, Thulin E, Radford SE, Dawson KA, Nucleation of protein fibrillation by nanoparticles. Proc Natl Acad Sci USA 2007, 104:8691-8696.

Liu HH and Cohen Y, Multimedia environmental distribution of engineered nanomaterials. Environ Sci Technol 2014, 48:3281–3292.

Liu HJ, Chang BY, Yan HW, Yu FH, Lu XX, Determination of amino acids in food and feed by derivatization with 6-aminoquinolyl-N-hydroxysuccinimidyl carbamate and reversed-phase liquid chromatographic separation. J AOAC Int 1995, 78:736-744.

Liu R and Lal R, Potentials of engineered nanoparticles as fertilizers for increasing agronomic productions. Sci Total Environ 2015, 514:131-139.

Liu R, Lal R, Nanoenhanced materials for reclamation of mine lands and other degraded soils: A review. J Nanotechnol 2012, 2012:18 pages.

Logothetidis S, Nanotechnology in medicine: The medicine of tomorrow and nanomedicine. Hippokratia 2006, 1:7-21.

López-Moreno ML, de la Rosa G, Hernández-Viezcas JA, Castillo-Michel H, Botez CE, Peralta-Videa JR, Gardea-Torresdey JL, Evidence of the differential biotransformation and genotoxicity of ZnO and CeO_2 nanoparticles on soybean (*Glycine max*) plants. Environ Sci Technol 2010b, 44:7315-7320.

López-Moreno ML, de la Rosa G, Hernández-Viezcas JA, Peralta-Videa JR, Gardea-Torresdey JL, X-ray Absorption Spectroscopy (XAS) corroboration of the uptake and storage of CeO_2 nanoparticles and assessment of their differential toxicity in four edible plant species. J Agric Food Chem 2010a, 58:3689-3693.

Lu CM, Zhang CY, Wen JQ, Wu GR, Tao MX, 2002, Research of the effect of nanometer materials on germination and growth enhancement of *Glycine max* and its mechanism.Soybean Sci, 21:168-172.

Lukman AI, Gong B, Marjo CE, Roessner U, Harris AT, Facile synthesis, stabilization, and anti-bacterial performance of discrete Ag nanoparticles using Medicago sativa seed exudates. J Colloid Interface Sci 2011, 353:433-444.

Lundin A, (1984). Extraction and Automatic Luminometric Assay of ATP, ADP and AMP. New York, New York:Academic Press.

Lv J, Zhang S, Luo L, Zhang J, Yang K, Christie P, Accumulation, speciation and uptake pathway of ZnO nanoparticles in maize. Environ Sci Nano 2015, 2:68-77.

Ma X, Geiser-Lee J, Deng Y, Kolmakov A, Interactions between engineered nanoparticles (ENPs) and plants: Phytotoxicity, uptake and accumulation. Sci Total Environ 2010, 408:3053-3061.

Ma Y, Kuang L, He X, Bai W, Ding Y, Zhang Z, Zhao Y, Chai Z, Effects of rare earth oxide nanoparticles on root elongation of plants. Chemosphere 2010, 78:273-279.

Ma Y, Zhang P, Zhang Z, He X, Li Y, Zhang J, Zheng L, Chu S, Yang K, Zhao Y, Chai Z, Origin of the different phytotoxicity and biotransformation of cerium and lanthanum oxide nanoparticles in cucumber. Nanotoxicol 2015, 9:262-270.

Ma Y, Zhang P, Zhang Z, He X, Zhang J, Ding Y, et al, Where does the transformation of precipitated ceria nanoparticles in hydroponic plants take place? Environ Sci Technol 2015, 49:10667-10674.

Mafuné F, Kohno J-Y, Takeda Y, Kondow T, Sawabe H, Formation of gold nanoparticles by laser ablation in aqueous solution of surfactant. J Phys Chem B 2001, 105:5114-5120.

Majumdar S, Peralta-Videa JR, Bandyopadhyay S, Castillo-Michel H, Hernandez-Viezcas J-A, Sahi S, Gardea-Torresdey JL, Exposure of cerium oxide nanoparticles to kidney bean shows disturbance in the plant defense mechanisms. J Haz Mat 2014, 278:279-287.

Manceau A, Nagy K, Marcus MWA, Lanson M, Geoffroy N, Jaquet TJ, Kirpichtikova T, Formation of metallic copper nanoparticles at the soil-root interface. Environ Sci Technol 2008, 42:1766-1772.

Marina OA, Pederson LR, US Patent, 2008, 7468218.

Marinova D, Ribarova F, Atanassova M, Total phenolics and total flavonoids in Bulgarian fruits and vegetables. J Chem Technol Metall 2005, 40:255-260.

Mariotti F, Tomé D, Mirand PP, Converting nitrogen into protein-beyond 6.25 and Jones' factors. Crit Rev Food Sci Nutr 2008, 48:177-184.

Marquet A, Enzymology of carbon–sulfur bond formation. Curr Opin Chem Biol 2001, 5:541-549.

Marschner H, (1995). Mineral nutrition of higher plants. Amsterdam, Netherlands:Academic Press.

Marshall AT, Haverkamp RG, Davies CE, Parsons JG, Gardea-Torresdey JL, van Agterveld D, Accumulation of gold nanoparticles in *Brassica juncea*. Int J Phytoremmediat 2007, 9:197-206.

Maskos M., Stauber RH, (2011). Materials Science and Materials Engineering, Oxford, Oxfordshire:Elsevier.

Masut T, Yamamoto M, Sakata T, Mori H, Adachi G, Synthesis of BN-coated CeO_2 fine powder as a new UV blocking material. J Mater Chem 2000, 10:353-357.

Matatov-Meytal YI, Sheintuch M, Catalytic abatement of water pollutants. Ind Eng Chem Res 1998, 37:309-326.

Mattiello A, Filippi A, Pošćić F, Musetti R, Salvatici MC, Giordano C, Vischi M, Bertolini A, Marchiol L, Evidence of phytotoxicity and genotoxicity in *Hordeum vulgare* L. exposed to CeO_2 and TiO_2 nanoparticles. Front Plant Sci 2015, 6:01043.

Maurer-Jones MA, Gunsolus IL, Murphy CJ, Haynes CL, Toxicity of engineered nanoparticles in the environment. Anal Chem 2013, 85:3036-3049.

Maynard AD, Kuempel ED, Airborne nanostructured particles and occupational health. J Nanopart Res 2005, 7:587-614.

McGrath SP, Zhao F-J, Phytoextraction of metals and metalloids from contaminated soils. Curr Opin Biotechnol 2003, 14:277-282.

Mendel RR and Hänsch R, Molybdoenzymes and molybdenum cofactor in plants. J Exp Bot 2002, 53:1689-1698.

Messing GL, Zhang S-C, Jayanthi GV, Ceramic powder synthesis by spray pyrolysis. J Am Ceram Soc 1993, 76:2707-2726.

Miralles P, Church TL, Harris AT, Toxicity, Uptake, and Translocation of engineered nanomaterials in vascular plants. Environ Sci Technol 2012, 46:9224-9239.

Mittal AK, Chisti Y, Banerjee UC, Synthesis of metallic nanoparticles using plant extracts. Biotechnol Adv 2013, 31:346-356.

Mohanpuria P, Rana NK, Yadav SK, Biosynthesis of nanoparticles: Technological concepts and future applications. J Nanopart Res 2008, 10:507-517.

Moreno-Olivas F, Gant VUJr, Johnson KL, Peralta-Videa JR, Gardea-Torresdey JL, Random amplified polymorphic DNA reveals that TiO_2 nanoparticles are genotoxic to *Cucurbita pepo*. J Zhejiang Univ Sci A 2014, 15:618-623.

Morimoto T, Tomonaga H, Mitani A, Ultraviolet ray absorbing coatings on glass for automobiles. Thin Solid films 1999, 351:61-65.

Moritz M, Geszke-Moritz M, The newest achievements in synthesis, immobilization and practical applications of antibacterial nanoparticles. Chem Eng J 2013, 228:596-613.

Morteza E, Moaveni P, Farahanim HA, Kiyani M, Study of photosynthetic pigments changes of maize (*Zea mays* L.) under nano TiO_2 spraying at various growth stages. SpringerPlus 2013, 2:247.

Mukherjee P, Ahmad A, Mandal D, Senapati S, Sainkar SR, Khan MI, et al., Fungus mediated synthesis of silver nanoparticles and their immobilization in the mycelial matrix: a novel biological approach to nanoparticle synthesis. Nano Lett 2001, 1:515-519.

Mukunthan KS, Balaji S, Cashew apple juice (*Anacardium occidentale* L.) speeds up the synthesis of silver nanoparticles. Int J Green Nanotechnol 2012, 4:71-79.

Mura S, Seddaiu G, Bacchini F, Roggero PP, Advances of nanotechnology in agro-environmental studies. Ital J Agron 2013, 8:e18.

Murr LE, Esquivel EV, Bang JJ, de la Rosa G, Gardea-Torresdey JL, Chemistry and nanoparticulate compositions of a 10,000 year-old ice core melt water. Water Res 2004, 38:4282-4296.

Murray CB, Sun S, Gaschler W, Doyle H, Betley TA, Kagan CR, Colloidal synthesis of nanocrystals and nanocrystal superlattices. IBM J Res & Dev 2001, 45:47-56.

Mushtaq YK, Effect of nanoscale Fe_3O_4, TiO_2 and carbon particles on cucumber seed germination. J Environ Sci Health A 2011, 46:1732-1735.

Nadeau S, Bouchard M, Debia M, De Marcellis-Warin N, Hallé S, Songmene V, Therrien M-C, Wilkinson K, Ateme-Nguema B, Dufour G, Dufresne A, Fatisson J, Haddad S, Hadioui M, Kouam J, Morency F, Tardif R, Viens M, Weichenthal S, Viau C, Camus M, ÉquiNanos: Innovative team for nanoparticle risk management. Nanomed Nanotechnol Biol Med 2013, 9:22-24.

Narayanan KB, Sakthivel N, Green synthesis of biogenic metal nanoparticles by terrestrial and aquatic phototrophic and heterotrophic eukaryotes and biocompatible agents. Adv Colloid Interface Sci 2011, 169:59-79.

Nascarella MA and Calabrese EJ, A method to evaluate hormesis in nanoparticle dose-response. Dose Response 2012, 10:344-354.

Nath D, Banerjee P, Green nanotechnology – A newhope for medical biology. Environ Toxicol Phar 2013, 36:997-1014.

Navarro E, Baun A, Behra R, Hartmann NB, Filser J, Miao A-J et al, Environmental behavior and ecotoxicity of engineered nanoparticles to algae, plants, and fungi. Ecotoxicology 2008, 17:372-386.

Newman, C.W., and Newman, R.K. (1992). Nutritional aspects of barley seed structure and composition, in Shewry, Wallingford, Oxfordshire: P.R..

Newman RK, Newman CW, (2008). Barley for Food and Health: Science, Technology and Products, New York, New York:Wiley Publishers.

Ni M, Leung MKH, Leung DYC, Sumathy K, A review and recent developments in photocatalytic water-splitting using TiO_2 for hydrogen production. Renew Sust Energ Rev 2007, 11:401-425.

Noctor G, Gomez L, Vanacker H, Foyer CH, Interactions between biosynthesis, compartmentation and transport in the control of glutathione homeostasis and signalling. J Exp Bot 2002, 53:1283-1304.

Noguez C, Surface plasmons on metal nanoparticles: The influence of shape and physical environment. J Phys Chem C 2007, 111:3806-3819.

Nowack B, Baalousha M, Bornhöft N, Chaudhry O, Cornelis G, Cotterill J, et al, Progress towards the validation of modelled environmental concentrations of engineered nanomaterials by analytical measurements. Environ Sci Nano 2015, 2:421-428.

Nowack B, Bucheli TD, Occurrence, behavior and effects of nanoparticles in the environment. Environ Pollut 2007, 150:5-22.

Nowack B, Ranville JF, Diamond S, Gallego-Urea JA, Metcalfe C, Rose J, et al., Potential scenarios for nanomaterial release and subsequent alternation in the environment. Environ Toxicol Chem 2012, 31:50-59.

O'Brien NJ, Cummins EJ, A Risk Assessment framework for assessing metallic nanomaterials of environmental concern: aquatic exposure and behavior. Risk Anal 2011, 31:706-726.

Oberdörster G, Oberdörster E, Oberdörster J, Nanotoxicology: An emerging discipline evolving from studies of ultrafine particles. Environ Health Persp 2005, 113:823-839.

OECD. List of Manufactured Nanomaterials and List of Endpoints for Phase One of the Sponsorship Programme for the Testing of Manufactured Nanomaterials: Revision. Paris: OECD Environment, Health and Safety Publications Series on the Safety of Manufactured Nanomaterials. 2010

Okumura M., Tsubota S., Iwamoto M., Haruta M., Chemical vapor deposition of gold nanoparticles on MCM-41 and their catalytic activities for the low-temperature oxidation of CO and of H_2. Chem Lett 1998, 4:315-316.

Ouacha H, Hendrich C, Hubenthal F, Träger F, Laser-assisted growth of gold nanoparticles: Shaping and optical characterization. Appl Phys B 2005, 81: 663-668.

Pacheco-Blandino II, Vanner R, Buzea C, (2012) Toxicity of Building Materials, Oxford, United Kingdom:Elsevier.

Pakrashi S, Jain N, Dalai S, Jayakumar J, Chandrasekaran PT, Raichur AM, Chandrasekaran N, Mukherjee A, In vivo genotoxicity assessment of titanium dioxide nanoparticles by *Allium cepa* root tip assay at high exposure concentrations. PLoS ONE 2014, 9:e87789.

Pan B, Xing B, Manufactured nanoparticles and their sorption of organic chemicals. Adv Agric 2010, 108:137-181.

Panariti A, Miserocchi G, Rivolta I, The effect of nanoparticle uptake on cellular behavior: disrupting or enabling functions? Nanotechnol Sci Appl 2012, 5:87-100.

Pansu M, Gautheyrou J, (2006). Handbook of soil analysis: mineralogical, organic and inorganic methods, Berlin, Germany:Springer-Verlag.

Parisi C, Vigani M, Rodríguez-Cerezo E, Agricultural nanotechnologies: What are the current possibilities? NanoToday 2015, 10:124-127.

Park Y, Hong YN, Weyers A, Kim YS, Linhardt RJ, Polysaccharides and phytochemicals: A natural reservoir for the green synthesis of gold and silver nanoparticles. IET Nanobiotechnol 2011, 5:69-78.

Patil S, Kuiry SC, Seal S, Vanfleet R, Synthesis of nanocrystalline ceria particles for high temperature oxidation resistant coating. J Nanopart Res 2002, 4:433-438.

Patil S, Sandberg A, Heckert E, Self W, Seal S, Protein adsorption and cellular uptake of cerium oxide nanoparticles as a function of zeta potential. Biomaterials 2007, 28:4600-4607.

Peakall R and Smouse PE, GenAlEx 6.5: genetic analysis in Excel. Population genetic software for teaching and research–an update. Bioinformatics 2012, 28:2537-2539.

Peralta-Videa JR, Hernandez-Viezcas JA, Zhao L, Corral Diaz B, Ge Y, Priester JH, Holden PA, Gardea-Torresdey JL, Cerium dioxide and zinc oxide nanoparticles alter the nutritional value of soil cultivated soybean plants. Plant Physiol Biochem 2014, 80:128-135.

Phenrat T, Liu Y, Tilton RD, Lowry GV, Adsorbed polyelectrolyte coatings decrease Fe^0 nanoparticle reactivity with TCE in water: Conceptual model and mechanisms. Environ Sci Technol 2009, 43:1507-1514.

Phenrat T, Saleh N, Sirk K, Kim H-J, Tilton RD, Lowry GV, Stabilization of aqueous nanoscale zerovalent iron dispersions by anionic polyelectrolytes: adsorbed anionic polyelectrolyte layer properties and their effect on aggregation and sedimentation. J Nanopart Res 2008, 10:795-814.

Philip D, Green synthesis of gold and silver nanoparticles using *Hibiscus rosa-sinensis*. Physica E 2010, 4:1417-1424.

Piccinno F, Gottschalk F, Seeger S, Nowack B, Industrial production quantities and uses of ten engineered nanomaterials in Europe and the world. J Nanopart Res 2012, 14:1109-9.

Pidgeon N, Harthorn BH, Bryant K, Rogers-Hayden T, Deliberating the risks of nanotechnologies for energy and health applications in the United States and United Kingdom. Nat Nanotechnol 2009, 4:95-98.

Pomeranz Y, Robbins GS, Smith RT, Craddock JC, Gilbertson JT, Protein content and amino acid composition of barleys from the world collection. Cereal Chem 1976, 53:497-504.

Pozzo RL, Baltanfis MA, Cassano AE, Supported titanium oxide as photocatalyst in water decontamination: State of the art. Catal today 1997, 39:219-231.

Priester JH, Ge Y, Mielke RE, Horst AM, Moritz SC, Espinosa K, Gelb J, Walker SL, Nisbet RM, An YJ, Schimel JP, Palmer RG, Hernandez-Viezcas JA, Zhao L, Gardea-Torresdey JL, Holden PA, Soybean susceptibility to manufactured nanomaterials with evidence for food quality and soil fertility interruption. Proc Natl Acad Sci 2012, 109:E2451-6.

Qi M, Liu Y, Li T, Nano-TiO_2 improve the photosynthesis of tomato leaves under mild heat stress. Biol Trace Elem Res 2013, 156:323-328.

Quester K, Avalos-Borja M, Castro-Longoria E, Biosynthesis and microscopic study of metallic nanoparticles. Micron 2013, 54-55:1-27.

Rajakumar G, Rahuman AA, Roopan SM, Khanna VG, Elango G, Kamaraj C, Zahir AA, Velayutham K, Fungus-mediated biosynthesis and characterization of TiO_2 nanoparticles and their activity against pathogenic bacteria. Spectrochim Acta Mol Biomol Spectrosc 2012, 91:23-29.

Reina A, Jia XT, Ho J, Nezich D, Son HB, Bulovic V, Dresselhaus MS, Kong J, Large area, few-layer graphene films on arbitrary substrates by chemical vapor deposition. Nano Lett 2009, 9:30-35.

Ribas Ferreira JL, Lonné MN, Franc TA, Maximilla NM, Lugokenski TH, Costa PG, Fillmann G, Antunes Soares FA, de la Torre FR, Monserrat JM, Co-exposure of the organic nanomaterial fullerene C60 with benzo[a]pyrene in *Danio rerio* (zebrafish) hepatocytes: Evidence of toxicological interactions. Aquat Toxicol 2014, 147:76-83.

Rico C, Morales M, Barrios A, McCreary R, Hong J, Lee W, et al., Effect of cerium oxide nanoparticles on the quality of rice (*Oryza sativa* L.) grains. J Agric Food Chem 2013, 61:11278-11285.

Rico CM, Barrios AC, Tan W, Rubenecia R, Lee SC, Varela-Ramirez A, Peralta-Videa JR, Gardea-Torresdey JL, Physiological and biochemical response of soil-grown barley (*Hordeum vulgare* L.) to cerium oxide nanoparticles. Environ Sci Pollut Res Int 2015b, 22:10551-10558.

Rico CM, Lee SC, Rubenecia R, Mukherjee A, Hong J, Peralta-Videa JR, Gardea-Torresdey JL, Cerium oxide nanoparticles impact yield and modify nutritional parameters in wheat (*Triticum aestivum* L.). J Agric Food Chem 2014, 62:9669-9675.

Rico CM, Majumdar S, Duarte-Gardea M, Peralta-Videa JR, Gardea-Torresdey JL, Interaction of nanoparticles with edible plants and their possible implications in the food chain. J Agric Food Chem 2011, 59:3485-3498.

Rico CM, Peralta-Videa JR, Gardea-Torresdey JL, Differential effects of cerium oxide nanoparticles on rice, wheat, and barley roots: a Fourier Transform Infrared (FT-IR) microspectroscopy study. Appl Spectrosc 2015a, 69:287-295.

Robinson AL, Donahue NM, Shrivastava MK, Weitkamp EA, Sage AM, Grieshop AP, Lane TE, Pierce JR, Pandis SN, Rethinking organic aerosols: Semivolatile emissions and photochemical aging. Science 2007, 315:1259-1262.

Roco MC (2010). Nanotechnology research directions for societal needs in 2020: Retrospective and outlook. Boston, Massachusetts:Springer.

Roco MM, The long view of nanotechnology development: The National Nanotechnology Initiative at 10 years. J Nanopart Res 2011, 13:427-445.

Rodríguez-León E, Iñiguez-Palomares R, Navarro RE, Herrera-Urbina R, Tánoris J, Iñiguez-Palomares C, Maldonano A, Synthesis of silver nanoparticles using reducing agents obtained from natural sources (*Rumex hymenosepalus* extracts). Nanoscale Res Lett 2013, 8:318.

Rogers F, Arnott P, Zielinska B, Sagebiel J, Kelly KE, Wagner D, Lighty JS, Sarofim AF Realtime measurements of jet aircraft engine exhaust. J. Air Waste Manag Assoc 2005, 55:583-593.

Rosati JA (2005). Final Report on the World Trade Center (WTC) Dust Screening Method Study. U.S. Environmental Protection Agency,Office of Research and Development.

Ruffini Castiglione M, Giorgetti L, Geri C, Cremonini R, Response of tomato plants exposed to treatment with nanoparticles. J Nanopart Res 2011, 1:2443-2449.

Saito K, Regulation of sulfate transport and synthesis of sulfur-containing amino-acids. Curr Opin Plant Biol 2000, 3: 188–195.

Saleh N, Phenrat T, Sirk K, Dufour B, Ok J, Sarbu T, Matyjaszewski K, Tilton RD, Lowry GV, Adsorbed triblock copolymers deliver reactive iron nanoparticles to the oil/water interface. Nano Lett 2005, 5:2489-2494.

Salt DE, Smith RD, Raskin I, Phytoremediation. Annu Rev Plant Physiol Plant Mol Biol 1998, 49:643-668.

Sastry M, Ahmad A, Khan MI, Kumar R, Biosynthesis of metal nanoparticles using fungi and actinomycete. Curr Sci 2003, 85:162-170.

Savolainen K, Backman U, Brouwer D, Fadeel B, Fernandes T, Kuhlbusch T, Landsiedel R, Lynch I, Pylkkänen L, (2013). Nanosafety in Europe 2015-2025: Towards Safe and Sustainable Nanomaterials and Nanotechnology Innovations, Helsinki, Finland:EDITA.

Schlich K, Hund-Rinke K, Influence of soil properties on the effect of silver nanomaterials on microbial activity in five soils. Env Poll 2015, 196:321-330.

Schmid G, Large clusters and colloids. Metals in the embryonic state. Chem Rev 1992, 92:1709-1727.

Schneider CA, Rasband WS, Eliceiri KW, NIH Image to ImageJ: 25 years of image analysis. Nat Methods 2012, 9:671-675.

Schnützendübel A, Polle A, Plant response to abiotic stresses: Heavy metal-induced oxidative stress and protection by mycorrhization. J Exp Bot 2002, 53:1351-1365.

Schwabe F, Schulin R, Limbach LK, Stark W, Bürge D, Nowack B, Influence of two types of organic matter on interaction of CeO_2 nanoparticles with plants in hydroponic culture. Chemosphere 2013, 91:512-520.

Schwabe F, Tanner S, Schulin R, Rotzetter A, Stark W, von Quadt A, Nowack B, Dissolved cerium contributes to uptake of Ce in the presence of differently sized CeO_2-nanoparticles by three crop plants. Metallomics 2015, 7:466-477.

Seames WS, Fernandez A, Wendt JO, A study of fine particulate emissions from combustion of treated pulverized municipal sewage sludge. Environ Sci Technol 2002, 36:2772-2776.

Servin AD, Castillo-Michel H, Hernández-Viezcas JA, Corral Diaz B, Peralta-Videa JR, Gardea-Torresdey JL, Synchrotron micro-XRF and micro-XANES confirmation of the uptake and translocation of TiO_2 nanoparticles in cucumber (*Cucumis sativus*) plants. Environ Sci Technol 2012, 46:7637-7643.

Servin AD, Morales MI, Castillo-Michel H, Hernandez-Viezcas JA, Munoz B, Zhao L, Nunez JE, Peralta-Videa JR, Gardea-Torresdey JL, Synchrotron verification of TiO_2 accumulation in cucumber fruit: a possible pathway of TiO_2 nanoparticle transfer from soil into the food chain. Environ Sci Technol 2013, 47, 11592-11598.

Servin AD and White JC, Nanotechnology in agriculture: Next steps for understanding engineered nanoparticle exposure and risk. NanoImpact 2016.

Shahin AM, Grandjean F, Long GJ, Schuman TP, Cerium LIII-Edge XAS investigation of the structure of crystalline and amorphous cerium oxides. Chem Mater 2005,17:315-321.

Shankar SS, Rai A, Ahmad A, Sastry M, Controlling the optical properties of lemongrass extract synthesized gold nanotriangles and potential application in infrared-absorbing optical coatings. Chem Mater 2005, 17:566-572

Sharma NC, Gardea-Torresdey JL, Nath S, Pal T, Parsons JG, Sahi SV: Synthesis of plant mediated gold nanoparticle and catalytic role of biomatrix embedded nanomaterials. Environ Sci Technol 2007, 936:2929-2933.

Sharma SS, Dietz K-J, The relationship between metal toxicity and cellular redox imbalance. Trends Plant Sci 2008, 14:43-50.

Shen CS, Zhang Q-F, Li J, Bi F-C, Yan N, Induction of programmed cell death in Arabidopsis and rice by single-wall carbon nanotubes. Am J Bot 2010, 97:1602-1609.

Shivaji S, Madhu S, Singh S, Extracellular synthesis of antibacterial silver nanoparticles using psychrophilic bacteria. Process Biochem 2011, 46: 1800-1807.

Shu X, Rasmussen SK, Quantification of amylose, amylopectin, and β-glucan in search for genes controlling the three major quality traits in barley by genome-wide association studies. Front Plant Sci 2014, 5:00197

Sim KS, Hilaire L, Le Normand F, Touroude R, Paul-Boncour V, Percheron-Guegan A, Catalysis by palladium-rare-earth-metal (REP3) Intermetallic compounds: Hydrogenation of But-1-ene, Buta-l,3-diene and But-1-yne. J Chem Soc Faraday Trans 1991, 87:1453-1460.

Simon P, Olveira S, Seege S, Nanotechnology in the market: Promises and realities. Int J Nanotechnol 2011, 8:592-613.

Singh D and Kumar A, Human exposures of engineered nanoparticles from plants irrigated with contaminated water: Mixture toxicity issues and challenges ahead. Adv Sci Lett 2014, 20:1204-1207.

Singleton VL, Rossi JAJ, Colorimetry of total phenolics with phosphomolybdic-phosphotungstic acid reagents. Am J Enol Vitic 1965, 16:144-158.

Sivula K., Le Formal F., Gratzel M., WO_3-Fe_2O_3 photoanodes for water splitting: A host scaffold, guest absorber approach. Chem Mater 2009, 21:2862-2867.

Skinner HCW, Jahren AH (2003). Treatise on Geochemistry, Amsterdam, Holland:Elsevier.

Smart SK, Cassady AI, Lu GQ, Martin DJ, The biocompatibility of carbon nanotubes. Carbon 2005, 44:1034-1047.

Smith IC, Carson BL (1977). Trace Elements in the Environment. Volume – Silver, Ann Arbor, Michigan:Ann Arbor Science.

Sohaebuddin SK, Thevenot PT, Baker D, Eaton JW, Tang L, Nanomaterial cytotoxicity is composition, size, and cell type dependent. Part Fibre Toxicol 2010, 7:22-39.

Sokal RR, Rohlf FJ, (2010). Biometry. The principles and practice of statistics in biological research, New York, New York:WH Freeman and Company.

Song JY, Jang H-K, Kim BS, Biological synthesis of gold nanoparticles using *Magnolia Kobus* and *Diopyros kaki* leaf extracts. Process Biochem 2009, 44:1133-1138.

Song U, Jun H, Waldman B, Roh J, Kim Y, Yi J, et al., Functional analysis of nanoparticle toxicity: a comparative study of the effects of TiO_2 and Ag on tomatoes (*Lycopersicon esculentum*). Ecotoxicol Environ Safe. 2013a, 93:60-67.

Song U, Shin M, Lee G, Roh J, Kim Y, Lee EJ, Functional analysis of TiO_2 nanoparticle toxicity in three plant species. Biol Trace Elem Res 2013b, 155:93-103.

Soto KF, Carrasco A, Powell TG, Garza KM, Murr LE, Comparative in vitro cytotoxicity assessment of some manufactured nanoparticulate materials characterized by transmission electron microscopy. J Nanopart Res 2005, 7: 145–169.

Starnes D, Jayjain A, Sahi S, In planta engineering of gold nanoparticles of desirable geometries by modulating growth conditions: an environment-friendly approach. Environ Sci Technol 2010, 44:7110-7115.

Stefanik TS, Tuller HL, Ceria-based gas sensors. J Eur Ceram Soc 2001, 21:1967-1970.

Stietz F, Laser manipulation of the size and shape of supported nanoparticles. Appl Phys A 2001, 72:381-394.

Su M, Liu H, Liu C, Qu C, Zheng L, Hong F, Promotion of nano-anatase TiO_2 on the spectral responses and photochemical activities of D1/D2/Cyt b559 complex of spinach. Spectroc Acta Pt A-Molec Biomolec Spectr 2009, 72:1112-1116.

Suppan S, Nanomaterials in soil: Our future food chain? Institute for Agriculture and Trade Policy, 2013.

Takeuchi MT, Kojima M, Luetzow M, State of the art on the initiatives and activities relevant to risk assessment and risk management of nanotechnologies in the food and agriculture sectors. Food Res Int 2014, 64:976-981.

Tao AR, Habas S, Yang P, Shape control of colloidal metal nanocrystals. Small 2008, 4:310-325.

Tarnuzzer RW, Colon J, Patil S, Seal S, Vacancy engineered ceria nanostructures for protection from radiation-induced cellular damage. Nano Lett 2005, 5:2573-2577.

Tashiro J, Sasaki A, Akiba S, Satoh S, Watanabe T, Funakubo H, Yoshimoto M, Room-temperature epitaxial growth of indium tin oxide thin films on Si substrates with an epitaxial CeO_2 ultrathin buffer. Thin Solid Films 2002, 415:272-275.

Thakkar KN, Mhatre SS, Parikh RY, Biological synthesis of metallic nanoparticles. Nanomedicine 2010, 6:257-262.

Tourinho PS, Van Gestel CAM, Lofts S, Svedsen C, Soares AMVM, Loureiro S, Metal-based nanoparticles in soil: Fate, behavior, and effects on soil invertebrates. Environ Toxicol Chem 2012, 31:1679-1692.

Trovarelli A, de Leitenburg C, Boaro M, Dolcetti G, The utilization of ceria in industrial catalysis. Catal Today 1999, 50:353-367.

Truffault L, Andrezza C, Santilli CV, Pulcinelli SH, Synthesis of PTSH-modified CeO_2 nanoparticles: Effect of the modifier on structure, optical properties, and dispersibility. Coloid Surf A 2013, 426:63-69.

Tsunekawa S, Fukuda T, Kasuya A, Blue shift in ultraviolet absorption spectra of monodisperse CeO_{2-x} nanoparticles. J Appl Phys 2000, 87:1318-1321.

Tsunekawa S, Sahara R, Kawazoe Y, Kasuya A, Origin of the blue shift in ultraviolet absorption spectra of nanocrystalline CeO_{2-x} particles. Mater T JIM 2000, 41:1104-1107.

Turkevich J, Stevenson PC, Hillier J, A study of the nucleation and growth processes in the synthesis of colloidal gold. Discuss Faraday Soc 1951, 11:55-75.

USEPA: Health assessment for Diesel exhaust. Washington, dc, U.S. Environmental Protection Agency. 2002.

USEPA: EPA Method 3052: Microwave Assisted Acid Digestion of Siliceous and Organically Based Matrices, 3rd Edn. Washington, DC: Test Methods for Evaluating Solid Waste. 1995.

USEPA: Nanotechnology White Paper External Review Draft. 2005.

van Assche F, Clijsters H, Effects of metals on enzyme activity in plants. Plant Cell Environ 1990, 13:195-206

Van Hoecke K, Quik JT, Mankiewicz-Boczek J, De Schamphelaere KA, Elsaesser A, Van der Meeren P, et al., Fate and effects of CeO_2 nanoparticles in aquatic ecotoxicity tests. Environ Sci Technol 2009, 15:4537-4546.

Van Nhan L, Ma C, Rui Y, Liu S, Li X, Xing B, et al., Phytotoxic mechanism of nanoparticles: destruction of chloroplasts and vascular bundles and alteration of nutrient absorption. Sci Rep 2015, 5:11618.

Veena Choudhary, Anju Gupta (2011). Polymer/Carbon Nanotube Nanocomposites, Carbon Nanotubes - Polymer Nanocomposites, Rijeka, Croatia:InTech,

Venkatpurwar V, Pokharkar V, Green synthesis of silver nanoparticles using marine polysaccharide: Study of in-vitro antibacterial activity. Mater Lett 2011, 65:999-1002.

Verma HC, Upadhyay C, Tripathi A, Tripathi RP, Bhandari N, Thermal decomposition pattern and particle size estimation of iron minerals. Meteorit Planet Sci 2002, 37:901-909.

Vranová E, Inzé D, VanBreusegem F, Signal transduction during oxidative stress. J Exp Bot 2002, 53:1227-1236.

Wang H and Joseph JA, Quantifying cellular oxidative stress by dichlorofluorescein assay using microplate reader. Free Radic Biol Med 1999,27:612-616.

Wang Q, Ma X, Zhang W, Pei H, Chen Y, The impact of cerium oxide nanoparticles on tomato (*Solanum lycopersicum* L.) and its implications for food safety. Metallomics 2012, 4:1105-1112.

Wang S, Li P, Liu H, Li J, Wei Y, The structure and optical properties of ZnO nanocrystals dependence on Co-doping levels. J Alloy Compd 2010, 505:362-366.

Watkins DM, Sayed-Sweet Y, Klimash JW, Turro NJ, Tomalia DA, Dendrimers with hydrophobic cores and the formation of supramolecular dendrimer-surfactant assemblies. Langmuir 1997, 13:3136-3141.

Weier E, Factors affecting the reduction of silver nitrate by chloroplasts. Am J Bot 1938, 23:501-507.

Wendera H, Migowskib P, Feil AF, Teixeirac SR, Dupont J, Sputtering deposition of nanoparticles onto liquid substrates: Recent advances and future trends. Coord Chem Rev 2013, 257:2468-2483.

Werlin R, Priester JH, Mielke RE, Kramer S, Jackson S, Stoimenov PK, Stucky GD, Cherr GN, Orias E, Holden PA, Biomagnification of cadmium selenide quantum dots in a simple experimental microbial food chain. Nat Nanotechnol 2011, 6:65-71.

White E, Life, death, and the pursuit of apoptosis. Genes Dev 1996, 10:1-15.

Wiesner MR, Lowry GV, Jones KL, Hochella MFJ, Di Giulio RT, Casman E, Bernhardt ES, Decreasing uncertainties in assessing environmental exposure, risk, and ecological implications of nanomaterials. Environ Sci Technol 2009, 43:6458-6462.

Wu SG, Huang L, Head J, Chen DR, Kong IC, Tang YJ, Phytotoxicity of metal oxide nanoparticles is related to both dissolved metals ion sand adsorption of particles on seed surfaces. J Pet Environ Biotechnol 2012, 3:126.

Yahiro H, Baba Y, Eguchi K, Arai H, High temperature fuel cell with ceria-yttria solid electrolyte. J Electrochem Soc 1988, 135:2077-2080.

Yakimova MS, Ivanov VK, Polezhaeva OS, Trushin AA, Lermontov AS, Tretyakov YD, Oxidation of CO on nanocrystalline ceria promoted by transition metal oxides. Dokl Chem 2009, 427:186-189.

Yamashita M, Kameyama K, Yabe S, Yoshida S, Fujishiro Y, Kawai T, Sato T, Synthesis and microstructure of calcia doped ceria as UV filters. J Mater Sci 2002, 37:683-687.

Yan RC, Thompson DB, Boyer CD, Fine structure of amylopectin in relation to gelatinization and retrogradation behavior of maize starches from three wx-Containing genotypes in two inbred lines. Cereal Chem, 1993, 70: 81-89.

Yang F, Hong F, You W, Liu C, Gao F, Wu C, Yang P, Influences of nano-anatase TiO_2 on the nitrogen metabolism of growing spinach. Biol Trace Elem Res 2006, 110:179-90.

Yang F, Liu C, Gao F, Su M, Wu X, Zheng L, Hong F, Yang P, The improvement of spinach growth by nano-anatase TiO_2 treatment is related to nitrogen photoreduction. Biol Trace Elem Res 2007, 119:77-88.

Yang L and Watts DJ, Particle surface characteristics may play an important role in phytotoxicity of alumina nanoparticles. Toxicol Lett 2005, 158:122-132.

Yokoyama T, Masuda H, Suzuki M, Ehara K, Nogi K, Fuji M, Fukui T, Suzuki H, Tatami J, Hayashi K, Toda K (2012). Nanoparticle Technology Handbook, Oxford, United Kingdom:Elsevier.

Yoon S-J, Kwaka JI, Lee W-M, Holden PA, Ana Y-J, Zinc oxide nanoparticles delay soybean development: A standard soil microcosm study. Ecotoxicol Environ Saf 2014, 100:131-137.

Zadoks JC, Chang TT, Konzak CF, A decimal code for the growth stages of cereals. Weed Res 1974, 14:415-421.

Zhai YQ, Zhang SY, Pang H, Preparation, characterization and photocatalytic activity of CeO_2 nanocrystalline using ammonium bicarbonate as precipitant. Mater Lett 2007, 61:1863-1867

Zhang M, Yudasaka M, Ajima K, Miyawaki J, Iijima S, Light assisted oxidation of single-wall carbon nanohorns for abundant creation of oxygenated groups that enable chemical modifications with proteins to enhance biocompatibility. ACS Nano 2007, 1:265-272.

Zhang P, Ma Y, Zhang Z, He X, Zhang J, Guo Z, Tai R, Zhao Y, Chai Z, Biotransformation of ceria nanoparticles in cucumber plants. ACS Nano 2012, 6:9943-9950.

Zhang P, Ma YH, Zhang ZY, He X, Li YY, Zhang J, Zheng LR, Zhao YL, Species-specific toxicity of ceria nanoparticles to Lactuca plants.Nanotoxicology 2013, 10:1-8.

Zhang W, Ebbs SD, Musante C, White JC, Gao C, Ma X, Uptake and accumulation of bulk and nanosized cerium oxide particles and ionic cerium by radish (*Raphanus sativus* L.). J Agric Food Chem 2015, 63:382-390.

Zhang W-X, Nanoscale iron particles for environmental remediation: An overview. J Nanopart Res 2003, 5:323-332.

Zhang WX, Wang C-B, Lien H-L, Treatment of chlorinated organic contaminants with nanoscale bimetallic particles. Catal Today 1998, 40:387-395.

Zhang Z, He X, Zhang H, Ma Y, Zhang P, Ding Y, et al., Uptake and distribution of ceria nanoparticles in cucumber plants. Metallomics 2011, 3:816-822.

Zhao H, Zhou Q, Zhou M, Li C, Gong X, Liu C, Qu C, Wang L, Si W, Hong F, Magnesium deficiency results in damage of nitrogen and carbon cross-talk of maize and improvement by cerium addition. Biol Trace Elem Res 2012, 148:102−109.

Zhao L, Peralta-Videa JR, Rico CM, Hernandez-Viezcas JA, Sun Y, Niu G, Servin A, Nunez JE, Duarte-Gardea M, Gardea-Torresdey JL, CeO_2 and ZnO nanoparticles change the nutritional qualities of cucumber (*Cucumis sativus*). J Agric Food Chem 2014, 62:2752–2759.

Zhao L, Sun Y, Hernandez-Viezcas JA, Hong J, Majumdar S, Niu G, Duarte-Gardea M, Peralta-Videa JR, Gardea-Torresdey JL, Monitoring the environmental effects of CeO_2 and ZnO nanoparticles through the life cycle of corn (*Zea mays*) plants and in situ μ-XRF mapping of nutrients in kernels. Environ Sci Technol 2015, 49:2921-2928.

Zhao L, Sun Y, Hernandez-Viezcas JA, Servin AD, Hong J, Niu G, Peralta-Videa JR, Duarte-Gardea M, Gardea-Torresdey JL, Influence of CeO_2 and ZnO nanoparticles on cucumber physiological markers and bioaccumulation of Ce and Zn: A life cycle study. J Agric Food Chem 2013, 61:11945-11951.

Zhao LJ, Peralta-Videa JR, Hernandez-Viezcas JA, Hong J, Gardea-Torresdey JL, Transport and retention behavior of ZnO nanoparticles in two natural soils: Effect of surface coating and soil composition. Journal of Nano Research 2012, 17:229-242.

Zheng L, Hong F, Lu S, Liu C, Effect of nano-TiO_2 on strength of naturally aged seeds and growth of spinach. Biol Trace Elem Res 2005, 104:83-92.

Zhong X, Li Q, Hu J, Lu Y, Characterization and corrosion studies of ceria thin film based on fluorinated AZ91D magnesium alloy. Corros Sci 2008, 50:2304-2309.

Zhou F, Ni X, Zhang Y, Zheng H, Size-controlled synthesis and electrochemical characterization of spherical CeO_2 crystallites. J Colloid Interface Sci 2007, 307:135-138.

Zhou F, Zhao X, Xu H, YuanC, CeO_2 spherical crystallites: Synthesis, formation mechanism, size control, and electrochemical property study. J Phys Chem C 2007, 111:1651-1657.

Zhu H, Han J, Xiao JQ, Jin Y, Uptake, translocation, and accumulation of manufactured iron oxide nanoparticles by pumpkin plants. J Environ Monitor 2008, 10:713-717.

Zhu X, Wang J, Zhang X, Chang Y, Chen Y, Trophic transfer of TiO_2 nanoparticles from daphnia to zebrafish in a simplified freshwater food chain. Chemosphere 2010, 79:928-933.

Zhuge LJ, Wu XM, Wu ZF, Yang XM, Chen XM, Chen Q, Structure and deep ultraviolet emission of Co-doped ZnO films with Co_3O_4 nano-clusters. Mater Chem Phys 2010, 120:480-483.